On the estimation of the electromagnetic, elastodynamic and piezoelectric properties of homogenized composite materials

Andrew J. Duncan

Doctor of Philosophy
University of Edinburgh
2009

Declaration

I declare that this thesis was composed by myself and that the work contained therein is my own, except where explicitly stated otherwise in the text.

(*Andrew J. Duncan*)

For Karen, my family and my supervisor Tom.

Abstract

The work in this thesis concerns the estimation of the electromagnetic, elastodynamic and piezoelectric properties of homogenized composite materials (HCMs). A composite may be considered homogeneous if wavelengths are sufficiently large in comparison to the size of the particles of each component material. This thesis examines HCMs constructed from two component materials and several methods of estimating the HCMs constitutive properties. Firstly, the Maxwell Garnett estimates and Bergman–Milton bounds on the electromagnetic properties of HCMs are examined. While both are widely used, we re–examine them, for isotropic dielectric HCMs, in light of recent advancements in material manufacture. Secondly, we examine the strong–property–fluctuation theory (SPFT). The SPFT estimate is calculated using iterations upon an initial ansatz, these iterations being dependent on statistical cumulants of the spatial distribution of the particles of the component materials. The zeroth–order SPFT estimate is identical to the first–order and both are taken to be identical to a comparison material. For the second–order estimate a two–point correlation function along with its associated correlation length are used to characterize the component materials' particle distribution. The general framework for the elastodynamic SPFT was established in 1999 by Zhuck and Lakhtakia. Here we further develop the elastodynamic SPFT for orthotropic HCMs, in order to undertake numerical studies. We simplify certain integrals in order to make them amenable to numerical computation. Also, we establish the piezoelectric SPFT for orthorhombic $mm2$ materials. The general theory is developed first in a manner analogous to the elastodynamic SPFT. We then implement a two–point covariance function, perform similar integral simplifications to those done in the elastodynamic SPFT and carry out

numerical experiments. From the numerical studies it is clear that, for both the elastodynamic and piezoelectric HCMs, the lowest–order SPFT estimate is similar to that provided by the corresponding Mori–Tanaka formalism. It is also apparent that the second–order SPFT estimate provides a significant correction to the lowest–order estimate, which reflects dissipative losses due to scattering.

Papers and Presentations

The work described within this thesis has to date yielded the following refereed journal papers:

P1. Duncan, A.J., Mackay, T.G. & Lakhtakia, A., 2007, On the Bergman-Milton bounds for the homogenization of dielectric composite materials, *Opt. Commun.*, **271**, 470–474.

P2. Duncan, A.J., Mackay, T.G. & Lakhtakia, A., 2009, On the homogenization of orthotropic elastic composites by the strong–property–fluctuation theory, *IMA J. Appl. Math*, http://imamat.oxfordjournals.org/cgi/content/abstract-/hxp001.

P3. Duncan, A.J., Mackay, T.G. & Lakhtakia, A., 2008, The homogenization of orthorhombic piezoelectric composites by the strong–property–fluctuation theory, *J. Phys. A: Math. Theor.*, **42**, 165402.

and the conference poster:

C1. Duncan, A.J., Mackay, T.G. & Lakhtakia, A., 2008, On conventional approaches to homogenization applied to unconventional composite materials, *Photon08 —- Quantum Electronics and Photonics 18*, Edinburgh Conference Centre, Heriot–Watt University.

Contents

Glossary of terms and notation

Symbol	Term
i	$\sqrt{-1}$
$\mathbf{D}$, D_j	electric displacement vector and its components
$\mathbf{E}$, E_j	electric field vector and its components
$\mathbf{H}$	magnetic field vector
$\mathbf{B}$	magnetic induction vector
ϵ_{lm}, $\underline{\underline{\boldsymbol{\epsilon}}}$	permittivity tensor and matrix
ϵ_0	permittivity of free-space
ϵ	relative permittivity
$\underline{\underline{\boldsymbol{\mu}}}$	permeability matrix
MG_α, MG_β	Maxwell Garnett estimates
HS_α, HS_β	Hashin–Shtrikman bounds
$\underline{\underline{\mathbf{I}}}$	3×3 identity matrix
$\underline{\underline{\mathbf{0}}}_{n\times n}$	$n \times n$ null matrix
$C^{(\ell)}_{lmpq}$, $\underline{\underline{\mathbf{C}}}^{(\ell)}$	stiffness tensor, matrix of component material ℓ
$\rho^{(\ell)}$, $\underline{\underline{\boldsymbol{\rho}}}^{(\ell)}$	density tensor, matrix of component material ℓ
t_{lm}, u_m, F_m	stress, displacement and applied force tensors
ω	angular frequency
S_{pq}, $\mathbf{S}$	strain tensor, vector
ξ_{lmpq}, $\underline{\underline{\boldsymbol{\xi}}}$	renormalization tensor, matrix
W_{rstu}, $\underline{\underline{\underline{\underline{\mathbf{W}}}}}$	renormalization tensor, matrix
$\langle \ldots \rangle$	ensemble average
$\mathbf{r}$	spatial variable
$\Phi^{(\ell)}$	characteristic function
B^{lmrs}_{tupq}, B	covariance functions
Γ	correlation function

continued on next page

continued from previous page

Symbol	Term
$\underline{\underline{\mathbf{G}}}$, G_{pm}	3×3 matrix Green function and its entries
$\underline{\underline{\mathbf{N}}}$, Δ	Numerator and denominator of $\underline{\underline{\mathbf{G}}}$
δ_{mp}	Kronecker delta
ϖ_{ij}, $\boldsymbol{\varpi}$	renormalization tensor, vector
$\underline{\underline{\mathbf{U}}}$	3×3 shape matrix
τ_{lmrs}, $\underline{\underline{\boldsymbol{\tau}}}$	identity tensor and its matrix representation
$f^{(\ell)}$	volume fraction of component material ℓ
$\lambda^{(\ell)}$, $\mu^{(\ell)}$	Lamé constants of material ℓ
$\kappa^{(\ell)}$, $\nu^{(\ell)}$	bulk modulus and Poisson ratio of material ℓ
$S_{ijkl}^{(esh)}$, $\underline{\underline{\mathbf{S}}}^{(esh)}$	Eshelby tensor, matrix
ϵ_{ijk}	Levi-Civita permutation tensor
k	wavenumber
$\bar{k}$	average wavenumber
$\underline{\underline{\tilde{\mathbf{C}}}}^{(spft)} = \underline{\underline{\mathbf{C}}}^{(spft)} - \underline{\underline{\mathbf{C}}}^{(ocm)}$	SPFT estimate of the stiffness matrix
$\underline{\underline{\tilde{\boldsymbol{\rho}}}}^{(spft)} = \underline{\underline{\boldsymbol{\rho}}}^{(spft)} - \underline{\underline{\boldsymbol{\rho}}}^{(ocm)}$	SPFT estimate of the density matrix
$\varphi^{(\ell)}$, q	electric potential and charge
$e_{qlm}^{(\ell)}$, $\underline{\underline{\mathbf{e}}}$	piezoelectric tensor and matrix
$\breve{C}_{lMPq}^{(\ell)}$, $\breve{\rho}_{MP}^{(\ell)}$	extended stiffness and density
$\breve{\sigma}_{iJ}$, $\breve{S}_{Ij}$, $\breve{\boldsymbol{\sigma}}$, $\breve{\mathbf{S}}$	extended stress and strain and their matrices
$\breve{u}_I$, $\breve{F}_J$	extended displacement and force
$\underline{\underline{\breve{\mathbf{C}}}}^{(\ell)}$, $\underline{\underline{\breve{\boldsymbol{\rho}}}}^{(\ell)}$	extended stiffness and density matrices
$\underline{\underline{\breve{\mathbf{G}}}}$, $\breve{G}_{PM}$	piezoelectric 4×4 matrix Green function and its entries
$\underline{\underline{\breve{\mathbf{N}}}}$, $\breve{\Delta}$	Numerator and denominator of $\underline{\underline{\breve{\mathbf{G}}}}$
$\breve{\xi}_{lMPq}$, $\underline{\underline{\breve{\boldsymbol{\xi}}}}$	piezoelectric extension of ξ_{lmpq} and $\underline{\underline{\boldsymbol{\xi}}}$
$\breve{W}_{RstU}$, $\underline{\underline{\breve{\mathbf{W}}}}$	piezoelectric extension of W_{lmpq} and $\underline{\underline{\mathbf{W}}}$
$\breve{\tau}_{lMRs}$, $\underline{\underline{\breve{\boldsymbol{\tau}}}}$	piezoelectric extension of τ_{lmrs}, $\underline{\underline{\boldsymbol{\tau}}}$
$\breve{\varpi}_{Ij}$, $\breve{\boldsymbol{\varpi}}$	piezoelectric extension of ϖ_{ij}, $\boldsymbol{\varpi}$

continued on next page

continued from previous page

Symbol	Term
$\breve{\underline{\underline{\mathbf{M}}}}$	extended compliance matrix
$\breve{\bar{k}}$	piezoelectric average wavenumber
$\tilde{\breve{\underline{\underline{\mathbf{C}}}}}^{(spft)} = \breve{\underline{\underline{\mathbf{C}}}}^{(spft)} - \breve{\underline{\underline{\mathbf{C}}}}^{(ocm)}$	SPFT estimate of the extended stiffness matrix
$\tilde{\breve{\underline{\underline{\boldsymbol{\rho}}}}}^{(spft)} = \breve{\underline{\underline{\boldsymbol{\rho}}}}^{(spft)} - \breve{\underline{\underline{\boldsymbol{\rho}}}}^{(ocm)}$	SPFT estimate of the extended density matrix
$\breve{S}^{(esh)}_{IjKl}$, $\breve{\underline{\underline{\mathbf{S}}}}^{(esh)}$	Piezoelectric extension of $S^{(esh)}_{ijkl}$, $\underline{\underline{\mathbf{S}}}^{(esh)}$

Within this thesis, matrices are denoted by double underlining and bold font $\underline{\underline{\mathbf{A}}}$, while vectors are in bold font with no underlining $\mathbf{a}$. Tensors are represented in normal font with their components indicated by subscripts (for nth–order tensors, with $n \leq 4$) or subscripts and superscripts (for eighth–order tensors). All tensor indexes range from 1 to 3. The pqth component of a matrix $\underline{\underline{\mathbf{A}}}$ is written as $\left[\underline{\underline{\mathbf{A}}}\right]_{pq}$, while the pth component of a vector $\mathbf{b}$ is written as $\left[\mathbf{b}\right]_p$. A repeated index implies summation. Thus, we have the matrix component $\left[\underline{\underline{\mathbf{A}}} \cdot \underline{\underline{\mathbf{B}}}\right]_{pr} = \left[\underline{\underline{\mathbf{A}}}\right]_{pq}\left[\underline{\underline{\mathbf{B}}}\right]_{qr}$, vector component $\left[\underline{\underline{\mathbf{A}}} \cdot \mathbf{b}\right]_p = \left[\underline{\underline{\mathbf{A}}}\right]_{pq}\left[\mathbf{b}\right]_q$, and scalar $\mathbf{a} \cdot \mathbf{b} = [\mathbf{a}]_p [\mathbf{b}]_p$. The adjoint, determinant and trace of a matrix $\underline{\underline{\mathbf{A}}}$ are denoted by $\mathrm{adj}\left(\underline{\underline{\mathbf{A}}}\right)$, $\det\left(\underline{\underline{\mathbf{A}}}\right)$ and $\mathrm{tr}\left(\underline{\underline{\mathbf{A}}}\right)$, respectively. The prefixes Re and Im are used to signify real and imaginary parts, respectively, while $i = \sqrt{-1}$.

Glossary of abbreviations and acronyms

Symbol	Description
HCM	Homogeneous composite material
OCM	Orthotropic/Orthorhombic comparison material
SPFT	Strong–property–fluctuation theory
HS	Hashin–Shtrikman
MG	Maxwell Garnett
BM	Bergman–Milton
MT	Mori–Tanaka
ECOs	Effective constitutive operators
EPOs	Effective perturbative operators

Chapter 1

Introduction

For over 150 years scientists have been trying to predict the constitutive properties of composite materials [1]. These composites can be considered homogeneous if the wavelengths are sufficiently large in comparison to the size of the particles of each component material. The work contained in this thesis describes the estimation of the constitutive properties of homogenized composite materials (HCMs) in electromagnetics, elastodynamics and piezoelectrics. Many different methods of estimation have been discussed [1, 2]. Some were derived for composites of a specific structure, whilst others apply to all composites. This thesis examines HCMs constructed from two component materials and several methods of estimating the HCMs' constitutive properties. Firstly, the Maxwell Garnett estimates and Bergman–Milton bounds on the electromagnetic properties of HCMs are examined. Secondly, the strong–property–fluctuation theory (SPFT) is examined for both elastodynamic and piezoelectric HCMs.

In Chapter 2 we examine the Maxwell Garnett estimates [1, 3] and the Bergman–Milton bounds [2, 4, 5, 6, 7, 8] on the relative permittivity of electromagnetic HCMs. Both are well known and depend only on the volume fraction of each component material and their respective permittivities. Although they have been widely used, we re-examine them for isotropic dielectric HCMs, in light of recent advancements in material manufacture. In particular, we consider HCMs arising from two component materials, with the real parts of their permittivities having different signs. Certain HCMs of this type are of interest because they may

support negative phase velocity, which is closely related to negative refraction [9].

The SPFT estimate has been developed for electromagnetic [10, 11, 12], acoustic [13] and elastodynamic [14] HCMs. In this case we consider the HCM to be a particulate composite with one component material randomly distributed as identically oriented ellipsoidal particles in a matrix composed of the second component material. The SPFT estimate is calculated using iterations upon an initial ansatz, these iterations being dependent on statistical cumulants of the spatial distribution of the particles of the component materials. The zeroth–order SPFT estimate is identical to the first–order and both are taken to be identical to a comparison material. For the second–order estimate a two–point correlation function along with its associated correlation length are used to characterize the component materials' particle distribution. Unlike conventional variational methods of homogenization [15, 16, 17, 18, 19], the SPFT incorporates a renormalized formulation which allows for relatively strong variations in the constitutive parameters of the component materials.

The general framework for the elastodynamic SPFT was established in 1999 by Zhuck and Lakhtakia [14]. In Chapter 3, we further develop the elastodynamic SPFT for orthotropic HCMs, in order to undertake numerical studies. In doing so we simplify certain integrals in order to make them amenable to numerical computation and implement the two–point covariance function which characterizes the distributions of the component materials. The results of the elastodynamic SPFT are compared to those from the mean–field Mori–Tanaka formalism [20] for two types of orthotropic component materials. Firstly, isotropic component materials with ellipsoidal inclusion particles and secondly, orthotropic component materials with spherical inclusion particles.

The piezoelectric SPFT for orthorhombic materials is established in Chapters 4 and 5. In Chapter 4, general theory is developed in a manner analogous to the elastodynamic SPFT. In Chapter 5, we implement a two–point covariance function, perform similar integral simplifications to those done in the elastodynamic SPFT and carry out numerical experiments. The piezoelectric SPFT results are also compared to the Mori–Tanaka formalism, in this case for orthorhombic $mm2$ component materials with ellipsoidal inclusion particles.

Chapter 2

Re-examination of the Maxwell Garnett estimates and the Bergman–Milton bounds

2.1 Theory

2.1.1 Introduction

The starting point of the solution to almost any problem in electromagnetic homogenization are the James Clerk Maxwell equations. In the frequency domain these equations are given by

$$i\omega \mathbf{D}(\mathbf{r},\omega) + \bigtriangledown \times \mathbf{H}(\mathbf{r},\omega) = \mathbf{0} \tag{2.1}$$

$$\bigtriangledown \times \mathbf{E}(\mathbf{r},\omega) - i\omega \mathbf{B}(\mathbf{r},\omega) = \mathbf{0} \tag{2.2}$$

$$\bigtriangledown \cdot \mathbf{D}(\mathbf{r},\omega) = 0 \tag{2.3}$$

$$\bigtriangledown \cdot \mathbf{B}(\mathbf{r},\omega) = 0, \tag{2.4}$$

where $\mathbf{D}(\mathbf{r},\omega)$, $\mathbf{E}(\mathbf{r},\omega)$, $\mathbf{H}(\mathbf{r},\omega)$ and $\mathbf{B}(\mathbf{r},\omega)$ are the electric displacement, electric field, magnetic field and magnetic induction vectors respectively [21], with ω the angular frequency and $i = \sqrt{-1}$. A further set of vector equations are necessary

for an explicit solution:

$$\mathbf{D} = \underline{\underline{\boldsymbol{\epsilon}}} \cdot \mathbf{E} + \underline{\underline{\boldsymbol{\xi}}} \cdot \mathbf{H} \tag{2.5}$$

$$\mathbf{B} = \underline{\underline{\boldsymbol{\zeta}}} \cdot \mathbf{E} + \underline{\underline{\boldsymbol{\mu}}} \cdot \mathbf{H}, \tag{2.6}$$

where $\underline{\underline{\boldsymbol{\mu}}}$ and $\underline{\underline{\boldsymbol{\epsilon}}}$ are the permeability and permittivity matrices respectively, with $\underline{\underline{\boldsymbol{\xi}}}$ and $\underline{\underline{\boldsymbol{\zeta}}}$ the magnetoelectric matrices. These equations are known as the constitutive relations and depend on the form that the component materials take [22]. Those presented above are for the most general linear medium, a bianisotropic medium. It is these constitutive relations that dictate the solution to Maxwell's equations and therefore the way in which any electromagnetic process behaves [22].

In this chapter we examine the Maxwell Garnett estimates and the Bergman–Milton bounds on the relative permittivity, ϵ, of a HCM . Both are well established [1, 2] but we re-examine them in light of recent advances in material manufacture.

2.1.2 Component materials

The materials presented in this chapter are isotropic dielectrics where $\underline{\underline{\boldsymbol{\epsilon}}} = \epsilon_0 \epsilon \underline{\underline{\mathbf{I}}}$, $\underline{\underline{\boldsymbol{\mu}}} = \mu_0 \mu \underline{\underline{\mathbf{I}}}$ and $\underline{\underline{\boldsymbol{\xi}}} = \underline{\underline{\boldsymbol{\zeta}}} = \underline{\underline{\mathbf{0}}}_{3\times 3}$. Herein ϵ and μ are the relative permittivity and permeability of the material, ϵ_0 and μ_0 the permittivity and permeability of free space, $\underline{\underline{\mathbf{I}}}$ the 3×3 identity matrix and $\underline{\underline{\mathbf{0}}}_{3\times 3}$ the 3×3 null matrix.

We consider the homogenization of two homogeneous isotropic dielectric component materials with relative permittivities $\epsilon^{(1)}$ and $\epsilon^{(2)}$, to produce a composite with relative permittivity $\epsilon^{(e)}$. Both nondissipative $\epsilon^{(1,2)} \in \mathbb{R}$ and dissipative $\epsilon^{(1,2)} \in \mathbb{C}$ component materials are considered. For the materials to be homogeneous, their constitutive properties must be independent of any spatial coordinate. Furthermore, the HCM is considered to occupy all space and be divisible into disjoint regions, containing only material '1' or material '2'. The volume fractions of each region are given by $f^{(1)}$ and $f^{(2)}$ respectively, with $f^{(1)} + f^{(2)} = 1$.

2.1.3 Maxwell Garnett estimates and Bergman–Milton bounds

We examine the Maxwell Garnett estimates and Bergman–Milton bounds whilst paying attention to the regime in which the parameter

$$\delta = \frac{\mathrm{Re}\left(\epsilon^{(1)}\right)}{\mathrm{Re}\left(\epsilon^{(2)}\right)}\,, \qquad\qquad (\epsilon^{(1)}, \epsilon^{(2)} \in \mathbb{C})\,, \tag{2.7}$$

is negative. Herein, we have $\mathrm{Re}\left(\epsilon^{(1,\,2)}\right)$ and $\mathrm{Im}\left(\epsilon^{(1,\,2)}\right)$ denoting the real and imaginary parts of $\epsilon^{(1,\,2)}$ respectively. The reason for examining the region $\delta < 0$ is due to recent advancements in material manufacture. Materials are being constructed which exhibit properties not traditionally encountered in electromagnetics [23, 24, 25]. The rise of such materials means that homogenization theories need to be revisited. As an example of such a material, with $\delta < 0$, we can examine a metal–in–insulator HCM [3, 26]. In this case we only have one of $\epsilon^{(1)}$ and $\epsilon^{(2)} \in \mathbb{R}$ and metal–in–insulator HCMs can be constructed to support planewave propagation with negative phase velocity [9].

We examine the Maxwell Garnett estimates [1, 3] which may be regarded as bounds that represent the extension of the Hashin–Shtrikman bounds [27] into the complex–valued permittivity regime:

$$\mathsf{MG}_\alpha \;=\; \epsilon^{(2)} + \frac{3f^{(1)}\epsilon^{(2)}(\epsilon^{(1)} - \epsilon^{(2)})}{\epsilon^{(1)} + 2\epsilon^{(2)} - f^{(1)}(\epsilon^{(1)} - \epsilon^{(2)})}, \qquad (\epsilon^{(1)}, \epsilon^{(2)} \in \mathbb{C})\,, \tag{2.8}$$

$$\mathsf{MG}_\beta \;=\; \epsilon^{(1)} + \frac{3f^{(2)}\epsilon^{(1)}(\epsilon^{(2)} - \epsilon^{(1)})}{\epsilon^{(2)} + 2\epsilon^{(1)} - f^{(2)}(\epsilon^{(2)} - \epsilon^{(1)})}, \qquad (\epsilon^{(1)}, \epsilon^{(2)} \in \mathbb{C})\,. \tag{2.9}$$

Concurrently, we investigate the set of bounds derived independently by Bergman [4, 5, 6, 7] and Milton [2, 8], for component materials with complex permittivities. The Bergman–Milton bounds are given by

$$\mathsf{BM}_\alpha(\gamma) \;=\; f^{(1)}\epsilon^{(1)} + f^{(2)}\epsilon^{(2)} - \frac{f^{(1)}f^{(2)}(\epsilon^{(2)} - \epsilon^{(1)})^2}{3\left[\gamma\epsilon^{(1)} + (1-\gamma)\,\epsilon^{(2)}\right]}\,, \quad (\epsilon^{(1)}, \epsilon^{(2)} \in \mathbb{C})\,, \tag{2.10}$$

$$\mathsf{BM}_\beta(\gamma) \;=\; \left\{\frac{f^{(1)}}{\epsilon^{(1)}} + \frac{f^{(2)}}{\epsilon^{(2)}} - \frac{2f^{(1)}f^{(2)}\left(\epsilon^{(1)} - \epsilon^{(2)}\right)^2}{3\,\epsilon^{(1)}\epsilon^{(2)}\left[\epsilon^{(2)}\gamma + \epsilon^{(1)}\,(1-\gamma)\right]}\right\}^{-1}, \; (\epsilon^{(1)}, \epsilon^{(2)} \in \mathbb{C})\,. \tag{2.11}$$

For the bound BM_α the parameter γ takes the values $\left(1-f^{(1)}\right)/3 \le \gamma \le 1 - f^{(1)}/3$, whereas for the bound BM_β the parameter γ takes the values $2\left(1-f^{(1)}\right)/3 \le \gamma \le 1 - 2f^{(1)}/3$.

The Bergman–Milton bounds are derived to give improved results on the Maxwell Garnett estimates, but they coincide with them for nondissipative component materials when the parameter γ attains its minimum and maximum values; i.e.,

$$\left.\begin{array}{rcccl} \mathsf{BM}_\alpha\left(\dfrac{1-f^{(1)}}{3}\right) & = & \mathsf{BM}_\beta\left(\dfrac{2-2f^{(1)}}{3}\right) & = & \mathsf{MG}_\alpha \\ \mathsf{BM}_\alpha\left(1-\dfrac{f^{(1)}}{3}\right) & = & \mathsf{BM}_\beta\left(1-\dfrac{2f^{(1)}}{3}\right) & = & \mathsf{MG}_\beta \end{array}\right\}. \tag{2.12}$$

In view of our particular interest in homogenization scenarios for which $\delta < 0$, we note that

$$\left|\mathsf{BM}_\alpha\left(\frac{1-f^{(1)}}{3}\right)\right| = \left|\mathsf{BM}_\beta\left(\frac{2-2f^{(1)}}{3}\right)\right| = |\mathsf{MG}_\alpha| \to \infty \qquad \text{as} \qquad \delta \to \frac{f^{(2)}-3}{f^{(2)}} \tag{2.13}$$

and

$$\left|\mathsf{BM}_\alpha\left(1-\frac{f^{(1)}}{3}\right)\right| = \left|\mathsf{BM}_\beta\left(1-\frac{2f^{(1)}}{3}\right)\right| = |\mathsf{MG}_\beta| \to \infty \qquad \text{as} \qquad \delta \to \frac{f^{(1)}}{f^{(1)}-3} \tag{2.14}$$

for nondissipative materials. Thus, there exist

(i) a volume fraction $f^{(1)} \in (0,1)$ at which MG_α is unbounded for all values of $\delta < -2$, and

(ii) a volume fraction $f^{(1)} \in (0,1)$ at which MG_β is unbounded for all values of $\delta \in (-1/2, 0)$.

When plotted for dissipative component materials, the Maxwell Garnett estimates and Bergman–Milton bounds sketch out an area in the complex plane. Numerical results describing the comparison of these bounds for $\delta < 0$ are given in the next section.

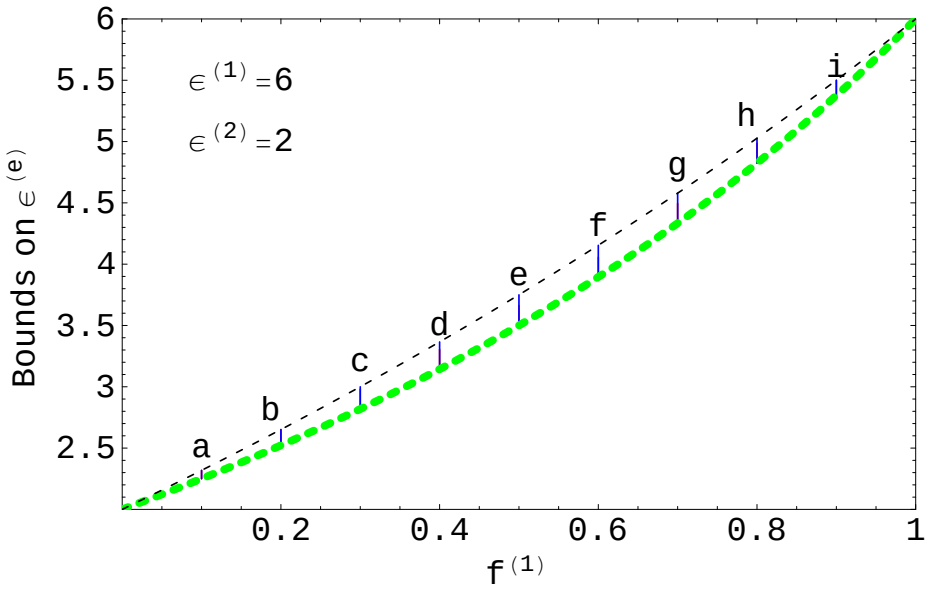

Figure 2.1: The MG_α (thick dashed line) and MG_β (thin dashed line) estimates of $\epsilon^{(e)}$ plotted against $f^{(1)}$ for $\epsilon^{(1)} = 6$, $\epsilon^{(2)} = 2$. The vertical solid lines represent the variation of the Bergman–Milton bound BM_α with γ for $f^{(1)} \in \{0.1(a), 0.2(b), 0.3(c), 0.4(d), 0.5(e), 0.6(f), 0.7(g), 0.8(h), 0.9(i)\}$; and these coincide with the corresponding variation of BM_β with γ.

2.2 Numerical illustrations

Let us now numerically explore the Bergman–Milton bounds, along with the Maxwell Garnett estimates, for some illustrative examples of nondissipative and dissipative HCMs. The parameter δ, defined in (2.7), is used to classify the two component materials of the chosen HCMs. We begin in §2.2.1 by considering nondissipative HCMs. While these do not represent realistic materials, they provide valuable insights into the limiting process in which weakly dissipative materials become nondissipative. Furthermore, they provide a useful yardstick in the evaluation of dissipative HCMs, which are considered in §2.2.2.

2.2.1 Nondissipative HCMs

We begin with the most straightforward situation: nondissipative, $\epsilon^{(1,2)} \in \mathbb{R}$, HCMs arising from component materials with $\delta > 0$.

In Figure 2.1, the Maxwell Garnett estimates MG_α and MG_β (which in this case are identical to the Hashin–Shtrikman bounds) are plotted against $f^{(1)} \in (0, 1)$

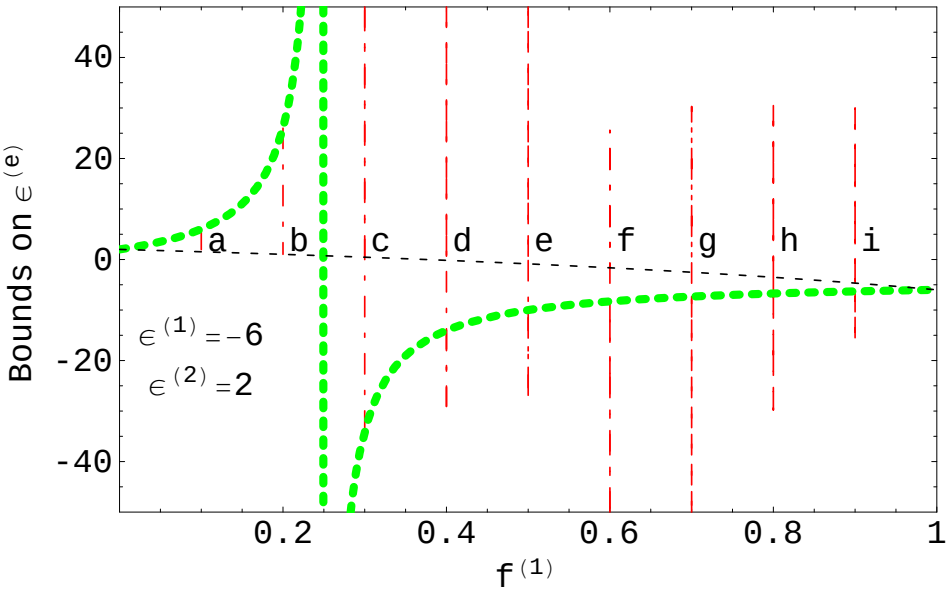

Figure 2.2: The MG_α (thick dashed line) and MG_β (thin dashed line) estimates of $\epsilon^{(e)}$ plotted against $f^{(1)}$ for $\epsilon^{(1)} = -6$ and $\epsilon^{(2)} = 2$. The Bergman–Milton bound BM_α is plotted as the vertical broken lines for $f^{(1)} \in \{0.1(a), 0.2(b), 0.3(c), 0.4(d), 0.5(e), 0.6(f), 0.7(g), 0.8(h), 0.9(i)\}$.

for $\epsilon^{(1)} = 6$ and $\epsilon^{(2)} = 2$. The Bergman–Milton bound BM_α is given for $f^{(1)} \in \{0.1, 0.2, 0.3, 0.4, 0.5, 0.6, 0.7, 0.8, 0.9\}$. The corresponding plots of BM_β overly those of BM_α. The Bergman–Milton bounds are entirely contained within the envelope constructed by the Maxwell Garnett estimates.

Let us turn now to the nondissipative scenario wherein $\delta < 0$. In Figure 2.2, the Maxwell Garnett estimates MG_α and MG_β are presented as functions of $f^{(1)}$ for $\epsilon^{(1)} = -6$ and $\epsilon^{(2)} = 2$. The Bergman–Milton bound BM_α is given for $f^{(1)} \in \{0.1, 0.2, 0.3, 0.4, 0.5, 0.6, 0.7, 0.8, 0.9\}$. The corresponding Bergman–Milton bound BM_β is plotted in Figure 2.3. In consonance with (2.12) and (2.13), we see that MG_α becomes unbounded as $f^{(1)} \to 0.25$. It is clear that $\mathsf{MG}_\beta \leq \mathsf{BM}_\alpha \leq \mathsf{MG}_\alpha$ for $f^{(1)} < 0.25$, whereas $\mathsf{MG}_\alpha \leq \mathsf{BM}_\beta \leq \mathsf{MG}_\beta$ for $f^{(1)} > 0.25$. For $f^{(1)} > 0.25$, the Bergman–Milton bound BM_α lies outside both Maxwell Garnett estimates MG_α and MG_β, and similarly BM_β lies outside both Maxwell Garnett estimates MG_α and MG_β for $f^{(1)} < 0.25$, although the relations (2.12) still hold.

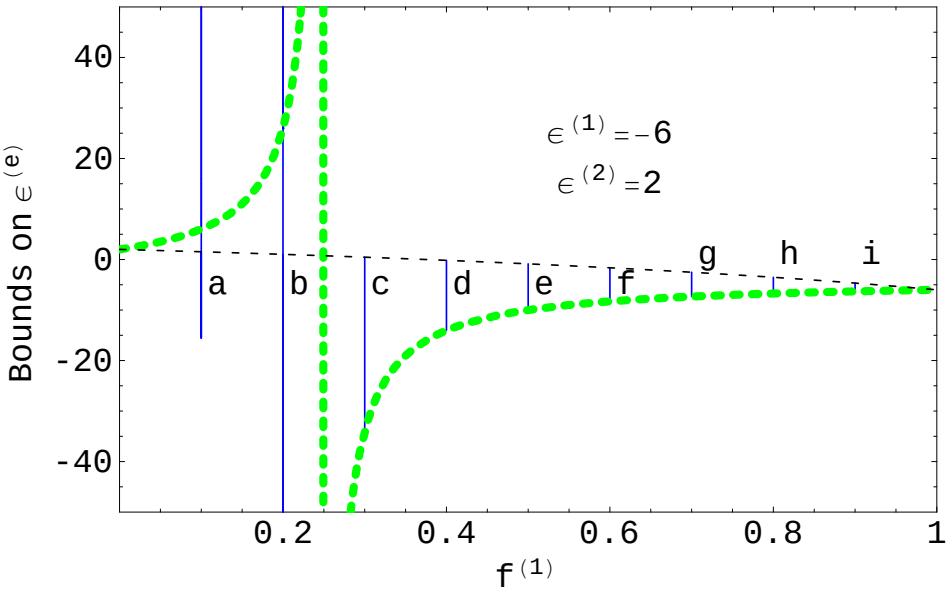

Figure 2.3: As Figure 2 but with BM_β (vertical solid lines) in place of BM_α.

2.2.2 Dissipative HCMs

We turn to homogenization scenarios based on dissipative component materials; i.e., $\epsilon^{(1,2)} \in \mathbb{C}$. Let us begin with the $\delta > 0$ scenario. In Figure 2.4, the homogenization of components characterized by the relative permittivities $\epsilon^{(1)} = 6 + 0.3i$ and $\epsilon^{(2)} = 2 + 0.2i$ is illustrated. In this figure, the Maxwell Garnett estimates on complex–valued $\epsilon^{(e)}$ are plotted as $f^{(1)}$ varies from 0 to 1. The Bergman–Milton bounds, which are graphed for $f^{(1)} \in \{0.1, 0.2, 0.3, 0.4, 0.5, 0.6, 0.7, 0.8, 0.9\}$, are fully contained within the Maxwell Garnett envelope. That is, we have $\mathsf{MG}_\beta \leq \mathsf{BM}_{\alpha,\beta} \leq \mathsf{MG}_\alpha$ for all values of $f^{(1)}$.

Now we consider dissipative component materials with $\delta < 0$. In Figure 2.5, the homogenization of component materials given by $\epsilon^{(1)} = -6 + 3i$ and $\epsilon^{(2)} = 2 + 2i$ is represented. The Bergman–Milton bounds are given for $f^{(1)} \in \{0.1, 0.2, 0.3, 0.4, 0.5, 0.6, 0.7, 0.8, 0.9\}$, whereas the Maxwell Garnett estimates are plotted for $f^{(1)} \in (0, 1)$. As is the case in Figure 2.4, BM_β lies entirely within the envelope constructed by MG_α and MG_β. We see that $\mathsf{BM}_\alpha \geq \mathsf{MG}_\beta$ for all values of $f^{(1)}$; but, for mid–range values of $f^{(1)}$, BM_α slightly exceeds MG_α for certain values of the parameter γ.

As the degree of dissipation exhibited by the component materials is de-

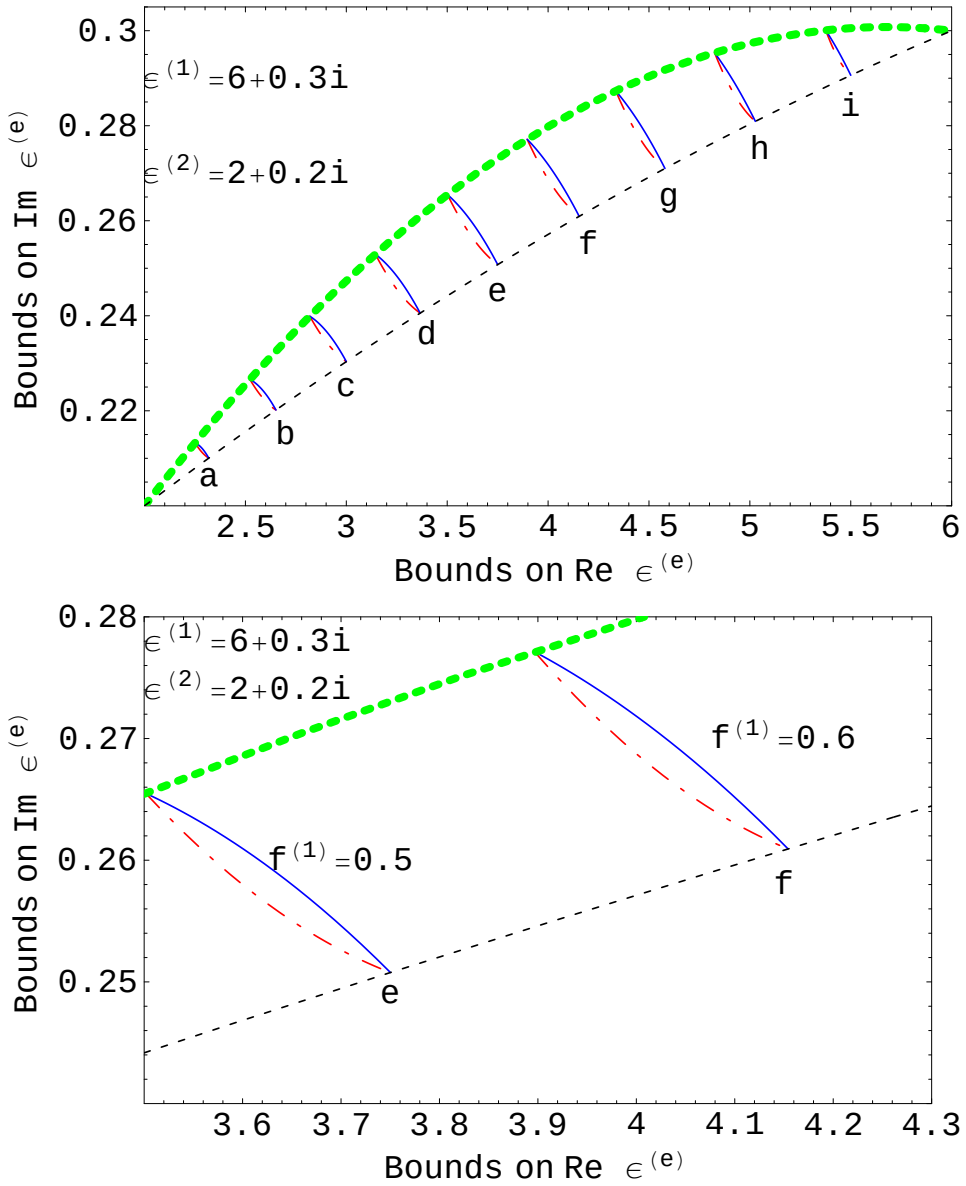

Figure 2.4: The MG_α (thick dashed line) and MG_β (thin dashed line) estimates in relation to $\mathrm{Re}\,\epsilon^{(e)}$ and $\mathrm{Im}\,\epsilon^{(e)}$ as $f^{(1)}$ varies from 0 to 1, for $\epsilon^{(1)} = 6 + 0.3i$, $\epsilon^{(2)} = 2 + 0.2i$. The Bergman–Milton bounds BM_α (thin broken dashed lines) and BM_β (thin solid lines) in the top diagram are plotted for $f^{(1)} \in \{0.1(a), 0.2(b), 0.3(c), 0.4(d), 0.5(e), 0.6(f), 0.7(g), 0.8(h), 0.9(i)\}$. The bottom diagram shows the Bergman–Milton bounds in greater detail but for $f^{(1)} = 0.5(e)$ and $f^{(1)} = 0.6(f)$.

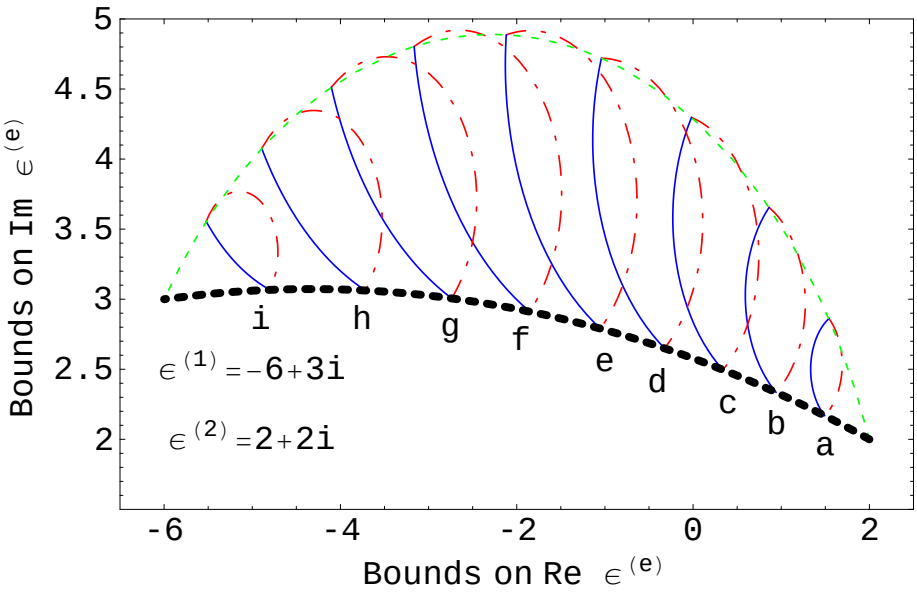

Figure 2.5: The MG_α (thin dashed line) and MG_β (thick dashed line) estimates in relation to $\operatorname{Re}\epsilon^{(e)}$ and $\operatorname{Im}\epsilon^{(e)}$ as $f^{(1)}$ varies from 0 to 1, for $\epsilon^{(1)} = -6+3i$ and $\epsilon^{(2)} = 2+2i$. The Bergman–Milton bounds BM_α (thin broken dashed lines) and BM_β (thin solid lines) are plotted for $f^{(1)} \in \{0.1(a), 0.2(b), 0.3(c), 0.4(d), 0.5(e), 0.6(f), 0.7(g), 0.8(h), 0.9(i)\}$.

creased, the extent to which BM_α exceeds MG_α is increased. This is illustrated in Figure 2.6 wherein the homogenization is repeated with $\epsilon^{(1)} = -6 + i$ and $\epsilon^{(2)} = 2 + 2i/3$. As in Figure 2.4, the Bergman–Milton bounds are given for $f^{(1)} \in \{0.1, 0.2, 0.3, 0.4, 0.5, 0.6, 0.7, 0.8, 0.9\}$, while the Maxwell Garnett estimates are plotted for $f^{(1)} \in (0, 1)$. The Bergman–Milton bound BM_β lies within the Maxwell Garnett envelope for all values of $f^{(1)}$, but substantial parts of BM_α lie well outside the envelope of the two Maxwell Garnett estimates.

The behaviour observed in Figures 2.5 and 2.6 is further exaggerated in Figure 2.7, where the homogenization of component materials with $\epsilon^{(1)} = -6 + 0.3i$ and $\epsilon^{(2)} = 2 + 0.2i$ is represented. The Maxwell Garnett estimates are plotted for $f^{(1)} \in (0, 1)$; for reasons of clarity, the Bergman–Milton bounds are plotted only for $f^{(1)} \in \{0.1, 0.3, 0.5\}$. The Maxwell Garnett estimates are exceedingly large and the Bergman–Milton bounds are larger still.

Finally, let us focus on the scenario referred to earlier, namely the homogenization of a conducting component material and a nonconducting component material or metal–in–insulator, wherein $\delta < 0$. Suppose we consider components characterized by the relative permittivities $\epsilon^{(1)} = -6 + 3i$ and $\epsilon^{(2)} = 2$. In Figure 2.8

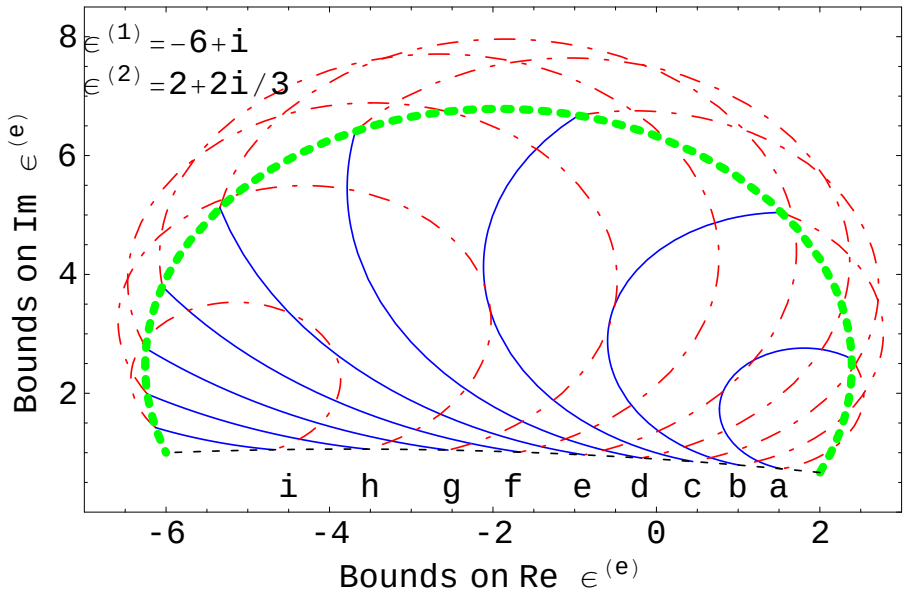

Figure 2.6: As Figure 2.4 but for $\epsilon^{(1)} = -6 + i$, $\epsilon^{(2)} = 2 + 2i/3$.

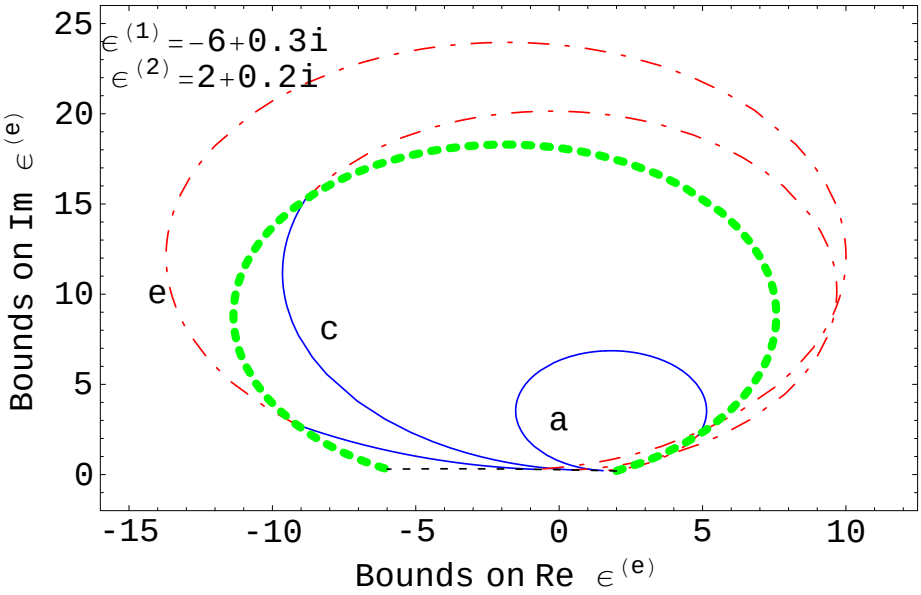

Figure 2.7: As Fig. 2.4 but for $\epsilon^{(1)} = -6 + 0.3i$ and $\epsilon^{(2)} = 2 + 0.2i$. The Bergman–Milton bounds are plotted for $f^{(1)} \in \{0.1(a), 0.3(c), 0.5(e)\}$.

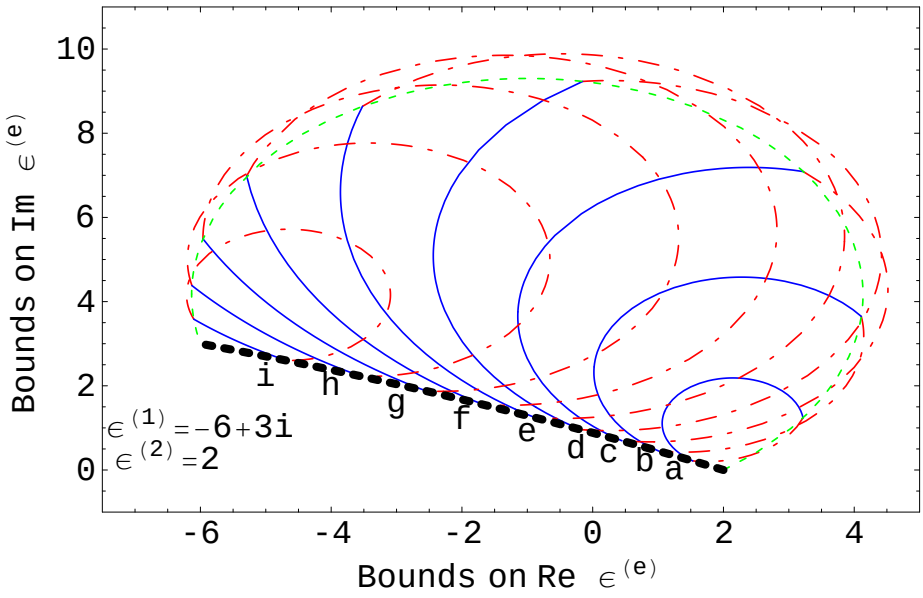

Figure 2.8: As Fig. 2.5 but for $\epsilon^{(1)} = -6 + 3i$ and $\epsilon^{(2)} = 2$.

the Maxwell Garnett estimates are plotted for $f^{(1)} \in (0, 1)$, whereas the Bergman–Milton bounds are given for $f^{(1)} \in \{0.1, 0.2, 0.3, 0.4, 0.5, 0.6, 0.7, 0.8, 0.9\}$. As we observed in Figure 2.6, the Maxwell Garnett envelope does not contain substantial parts of the Bergman–Milton bound BM_α, whereas the BM_β bound lies entirely within the envelope constructed from the two Maxwell Garnett estimates.

2.3 Discussion and conclusions

The Bergman–Milton bounds, as well as the Maxwell Garnett estimates, are valuable for estimating the effective constitutive parameters of HCMs in many commonly encountered circumstances. However, the advent of exotic new materials has led to the examination of such bounds within unconventional parameter regimes. It has been demonstrated in this chapter, that the Bergman–Milton bounds do not provide tight limits on the value of $\epsilon^{(e)}$ when the relative permittivities of the component materials $\epsilon^{(1)}$ and $\epsilon^{(2)}$ are such that [28]

(i) $\mathrm{Re}\left(\epsilon^{(1)}\right)$ and $\mathrm{Re}\left(\epsilon^{(2)}\right)$ have opposite signs; and

(ii) $|\mathrm{Re}\left(\epsilon^{(1,2)}\right)| \gg |\mathrm{Im}\left(\epsilon^{(1,2)}\right)|$.

We note that if the real parts of $\epsilon^{(1)}$ and $\epsilon^{(2)}$ have opposite signs, but are of the same order of magnitude as their imaginary parts, then the Bergman–Milton bounds are indeed useful, and they then lie within the envelope constructed by the Maxwell Garnett estimates.

Chapter 3

Implementation of Elastodynamic SPFT

3.1 Theory

3.1.1 Introduction

In elastodynamic homogenization we begin with the equation of motion

$$\partial_l \sigma_{lm}^{(\ell)}(\mathbf{r}) + \omega^2 \rho^{(\ell)} u_m^{(\ell)}(\mathbf{r}) = -F_m(\mathbf{r}), \tag{3.1}$$

where $\sigma_{lm}^{(\ell)}(\mathbf{r})$, $u_m^{(\ell)}(\mathbf{r})$ and $F_m(\mathbf{r})$ are the stress, displacement and applied force tensors of material 'ℓ' respectively. Here the constitutive relation is given by

$$\sigma_{lm}^{(\ell)}(\mathbf{r}) = C_{lmpq}^{(\ell)} S_{pq}^{(\ell)}(\mathbf{r}) \tag{3.2}$$

where the elastic strain tensor is given by

$$S_{pq}^{(\ell)}(\mathbf{r}) = \frac{1}{2}\left(\partial_p u_q^{(\ell)}(\mathbf{r}) + \partial_q u_p^{(\ell)}(\mathbf{r})\right) \tag{3.3}$$

and $C_{lmpq}^{(\ell)}$ represents the stiffness tensor, which describes the constitutive properties of material 'ℓ '.

In this chapter we apply the elastodynamic SPFT, established by Zhuck and Lakhtakia [14], to calculate numerically $C_{lmpq}^{(hcm)}$ for HCMs constructed as oriented

ellipsoidal particles of one component material randomly distributed in a matrix of the second component material. Prior to undertaking the numerical study, we derive new theoretical results in two particular areas:

(i) in the implementation of a two–point covariance function which characterizes the distributions of the component materials, and

(ii) in the simplification of certain integrals in order to make them amenable to numerical computation.

The SPFT estimate is also compared analytically to the self-consistent approaches provided by the Hill and Budiansky estimates [29, 30, 31], whilst the numerical examples are compared to the Mori–Tanaka mean–field formalism [20] and the Hashin–Shtrikman bounds [2, 15].

3.1.2 Preliminaries

In applying the elastodynamic SPFT formalism, it is expedient to adopt both matrix and tensor representations [32]. The correspondence between the two representations is described in §3.1.3. Matrices are denoted by double underlining and bold font, while vectors are in bold font with no underlining. Tensors are represented in normal font with their components indicated by subscripts (for nth–order tensors, with $n \leq 4$) or subscripts and superscripts (for eighth–order tensors). All tensor indexes range from 1 to 3. The pqth component of a matrix $\underline{\underline{\mathbf{A}}}$ is written as $\big[\,\underline{\underline{\mathbf{A}}}\,\big]_{pq}$, while the pth component of a vector $\mathbf{b}$ is written as $[\,\mathbf{b}\,]_p$. A repeated index implies summation. Thus, we have the matrix component $\big[\,\underline{\underline{\mathbf{A}}} \cdot \underline{\underline{\mathbf{B}}}\,\big]_{pr} = \big[\,\underline{\underline{\mathbf{A}}}\,\big]_{pq}\big[\,\underline{\underline{\mathbf{B}}}\,\big]_{qr}$, vector component $\big[\,\underline{\underline{\mathbf{A}}} \cdot \mathbf{b}\big]_p = \big[\,\underline{\underline{\mathbf{A}}}\,\big]_{pq}\big[\mathbf{b}\big]_q$, and scalar $\mathbf{a} \cdot \mathbf{b} = [\mathbf{a}]_p\,[\mathbf{b}]_p$. The adjoint, determinant and trace of a matrix $\underline{\underline{\mathbf{A}}}$ are denoted by $\mathrm{adj}\,\big(\,\underline{\underline{\mathbf{A}}}\,\big)$, $\det\big(\,\underline{\underline{\mathbf{A}}}\,\big)$ and $\mathrm{tr}\,\big(\,\underline{\underline{\mathbf{A}}}\,\big)$, respectively. The prefixes Re and Im are used to signify real and imaginary parts, respectively, while $i = \sqrt{-1}$.

The SPFT is developed in the frequency domain wherein the stress, strain, and displacement have an implicit $\exp(-i\omega t)$ dependency on time t, ω being the angular frequency. Thus, these are generally complex–valued quantities. The possibility of viscoelastic behaviour is accommodated through complex–valued

constitutive parameters. Stiffness tensors are taken to exhibit the usual symmetries

$$C_{lmpq} = C_{mlpq} = C_{lmqp} = C_{pqlm}, \tag{3.4}$$

whilst bearing in mind that the symmetry $\mathrm{Im}\, C_{lmpq} = \mathrm{Im}\, C_{pqlm}$ has not been proved generally [33]. On account of the symmetries (3.4), the matrix counterpart of tensor C_{lmpq} — namely, the 9×9 stiffness matrix $\underline{\underline{\mathbf{C}}}$ — is symmetric.

3.1.3 Matrix/tensor algebra

A fourth–order tensor A_{rstu} $(r, s, t, u \in \{1, 2, 3\})$ has 81 components. If it obeys the symmetries $A_{rstu} = A_{srtu} = A_{rsut} = A_{turs}$, it can be represented by a 9×9 matrix $\underline{\underline{\mathbf{A}}}$ with components $\left[\underline{\underline{\mathbf{A}}}\right]_{RS}$ $(R, S \in \{1, \ldots, 9\})$. Similarly, the nine entries of a second–order tensor B_{rs} $(r, s \in \{1, 2, 3\})$ may be expressed as a column 9–vector $\mathbf{B}$ with components $[\mathbf{B}]_R$ $(R \in \{1, \ldots, 9\})$. The scheme for converting between the tensor subscript pairs rs and tu and the matrix indexes RS or vector index R is provided in Table 3.1.

R, S	rs, tu	R, S	rs, tu	R, S	rs, tu
1	11	4	23 or 32	7	23 or 32
2	22	5	13 or 31	8	13 or 31
3	33	6	12 or 21	9	12 or 21

Table 3.1: Conversion between tensor and matrix/vector subscripts.

The most general 9×9 matrix $\underline{\underline{\mathbf{A}}}$ considered in this chapter has the form

$$\underline{\underline{\mathbf{A}}} = \begin{pmatrix} \underline{\underline{\boldsymbol{\alpha}}} & \underline{\underline{\mathbf{0}}}_{3\times3} & \underline{\underline{\mathbf{0}}}_{3\times3} \\ \underline{\underline{\mathbf{0}}}_{3\times3} & \underline{\underline{\boldsymbol{\beta}}} & \underline{\underline{\boldsymbol{\beta}}} \\ \underline{\underline{\mathbf{0}}}_{3\times3} & \underline{\underline{\boldsymbol{\beta}}} & \underline{\underline{\boldsymbol{\beta}}} \end{pmatrix}, \tag{3.5}$$

where $\underline{\underline{\boldsymbol{\alpha}}}$ is a general 3×3 matrix, $\underline{\underline{\boldsymbol{\beta}}}$ is a diagonal 3×3 matrix, and $\underline{\underline{\mathbf{0}}}_{3\times3}$ is the

3×3 null matrix. If we define a 9×9 matrix $\underline{\underline{\mathbf{A}}}^{\dagger}$ as [32]

$$\underline{\underline{\mathbf{A}}}^{\dagger} = \begin{pmatrix} \underline{\underline{\boldsymbol{\alpha}}}^{-1} & \underline{\underline{\mathbf{0}}}_{3\times3} & \underline{\underline{\mathbf{0}}}_{3\times3} \\ \underline{\underline{\mathbf{0}}}_{3\times3} & \frac{1}{4}\underline{\underline{\boldsymbol{\beta}}}^{-1} & \frac{1}{4}\underline{\underline{\boldsymbol{\beta}}}^{-1} \\ \underline{\underline{\mathbf{0}}}_{3\times3} & \frac{1}{4}\underline{\underline{\boldsymbol{\beta}}}^{-1} & \frac{1}{4}\underline{\underline{\boldsymbol{\beta}}}^{-1} \end{pmatrix}, \tag{3.6}$$

then $\underline{\underline{\mathbf{A}}}^{\dagger} \cdot \underline{\underline{\mathbf{A}}} = \underline{\underline{\mathbf{A}}} \cdot \underline{\underline{\mathbf{A}}}^{\dagger} = \underline{\underline{\boldsymbol{\tau}}}$, where $\underline{\underline{\boldsymbol{\tau}}}$ is the 9×9 matrix counterpart of the identity tensor

$$\tau_{rstu} = \frac{1}{2}\left(\delta_{rt}\delta_{su} + \delta_{ru}\delta_{st}\right). \tag{3.7}$$

3.1.4 Component materials

We consider the homogenization of a two–component composite material. Both component materials are homogeneous and we randomly distribute identically–oriented, conformal, ellipsoidal particles of one component material in a matrix of the second component material. For convenience, the principal axes of the ellipsoidal particles are taken to be aligned with the Cartesian axes. Thus, the surface of each ellipsoidal particle may be parameterized by the vector

$$\mathbf{r}^{(e)} = \eta \underline{\underline{\mathbf{U}}} \cdot \hat{\mathbf{r}}, \tag{3.8}$$

where η is a linear measure of size, $\hat{\mathbf{r}}$ is the radial unit vector and the diagonal shape matrix

$$\underline{\underline{\mathbf{U}}} = \frac{1}{\sqrt[3]{abc}} \begin{pmatrix} a & 0 & 0 \\ 0 & b & 0 \\ 0 & 0 & c \end{pmatrix}, \qquad (a, b, c \in \mathbb{R}^{+}). \tag{3.9}$$

The composite material is considered to occupy all space, denoted by V. It is partitioned into parts $V^{(1)}$ and $V^{(2)}$ containing the two component materials labeled as '1' and '2', respectively. The distributional statistics of the component material distributed as ellipsoidal particles are described in terms of moments of

the characteristic functions

$$\Phi^{(\ell)}(\mathbf{r}) = \begin{cases} 1, & \mathbf{r} \in V^{(\ell)}, \\ \\ 0, & \mathbf{r} \notin V^{(\ell)}, \end{cases} \qquad (\ell = 1, 2). \tag{3.10}$$

The volume fraction of component material 'ℓ', namely $f^{(\ell)}$, is given by the first statistical moment of $\Phi^{(\ell)}$; i.e.,

$$\langle\, \Phi^{(\ell)}(\mathbf{r}) \,\rangle = f^{(\ell)}, \qquad (\ell = 1, 2)\,. \tag{3.11}$$

Notice that $f^{(1)} + f^{(2)} = 1$. The second statistical moment of $\Phi^{(\ell)}$ constitutes a two–point covariance function. The physically–motivated form [34]

$$\langle\, \Phi^{(\ell)}(\mathbf{r})\, \Phi^{(\ell)}(\mathbf{r}') \,\rangle = \begin{cases} \langle\, \Phi^{(\ell)}(\mathbf{r}) \,\rangle \langle \Phi^{(\ell)}(\mathbf{r}') \,\rangle\,, & |\, \underline{\underline{U}}^{-1} \cdot (\mathbf{r} - \mathbf{r}') \,| > L\,, \\ \\ \langle\, \Phi^{(\ell)}(\mathbf{r}) \,\rangle\,, & |\, \underline{\underline{U}}^{-1} \cdot (\mathbf{r} - \mathbf{r}') \,| \leq L\,, \end{cases} \tag{3.12}$$

is adopted, where $L > 0$ is the correlation length which is taken to be much smaller than the elastodynamic wavelengths. In the context of the electromagnetic SPFT, the specific form of the covariance function has only a secondary influence on estimates of HCM constitutive parameters, for a range of physically–plausible covariance functions [12].

The elastodynamic properties of the component materials '1' and '2' are characterized by their stiffness tensors $C^{(1)}_{lmpq}$ and $C^{(2)}_{lmpq}$ (or, equivalently, their 9×9 stiffness matrices $\underline{\underline{\mathbf{C}}}^{(\ell)}$, $\ell \in \{1, 2\}$), and their densities $\rho^{(1)}$ and $\rho^{(2)}$. The stiffness tensors exhibit the symmetries represented in (3.4). The component materials are generally orthotropic [35] in the following developments; i.e., the stiffness matrix for each component material may be expressed as

$$\underline{\underline{\mathbf{C}}}^{(\ell)} = \begin{pmatrix} \underline{\underline{\mathcal{M}}}^{(\ell)} & \underline{\underline{\mathbf{0}}}_{3\times3} & \underline{\underline{\mathbf{0}}}_{3\times3} \\ \underline{\underline{\mathbf{0}}}_{3\times3} & \underline{\underline{\mathcal{D}}}^{(\ell)} & \underline{\underline{\mathcal{D}}}^{(\ell)} \\ \underline{\underline{\mathbf{0}}}_{3\times3} & \underline{\underline{\mathcal{D}}}^{(\ell)} & \underline{\underline{\mathcal{D}}}^{(\ell)} \end{pmatrix}, \qquad (\ell = 1, 2), \tag{3.13}$$

where $\underline{\underline{\mathcal{M}}}^{(\ell)}$ and $\underline{\underline{\mathcal{D}}}^{(\ell)}$ are symmetric and diagonal 3×3 matrices, respectively, and $\underline{\underline{\mathbf{0}}}_{3\times3}$ is the 3×3 null matrix. For the degenerate case in which the component material 'ℓ' is isotropic, we have

$$\left.\begin{aligned}
\left[\underline{\underline{\mathbf{C}}}^{(\ell)}\right]_{11} &= \left[\underline{\underline{\mathbf{C}}}^{(\ell)}\right]_{22} = \left[\underline{\underline{\mathbf{C}}}^{(\ell)}\right]_{33} = \lambda^{(\ell)} + 2\mu^{(\ell)} \\
\left[\underline{\underline{\mathbf{C}}}^{(\ell)}\right]_{12} &= \left[\underline{\underline{\mathbf{C}}}^{(\ell)}\right]_{13} = \left[\underline{\underline{\mathbf{C}}}^{(\ell)}\right]_{23} = \lambda^{(\ell)} \\
\left[\underline{\underline{\mathbf{C}}}^{(\ell)}\right]_{44} &= \left[\underline{\underline{\mathbf{C}}}^{(\ell)}\right]_{55} = \left[\underline{\underline{\mathbf{C}}}^{(\ell)}\right]_{66} = \mu^{(\ell)}
\end{aligned}\right\}, \qquad (\ell = 1, 2), \tag{3.14}$$

where $\lambda^{(\ell)}$ and $\mu^{(\ell)}$ are the Lamé constants [36].

3.2 Comparison material and the SPFT

3.2.1 Comparison material

A central concept in the SPFT is that of a homogeneous *comparison material*. This provides the initial ansatz for the SPFT estimate of the constitutive properties of the HCM. As such, the comparison material represents the lowest–order SPFT estimate of the HCM. Since we have taken the component materials to be generally orthotropic and the inclusion particles to be ellipsoidal, the comparison material is generally orthotropic[1]. The orthotropic comparison material (OCM) is characterized by its stiffness tensor $C_{lmpq}^{(ocm)}$ and density $\rho^{(ocm)}$, with $C_{lmpq}^{(ocm)}$ exhibiting the symmetries (3.4).

For the OCM the equation of motion is given by

$$\partial_l \sigma_{lm}^{(ocm)}(\mathbf{r}) + \omega^2 \rho^{(ocm)} u_m^{(ocm)}(\mathbf{r}) = -F_m(\mathbf{r}), \tag{3.15}$$

and the constitutive relation

$$\sigma_{lm}^{(ocm)}(\mathbf{r}) = C_{lmpq}^{(ocm)} S_{pq}^{(ocm)}(\mathbf{r}). \tag{3.16}$$

[1]In fact, the comparison material would also be orthotropic if (i) the components materials were isotropic but distributed as aligned ellipsoidal particles; or (ii) the components materials were orthotropic but distributed as spherical particles

Substituting (3.16) and (3.3) into (3.15) gives us

$$C_{lmpq}^{(ocm)}\partial_l\partial_q u_p(\mathbf{r}) + \omega^2\rho^{(ocm)}u_m(\mathbf{r}) = -F_m(\mathbf{r}). \tag{3.17}$$

The solution to this equation of motion is given by

$$u_p^{(ocm)}(\mathbf{r}) = G_{pm}^{(ocm)}(\mathbf{r}) * F_m(\mathbf{r}), \tag{3.18}$$

where $*$ represents a convolution integral and $G_{pm}^{(ocm)}(\mathbf{r})$ is the Green function of the OCM, which may be expressed in 3×3 spectral matrix form as [14]

$$\underline{\underline{\mathbf{G}}}^{(ocm)}(\mathbf{k}) = \left[k^2\underline{\underline{\mathbf{a}}}(\hat{\mathbf{k}}) - \omega^2\rho^{(ocm)}\underline{\underline{\mathbf{I}}}\right]^{-1}, \tag{3.19}$$

with $\underline{\underline{\mathbf{I}}}$ being the 3×3 identity matrix and $\underline{\underline{\mathbf{a}}}(\hat{\mathbf{k}})$ the 3×3 matrix with entries

$$\left[\,\underline{\underline{\mathbf{a}}}(\hat{\mathbf{k}})\,\right]_{mp} = \frac{k_l C_{lmpq}^{(ocm)} k_q}{k^2}. \tag{3.20}$$

Herein, $\mathbf{k} = k\,\hat{\mathbf{k}} \equiv (k_1, k_2, k_3)$ with $\hat{\mathbf{k}} = (\sin\theta\cos\phi, \sin\theta\sin\phi, \cos\theta)$. For use later on in §3.2.4, we remark that $\underline{\underline{\mathbf{G}}}^{(ocm)}(\mathbf{k})$ may be conveniently expressed as [14]

$$\underline{\underline{\mathbf{G}}}^{(ocm)}(\mathbf{k}) = \frac{\underline{\underline{\mathbf{N}}}(\mathbf{k})}{\Delta(\mathbf{k})}, \tag{3.21}$$

with the 3×3 matrix function

$$\underline{\underline{\mathbf{N}}}(\mathbf{k}) = k^4\mathrm{adj}\left[\underline{\underline{\mathbf{a}}}(\hat{\mathbf{k}})\right] + \omega^2\rho^{(ocm)}k^2\left\{\underline{\underline{\mathbf{a}}}(\hat{\mathbf{k}}) - \mathrm{tr}\left[\underline{\underline{\mathbf{a}}}(\hat{\mathbf{k}})\right]\,\underline{\underline{\mathbf{I}}}\right\} + \left(\omega^2\rho^{(ocm)}\right)^2\underline{\underline{\mathbf{I}}} \tag{3.22}$$

and the scalar function

$$\begin{aligned}\Delta(\mathbf{k}) \;=\; & k^6\det\left[\underline{\underline{\mathbf{a}}}(\hat{\mathbf{k}})\right] - \omega^2\rho^{(ocm)}\;k^4\mathrm{tr}\left\{\mathrm{adj}\left[\underline{\underline{\mathbf{a}}}(\hat{\mathbf{k}})\right]\right\} + \\ & \left(\omega^2\rho^{(ocm)}\right)^2 k^2\,\mathrm{tr}\left[\underline{\underline{\mathbf{a}}}(\hat{\mathbf{k}})\right] - \left(\omega^2\rho^{(ocm)}\right)^3.\end{aligned} \tag{3.23}$$

A key step in the SPFT — one which facilitates the calculation of $C_{lmpq}^{(ocm)}$ and

$\rho^{(ocm)}$ — is the imposition of the conditions [14, eqs. (2.72),(2.73)]

$$\langle \Phi^{(1)}(\mathbf{r})\, \xi^{(1)}_{lmpq} + \Phi^{(2)}(\mathbf{r})\, \xi^{(2)}_{lmpq} \rangle = 0, \tag{3.24}$$

$$\langle \Phi^{(1)}(\mathbf{r}) \left[\rho^{(1)} - \rho^{(ocm)}\right] + \Phi^{(2)}(\mathbf{r}) \left[\rho^{(2)} - \rho^{(ocm)}\right] \rangle = 0, \tag{3.25}$$

in order to remove all secular terms. In (3.24), the quantities

$$\xi^{(\ell)}_{lmpq} = \left(C^{(\ell)}_{lmst} - C^{(ocm)}_{lmst} \right) \eta^{(\ell)}_{stpq}, \qquad (\ell = 1, 2), \tag{3.26}$$

where $\eta^{(\ell)}_{stpq}$ is given implicitly via [14]

$$S^{(\ell)}_{pq}(\mathbf{r}) = \eta^{(\ell)}_{pqst} \varpi^{(\ell)}_{st}(\mathbf{r}), \tag{3.27}$$

$$\varpi^{(\ell)}_{ij}(\mathbf{r}) = S^{(\ell)}_{ij}(\mathbf{r}) + W_{ijlm} \left(C^{(\ell)}_{lmpq} - C^{(ocm)}_{lmpq} \right) S^{(\ell)}_{pq}(\mathbf{r}), \tag{3.28}$$

and the renormalization tensor is given by [14]

$$\begin{aligned} W_{rstu} \;=\; & \frac{1}{8\pi} \int_0^{2\pi} d\phi \int_0^{\pi} d\theta \sin\theta \times \frac{(\underline{\underline{\mathbf{U}}}^{-1} \cdot \hat{\mathbf{k}})_t}{(\underline{\underline{\mathbf{U}}}^{-1} \cdot \hat{\mathbf{k}}) \cdot (\underline{\underline{\mathbf{U}}}^{-1} \cdot \hat{\mathbf{k}})} \times \\ & \left\{ (\underline{\underline{\mathbf{U}}}^{-1} \cdot \hat{\mathbf{k}})_s \left[\underline{\underline{\mathbf{a}}}^{-1} (\underline{\underline{\mathbf{U}}}^{-1} \cdot \hat{\mathbf{k}}) \right]_{ru} + (\underline{\underline{\mathbf{U}}}^{-1} \cdot \hat{\mathbf{k}})_r \left[\underline{\underline{\mathbf{a}}}^{-1} (\underline{\underline{\mathbf{U}}}^{-1} \cdot \hat{\mathbf{k}}) \right]_{su} \right\}. \end{aligned} \tag{3.29}$$

3.2.2 Stiffness matrix of the OCM

To solve for $C^{(ocm)}_{lmpq}$ we must convert (3.26)–(3.28) to matrix notation as described in §3.1.3, giving us

$$\underline{\underline{\boldsymbol{\xi}}}^{(\ell)} = \left(\underline{\underline{\mathbf{C}}}^{(\ell)} - \underline{\underline{\mathbf{C}}}^{(ocm)} \right) \cdot \underline{\underline{\boldsymbol{\eta}}}^{(\ell)} \tag{3.30}$$

$$\mathbf{S}^{(\ell)}(\mathbf{r}) = \underline{\underline{\boldsymbol{\eta}}}^{(\ell)} \cdot \boldsymbol{\varpi}^{(\ell)}(\mathbf{r}) \tag{3.31}$$

$$\boldsymbol{\varpi}^{(\ell)}(\mathbf{r}) = \mathbf{S}^{(\ell)}(\mathbf{r}) + \underline{\underline{\underline{\mathbf{W}}}} \cdot \left(\underline{\underline{\mathbf{C}}}^{(\ell)} - \underline{\underline{\mathbf{C}}}^{(ocm)} \right) \cdot \mathbf{S}^{(\ell)}(\mathbf{r}) \tag{3.32}$$

for $\ell = 1, 2$. We can now utilize the matrix operation †, also defined in §3.1.3, to rearrange (3.30) as

$$\underline{\underline{\boldsymbol{\eta}}}^{(\ell)} = \left(\underline{\underline{\mathbf{C}}}^{(\ell)} - \underline{\underline{\mathbf{C}}}^{(ocm)} \right)^{\dagger} \cdot \underline{\underline{\boldsymbol{\xi}}}^{(\ell)}. \tag{3.33}$$

We can now substitute (3.31) and (3.33) into (3.32) to give

$$\begin{aligned}\boldsymbol{\varpi}^{(\ell)}(\mathbf{r}) &= \left(\underline{\underline{\mathbf{C}}}^{(\ell)} - \underline{\underline{\mathbf{C}}}^{(ocm)}\right)^{\dagger} \cdot \underline{\underline{\boldsymbol{\xi}}}^{(\ell)} \cdot \boldsymbol{\varpi}^{(\ell)}(\mathbf{r}) + \\ &\quad \underline{\underline{\mathbf{W}}} \cdot \left(\underline{\underline{\mathbf{C}}}^{(\ell)} - \underline{\underline{\mathbf{C}}}^{(ocm)}\right) \cdot \left(\underline{\underline{\mathbf{C}}}^{(\ell)} - \underline{\underline{\mathbf{C}}}^{(ocm)}\right)^{\dagger} \cdot \underline{\underline{\boldsymbol{\xi}}}^{(\ell)} \cdot \boldsymbol{\varpi}^{(\ell)}(\mathbf{r}) \quad (3.34) \\ &= \left[\left(\underline{\underline{\mathbf{C}}}^{(\ell)} - \underline{\underline{\mathbf{C}}}^{(ocm)}\right)^{\dagger} + \underline{\underline{\mathbf{W}}}\right] \cdot \underline{\underline{\boldsymbol{\xi}}}^{(\ell)} \cdot \boldsymbol{\varpi}^{(\ell)}(\mathbf{r}). \quad (3.35)\end{aligned}$$

This produces

$$\left[\left(\underline{\underline{\mathbf{C}}}^{(\ell)} - \underline{\underline{\mathbf{C}}}^{(ocm)}\right)^{\dagger} + \underline{\underline{\mathbf{W}}}\right] \cdot \underline{\underline{\boldsymbol{\xi}}}^{(\ell)} = \underline{\underline{\boldsymbol{\tau}}} \quad (3.36)$$

where $\underline{\underline{\boldsymbol{\tau}}}$ is the 9×9 matrix representation of the identity tensor τ_{rstu} as described in §3.1.3. We can now find $\underline{\underline{\boldsymbol{\xi}}}^{(\ell)}$ by multiplying through with

$$\left[\left(\underline{\underline{\mathbf{C}}}^{(\ell)} - \underline{\underline{\mathbf{C}}}^{(ocm)}\right)^{\dagger} + \underline{\underline{\mathbf{W}}}\right]^{\dagger} \quad (3.37)$$

giving

$$\underline{\underline{\boldsymbol{\xi}}}^{(\ell)} = \left[\left(\underline{\underline{\mathbf{C}}}^{(\ell)} - \underline{\underline{\mathbf{C}}}^{(ocm)}\right)^{\dagger} + \underline{\underline{\mathbf{W}}}\right]^{\dagger}. \quad (3.38)$$

Substituting (3.38) into the matrix representation of (3.24) provides an equation that can be solved for $\underline{\underline{\mathbf{C}}}^{(ocm)}$

$$\begin{aligned}f^{(1)}\underline{\underline{\boldsymbol{\xi}}}^{(1)} &= -f^{(2)}\underline{\underline{\boldsymbol{\xi}}}^{(2)}, \quad (3.39) \\ f^{(1)}\left[\left(\underline{\underline{\mathbf{C}}}^{(1)} - \underline{\underline{\mathbf{C}}}^{(ocm)}\right)^{\dagger} + \underline{\underline{\mathbf{W}}}\right]^{\dagger} &= -f^{(2)}\left[\left(\underline{\underline{\mathbf{C}}}^{(2)} - \underline{\underline{\mathbf{C}}}^{(ocm)}\right)^{\dagger} + \underline{\underline{\mathbf{W}}}\right]^{\dagger}. \quad (3.40)\end{aligned}$$

Multiplying through, in turn by, $\left[(\underline{\underline{\mathbf{C}}}^{(1)} - \underline{\underline{\mathbf{C}}}^{(ocm)})^{\dagger} + \underline{\underline{\mathbf{W}}}\right]$, $\left[(\underline{\underline{\mathbf{C}}}^{(2)} - \underline{\underline{\mathbf{C}}}^{(ocm)})^{\dagger} + \underline{\underline{\mathbf{W}}}\right]$, $(\underline{\underline{\mathbf{C}}}^{(1)} - \underline{\underline{\mathbf{C}}}^{(ocm)})$ and $(\underline{\underline{\mathbf{C}}}^{(2)} - \underline{\underline{\mathbf{C}}}^{(ocm)})$ in (3.40) leaves us with an equation for $\underline{\underline{\mathbf{C}}}^{(ocm)}$ of the form,

$$\underline{\underline{\mathbf{C}}}^{(ocm)} = f^{(1)}\underline{\underline{\mathbf{C}}}^{(1)} + f^{(2)}\underline{\underline{\mathbf{C}}}^{(2)} + (\underline{\underline{\mathbf{C}}}^{(2)} - \underline{\underline{\mathbf{C}}}^{(ocm)}) \cdot \underline{\underline{\mathbf{W}}} \cdot (\underline{\underline{\mathbf{C}}}^{(1)} - \underline{\underline{\mathbf{C}}}^{(ocm)}). \quad (3.41)$$

Finally, we can rearrange (3.41) to get

$$(\underline{\underline{\mathbf{C}}}^{(1)} - \underline{\underline{\mathbf{C}}}^{(ocm)}) + f^{(2)}(\underline{\underline{\mathbf{C}}}^{(2)} - \underline{\underline{\mathbf{C}}}^{(1)}) + (\underline{\underline{\mathbf{C}}}^{(2)} - \underline{\underline{\mathbf{C}}}^{(ocm)}) \cdot \underline{\underline{\mathbf{W}}} \cdot (\underline{\underline{\mathbf{C}}}^{(1)} - \underline{\underline{\mathbf{C}}}^{(ocm)}) = \underline{\underline{\mathbf{0}}}_{9\times 9} \quad (3.42)$$

and remove a common factor, giving

$$\left[\underline{\underline{\boldsymbol{\tau}}} + (\underline{\underline{\mathbf{C}}}^{(2)} - \underline{\underline{\mathbf{C}}}^{(ocm)}) \cdot \underline{\underline{\mathbf{W}}}\right] \cdot (\underline{\underline{\mathbf{C}}}^{(1)} - \underline{\underline{\mathbf{C}}}^{(ocm)}) = f^{(2)}(\underline{\underline{\mathbf{C}}}^{(1)} - \underline{\underline{\mathbf{C}}}^{(2)}). \tag{3.43}$$

Using the matrix operation † we have

$$(\underline{\underline{\mathbf{C}}}^{(1)} - \underline{\underline{\mathbf{C}}}^{(ocm)}) = f^{(2)} \left[\underline{\underline{\boldsymbol{\tau}}} + (\underline{\underline{\mathbf{C}}}^{(2)} - \underline{\underline{\mathbf{C}}}^{(ocm)}) \cdot \underline{\underline{\mathbf{W}}}\right]^\dagger \cdot (\underline{\underline{\mathbf{C}}}^{(1)} - \underline{\underline{\mathbf{C}}}^{(2)}) \tag{3.44}$$

and we rearrange to get our new estimate for $\underline{\underline{\mathbf{C}}}^{(ocm)}$ as

$$\underline{\underline{\mathbf{C}}}^{(ocm)} = \underline{\underline{\mathbf{C}}}^{(1)} + f^{(2)} \left[\underline{\underline{\boldsymbol{\tau}}} + (\underline{\underline{\mathbf{C}}}^{(2)} - \underline{\underline{\mathbf{C}}}^{(ocm)}) \cdot \underline{\underline{\mathbf{W}}}\right]^\dagger \cdot \left(\underline{\underline{\mathbf{C}}}^{(2)} - \underline{\underline{\mathbf{C}}}^{(1)}\right). \tag{3.45}$$

By standard numerical procedures, such as the Jacobi method [37], the nonlinear relation (3.45) is solved for $\underline{\underline{\mathbf{C}}}^{(ocm)}$. The iteration used in this case is given by

$$\begin{aligned} {}^{n+1}\underline{\underline{\mathbf{C}}}^{(ocm)} &= \underline{\underline{\mathbf{C}}}^{(1)} + f^{(2)} \left[\underline{\underline{\boldsymbol{\tau}}} + (\underline{\underline{\mathbf{C}}}^{(2)} - {}^{n}\underline{\underline{\mathbf{C}}}^{(ocm)}) \cdot \underline{\underline{\mathbf{W}}}\right]^\dagger \cdot \left(\underline{\underline{\mathbf{C}}}^{(2)} - \underline{\underline{\mathbf{C}}}^{(1)}\right) \\ {}^{n}\underline{\underline{\mathbf{C}}}^{(ocm)} &= \frac{1}{2}\left({}^{n}\underline{\underline{\mathbf{C}}}^{(ocm)} + {}^{(n-1)}\underline{\underline{\mathbf{C}}}^{(ocm)}\right), \\ {}^{0}\underline{\underline{\mathbf{C}}}^{(ocm)} &= f^{(1)}\underline{\underline{\mathbf{C}}}^{(1)} + f^{(2)}\underline{\underline{\mathbf{C}}}^{(2)}, \end{aligned} \tag{3.46}$$

where ${}^{n}\underline{\underline{\mathbf{C}}}^{(ocm)}$ is the n^{th} iteration of $C^{(ocm)}$. The iteration was said to have converged when the relative error of ${}^{n+1}\underline{\underline{\mathbf{C}}}^{(ocm)}$ and ${}^{n'}\underline{\underline{\mathbf{C}}}^{(ocm)}$ was less than 1×10^{-3}.

By combining (3.11) with (3.25), it follows immediately that the OCM density is the volume average of the densities of the component materials '1' and '2'; i.e.,

$$\rho^{(ocm)} = f^{(1)}\rho^{(1)} + f^{(2)}\rho^{(2)}. \tag{3.47}$$

3.2.3 Comparison of OCM with the Hill and Budiansky estimates

If both component materials are isotropic, with their stiffness matrices given by (3.14), then we can solve $\underline{\underline{\mathbf{C}}}^{(ocm)}$ for the Lamé constants $\lambda^{(ocm)}$ and $\mu^{(ocm)}$. The form of $\underline{\underline{\mathbf{C}}}^{(ocm)}$ given in (3.41) allows for easy calculation of the Lamé constants of the composite.

Lamé constants of the OCM

For an isotropic composite material, Zhuck and Lakhtakia [14] have found $\underline{\underline{\mathbf{W}}}$ in tensor form as

$$W_{rstu} = \frac{(3\lambda^{(ocm)} + 8\mu^{(ocm)})(\delta_{rt}\delta_{su} + \delta_{ru}\delta_{st}) - 2(\lambda^{(ocm)} + \mu^{(ocm)})\delta_{rs}\delta_{tu}}{30\mu^{(ocm)}(\lambda^{(ocm)} + 2\mu^{(ocm)})}, \quad (3.48)$$

wherein δ_{mp} is the Kronecker delta function.

We can now create two equations for $\lambda^{(ocm)}$ and $\mu^{(ocm)}$ by finding $\left[\underline{\underline{\mathbf{C}}}^{(ocm)}\right]_{12}$ and $\left[\underline{\underline{\mathbf{C}}}^{(ocm)}\right]_{44}$ in terms of the Lamé constants. From $\left[\underline{\underline{\mathbf{C}}}^{(ocm)}\right]_{12}$ we have

$$\begin{aligned}
&\left[\frac{1}{15\mu^{(ocm)}(\lambda^{(ocm)} + 2\mu^{(ocm)})}\right] \times \Big\{ -9\mu^{(ocm)}\lambda^{(ocm)}\mu^{(1)} - 14[\mu^{(ocm)}]^2\mu^{(1)} + \\
&15f^{(2)}\mu^{(ocm)}\lambda^{(ocm)}\mu^{(1)} + 30f^{(2)}[\mu^{(ocm)}]^2\mu^{(1)} - 15f^{(2)}\mu^{(1)}\mu^{(2)} - \\
&30f^{(2)}[\mu^{(ocm)}]^2\mu^{(2)} - 6\lambda^{(ocm)}\mu^{(1)}\mu^{(2)} + 6\mu^{(ocm)}\lambda^{(ocm)}\mu^{(2)} - 16\mu^{(ocm)}\mu^{(1)}\mu^{(2)} + \\
&16[\mu^{(ocm)}]^2\mu^{(2)} + 9\lambda^{(ocm)}[\mu^{(ocm)}]^2 + 14[\mu^{(ocm)}]^3\Big\} = 0, \quad (3.49)
\end{aligned}$$

which can be solved for $\lambda^{(ocm)}$ to give

$$\begin{aligned}
\lambda^{(ocm)} \;=\; &\left\{\frac{1}{3\left[-3\mu^{(ocm)}\mu^{(1)} + 5f^{(2)}\mu^{(ocm)}(\mu^{(1)} - \mu^{(2)}) - 2\mu^{(2)}(\mu^{(1)} - \mu^{(ocm)})\right]}\right\} \times \\
&-2\mu^{(ocm)}\Big\{ -7\mu^{(ocm)}\mu^{(1)} + 15f^{(2)}\mu^{(ocm)}[\mu^{(1)} - \mu^{(2)}] - \\
&8\mu^{(2)}[\mu^{(1)} - \mu^{(ocm)}] + 7\left[\mu^{(ocm)}\right]^2\Big\}. \quad (3.50)
\end{aligned}$$

Now we also have an equation for $\mu^{(ocm)}$ from $\left[\underline{\underline{\mathbf{C}}}^{(ocm)}\right]_{44}$

$$\begin{aligned}
&\left[\frac{1}{15\mu^{(ocm)}(\lambda^{(ocm)} + 2\mu^{(ocm)})}\right] \times \Big\{6\mu^{(ocm)}\lambda^{(ocm)}\mu^{(1)} + 4\mu^{(ocm)}\mu^{(1)}\mu^{(2)} + \\
&4\lambda^{(ocm)}\mu^{(1)}\mu^{(2)} - 30f\left[\mu^{(ocm)}\right]^2\lambda^{(2)} + 4\left[\mu^{(ocm)}\right]^3 - 20\left[\mu^{(ocm)}\right]^2\lambda^{(1)} - \\
&4\left[\mu^{(ocm)}\right]^2\mu^{(1)} + 14\lambda^{(ocm)}\left[\mu^{(ocm)}\right]^2 + 15\lambda^{(ocm)}\mu^{(ocm)}\lambda^{(2)} + 6\lambda^{(ocm)}\mu^{(ocm)}\mu^{(2)} + \\
&10\left[\mu^{(ocm)}\right]^2\lambda^{(2)} - 4\left[\mu^{(ocm)}\right]^2\mu^{(2)} + 15f^{(2)}\lambda^{(ocm)}\mu^{(ocm)}\lambda^{(1)} - \\
&15f^{(2)}\mu^{(1)}\lambda^{(2)} + 30f^{(2)}\left[\mu^{(ocm)}\right]^2\lambda^{(1)} - 15\mu^{(ocm)}\lambda^{(1)}\lambda^{(2)} - 10\mu^{(ocm)}\mu^{(2)}\lambda^{(1)} - \\
&10\mu^{(ocm)}\mu^{(1)}\lambda^{(ocm)}\Big\} = 0 \quad (3.51)
\end{aligned}$$

and when we substitute in (3.50), we get the solution for $\mu^{(ocm)}$ as

$$\begin{aligned}\mu^{(ocm)} &= \frac{\mu^{(1)}}{2} - \frac{5f^{(2)}\mu^{(1)}}{6} + \frac{5f^{(2)}\mu^{(2)}}{6} - \frac{\mu^{(2)}}{3} \pm \\ &\quad \frac{1}{6}\sqrt{9\left[\mu^{(1)}\right]^2 + 12\mu^{(1)}\mu^{(2)} - 30f^{(2)}\left[\mu^{(1)}\right]^2 - 20f^{(2)}\left[\mu^{(2)}\right]^2 + \\ &\quad 50f^{(1)}f^{(2)}\mu^{(1)}\mu^{(2)} + 25\left[f^{(2)}\right]^2\left(\left[\mu^{(1)}\right]^2 + \left[\mu^{(2)}\right]^2\right) + 4\left[\mu^{(2)}\right]^2}.\end{aligned} \tag{3.52}$$

The Hill and Budiansky estimates

The Hill estimate is given by [29, 30]

$$\frac{f^{(1)}}{\kappa^{(hill)} - \kappa^{(2)}} + \frac{f^{(2)}}{\kappa^{(hill)} - \kappa^{(1)}} = \frac{1}{\kappa^{(hill)} + \frac{4}{3}\mu^{(hill)}}, \tag{3.53}$$

$$\frac{f^{(1)}}{\mu^{(hill)} - \mu^{(2)}} + \frac{f^{(2)}}{\mu^{(hill)} - \mu^{(1)}} = \frac{2\kappa^{(hill)} + 4\mu^{(hill)}}{5(\kappa^{(hill)} + \frac{4}{3}\mu^{(hill)})} \tag{3.54}$$

and the Budiansky estimate by [31]

$$\frac{1}{\kappa^{(bud)}} = \frac{1}{\kappa^{(2)}} + \left(1 - \frac{\kappa^{(1)}}{\kappa^{(2)}}\right)\frac{f^{(1)}}{\kappa^{(bud)} + \alpha(\kappa^{(1)} - \kappa^{(bud)})}, \tag{3.55}$$

$$\frac{1}{\mu^{(bud)}} = \frac{1}{\mu^{(2)}} + \left(1 - \frac{\mu^{(1)}}{\mu^{(2)}}\right)\frac{f^{(1)}}{\mu^{(bud)} + \beta(\mu^{(1)} - \mu^{(bud)})}, \tag{3.56}$$

where $\alpha = \dfrac{1+\nu^{(bud)}}{3[1-\nu^{(bud)}]}$, $\beta = \dfrac{2[4-5\nu^{(bud)}]}{15[1-\nu^{(bud)}]}$ and $\nu^{(bud)} = \dfrac{\lambda^{(bud)}}{2[\lambda^{(bud)} + \mu^{(bud)}]}$. Both of these estimates are written in terms of the bulk modulus $\kappa^{(\ell)} = \lambda^{(\ell)} + 2\mu^{(\ell)}$, ($\ell = 1$, 2, bud, hill) so we can solve for the Lamé constants of the composite.

If we substitute (3.50) and (3.52) into the Hill and Budiansky estimates then the equations are satisfied and we find that the Hill and Budiansky estimates are identical to each other and also identical to the OCM estimate for isotropic composites. It is of interest to note Zhuck and Lakhtakia [14] made reference to this result but produced no results.

3.2.4 Second–order SPFT

The expressions for the second–order[2] estimates of the HCM stiffness and density tensors, as derived elsewhere [14, eqs. (2.77),(2.78)], are

$$\begin{aligned} C_{lmpq}^{(spft)} &= C_{lmpq}^{(ocm)} - \frac{\omega^2 \rho^{(ocm)}}{2} \int d^3k \, \frac{k_t}{k^2} \, B_{tupq}^{lmrs}(\mathbf{k}) \, \left[\underline{\underline{\mathbf{G}}}^{(ocm)}(\mathbf{k}) \right]_{vu} \times \\ & \left\{ k_s \left[\underline{\underline{\mathbf{a}}}^{-1}(\hat{\mathbf{k}}) \right]_{rv} + k_r \left[\underline{\underline{\mathbf{a}}}^{-1}(\hat{\mathbf{k}}) \right]_{sv} \right\} \end{aligned} \tag{3.57}$$

and

$$\rho_{mp}^{(spft)} = \rho^{(ocm)} \delta_{mp} + \omega^2 \int d^3k \; B(\mathbf{k}) \left[\underline{\underline{\mathbf{G}}}^{(ocm)}(\mathbf{k}) \right]_{mp}, \tag{3.58}$$

respectively. The eighth–order tensor $B_{tupq}^{lmrs}(\mathbf{k})$ and scalar $B(\mathbf{k})$ represent the spectral covariance functions given as

$$\left. \begin{aligned} B_{tupq}^{lmrs}(\mathbf{k}) &= \frac{\left(\xi_{lmrs}^{(2)} - \xi_{lmrs}^{(1)} \right) \left(\xi_{tupq}^{(2)} - \xi_{tupq}^{(1)} \right)}{8\pi^3} \int d^3R \; \Gamma(\mathbf{R}) \, \exp\left(-i\mathbf{k} \cdot \mathbf{R}\right) \\ B(\mathbf{k}) &= \frac{\left(\rho^{(2)} - \rho^{(1)} \right)^2}{8\pi^3} \int d^3R \, \Gamma(\mathbf{R}) \, \exp\left(-i\mathbf{k} \cdot \mathbf{R}\right) \end{aligned} \right\}, \tag{3.59}$$

with

$$\begin{aligned} \Gamma(\mathbf{R}) = \Gamma(\mathbf{r} - \mathbf{r}') &= \langle \, \Phi^{(1)}(\mathbf{r}) \, \Phi^{(1)}(\mathbf{r}') \, \rangle - \langle \, \Phi^{(1)}(\mathbf{r}) \, \rangle \, \langle \, \Phi^{(1)}(\mathbf{r}') \, \rangle \\ &\equiv \langle \, \Phi^{(2)}(\mathbf{r}) \, \Phi^{(2)}(\mathbf{r}') \, \rangle - \langle \, \Phi^{(2)}(\mathbf{r}) \, \rangle \, \langle \, \Phi^{(2)}(\mathbf{r}') \, \rangle . \end{aligned} \tag{3.60}$$

We now proceed to simplify the expressions for $C_{lmpq}^{(spft)}$ and $\rho_{mp}^{(spft)}$ presented in (3.57) and (3.58), in order to make them numerically tractable. We begin with the integral on the right sides of (3.59) which, upon implementing the step function–shaped covariance function (3.12), may be expressed as

$$\int d^3R \; \Gamma(\mathbf{R}) \, \exp\left(-i\mathbf{k} \cdot \mathbf{R}\right) = f^{(1)} f^{(2)} \int_{|\mathbf{R}| \leq L} d^3R \; \exp\left[-i \left(\underline{\underline{\mathbf{U}}} \cdot \mathbf{k} \right) \cdot \mathbf{R} \right]. \tag{3.61}$$

[2]The first–order SPFT estimate is identical to the zeroth–order SPFT estimate which is represented by the comparison material.

Thus, we find that $B^{lmrs}_{tupq}(\mathbf{k})$ and $B(\mathbf{k})$ are given by [38]

$$\left.\begin{aligned} B^{lmrs}_{tupq}(\mathbf{k}) &= \frac{f^{(1)}f^{(2)}\left(\xi^{(2)}_{lmrs}-\xi^{(1)}_{lmrs}\right)\left(\xi^{(2)}_{tupq}-\xi^{(1)}_{tupq}\right)}{2\left(\pi k\sigma\right)^2}\left[\frac{\sin\left(k\sigma L\right)}{k\sigma}-L\cos\left(k\sigma L\right)\right] \\ B(\mathbf{k}) &= \frac{f^{(1)}f^{(2)}\left(\rho^{(2)}-\rho^{(1)}\right)^2}{2\left(\pi k\sigma\right)^2}\left[\frac{\sin\left(k\sigma L\right)}{k\sigma}-L\cos\left(k\sigma L\right)\right] \end{aligned}\right\}, \tag{3.62}$$

wherein the scalar function

$$\sigma \equiv \sigma(\theta,\phi) = \sqrt{a^2\sin^2\theta\cos^2\phi + b^2\sin^2\theta\sin^2\phi + c^2\cos^2\theta}. \tag{3.63}$$

Upon substituting (3.62) into (3.57) and (3.58), the integrals therein with respect to k can be evaluated by means of calculus of residues: The roots of $\Delta(\mathbf{k})=0$ give rise to six poles in the complex–k plane, located at $k=\pm p_1$, $\pm p_2$ and $\pm p_3$, chosen such that $\mathrm{Im}\, p_i \geq 0$ $(i=1,2,3)$. From (3.23), we find that.

$$p_1^2 = P_A - \frac{1}{3}\left(\frac{2^{1/3}P_B}{P_C\det\left[\underline{\underline{\mathbf{a}}}(\hat{\mathbf{k}})\right]} - \frac{P_C}{2^{1/3}\det\left[\underline{\underline{\mathbf{a}}}(\hat{\mathbf{k}})\right]}\right), \tag{3.64}$$

$$p_2^2 = P_A + \frac{1}{3}\left(\frac{(1+i\sqrt{3})P_B}{2^{2/3}P_C\det\left[\underline{\underline{\mathbf{a}}}(\hat{\mathbf{k}})\right]} - \frac{(1-i\sqrt{3})P_C}{2^{4/3}\det\left[\underline{\underline{\mathbf{a}}}(\hat{\mathbf{k}})\right]}\right), \tag{3.65}$$

$$p_3^2 = P_A + \frac{1}{3}\left(\frac{(1-i\sqrt{3})P_B}{2^{2/3}P_C\det\left[\underline{\underline{\mathbf{a}}}(\hat{\mathbf{k}})\right]} - \frac{(1+i\sqrt{3})P_C}{2^{4/3}\det\left[\underline{\underline{\mathbf{a}}}(\hat{\mathbf{k}})\right]}\right), \tag{3.66}$$

wherein

$$P_A = \frac{\omega^2\rho^{(ocm)}\mathrm{tr}\left\{\mathrm{adj}\left[\underline{\underline{\mathbf{a}}}(\hat{\mathbf{k}})\right]\right\}}{3\det\left[\underline{\underline{\mathbf{a}}}(\hat{\mathbf{k}})\right]}, \tag{3.67}$$

$$P_B = \left(\omega^2\rho^{(ocm)}\right)^2\left(3\det\left[\underline{\underline{\mathbf{a}}}(\hat{\mathbf{k}})\right]\,\mathrm{tr}\left[\underline{\underline{\mathbf{a}}}(\hat{\mathbf{k}})\right] - \mathrm{tr}\left\{\mathrm{adj}\left[\underline{\underline{\mathbf{a}}}(\hat{\mathbf{k}})\right]\right\}^2\right), \tag{3.68}$$

$$P_C^3 = P_D + \sqrt{4P_B^3+P_D^2}, \tag{3.69}$$

$$\begin{aligned} P_D = {} & \left(\omega^2\rho^{(ocm)}\right)^3\left(2\,\mathrm{tr}\left\{\mathrm{adj}\left[\underline{\underline{\mathbf{a}}}(\hat{\mathbf{k}})\right]\right\}^3 - \right. \\ & \left. 9\det\left[\underline{\underline{\mathbf{a}}}(\hat{\mathbf{k}})\right]\,\mathrm{tr}\left\{\mathrm{adj}\left[\underline{\underline{\mathbf{a}}}(\hat{\mathbf{k}})\right]\right\}\,\mathrm{tr}\left[\underline{\underline{\mathbf{a}}}(\hat{\mathbf{k}})\right] + 27\det\left[\underline{\underline{\mathbf{a}}}(\hat{\mathbf{k}})\right]^2\right). \end{aligned} \tag{3.70}$$

These six poles are all simple poles of $\Delta(\mathbf{k})$ and we must calculate the residue of $\underline{\underline{\mathbf{G}}}^{(ocm)}$ at each of them. The situation is further complicated by the simple pole introduced by the covariance functions (3.62). The function we wish to find the residue of is

$$\frac{\underline{\underline{\mathbf{N}}}(\mathbf{k})}{\acute{\mathcal{F}}(k)}\left[\frac{e^{iL\sigma k}-e^{-iL\sigma k}}{2i\sigma k}-\frac{L(e^{iL\sigma k}+e^{-iL\sigma k})}{2}\right], \tag{3.71}$$

with

$$\acute{\mathcal{F}}(k)=(k-p_1)(k-p_2)(k-p_3)(k+p_1)(k+p_2)(k+p_3). \tag{3.72}$$

We calculate the residue using contour integration. Splitting (3.71) into 4 separate functions;

$$\mathcal{F}_1(k) = \frac{\underline{\underline{\mathbf{N}}}(\mathbf{k})}{\acute{\mathcal{F}}(k)}\frac{e^{iL\sigma k}}{2i\sigma k} \tag{3.73}$$

$$\mathcal{F}_2(k) = \frac{\underline{\underline{\mathbf{N}}}(\mathbf{k})}{\acute{\mathcal{F}}(k)}\frac{-Le^{iL\sigma k}}{2} \tag{3.74}$$

$$\mathcal{F}_3(k) = \frac{\underline{\underline{\mathbf{N}}}(\mathbf{k})}{\acute{\mathcal{F}}(k)}\frac{-e^{-iL\sigma k}}{2i\sigma k} \tag{3.75}$$

$$\mathcal{F}_4(k) = \frac{\underline{\underline{\mathbf{N}}}(\mathbf{k})}{\acute{\mathcal{F}}(k)}\frac{-Le^{-iL\sigma k}}{2}. \tag{3.76}$$

For the functions $\mathcal{F}_1(k)$ and $\mathcal{F}_2(k)$ we use the a semi–circle in the upper half plane as the contour, calculating the residue of $\mathcal{F}_1(k)$ at p_1, p_2, p_3 and 0 but the residue of $\mathcal{F}_2(k)$ only at p_1, p_2, p_3. The residues are given by

$$\mathrm{Res}(\mathcal{F}_1(p_1))=\frac{-i\underline{\underline{\mathbf{N}}}(p_1\underline{\underline{\mathbf{U}}}\cdot\hat{\mathbf{k}})e^{iL\sigma p_1}}{4\sigma p_1^2(p_1^2-p_2^2)(p_1^2-p_3^2)} \tag{3.77}$$

$$\mathrm{Res}(\mathcal{F}_1(p_2))=\frac{i\underline{\underline{\mathbf{N}}}(p_2\underline{\underline{\mathbf{U}}}\cdot\hat{\mathbf{k}})e^{iL\sigma p_2}}{4\sigma p_2^2(p_1^2-p_2^2)(p_2^2-p_3^2)} \tag{3.78}$$

$$\mathrm{Res}(\mathcal{F}_1(p_3))=\frac{-i\underline{\underline{\mathbf{N}}}(p_3\underline{\underline{\mathbf{U}}}\cdot\hat{\mathbf{k}})e^{iL\sigma p_3}}{4\sigma p_3^2(p_1^2-p_3^2)(p_2^2-p_3^2)} \tag{3.79}$$

$$\mathrm{Res}(\mathcal{F}_1(0))=\frac{i\underline{\underline{\mathbf{N}}}(\mathbf{0})}{2\sigma p_1^2p_2^2p_3^2} \tag{3.80}$$

$$\mathrm{Res}(\mathcal{F}_2(p_1))=\frac{-L\underline{\underline{\mathbf{N}}}(p_1\underline{\underline{\mathbf{U}}}\cdot\hat{\mathbf{k}})e^{iL\sigma p_1}}{4\sigma p_1(p_1^2-p_2^2)(p_1^2-p_3^2)} \tag{3.81}$$

$$\mathrm{Res}(\mathcal{F}_2(p_2)) = \frac{L\underline{\underline{\mathbf{N}}}(p_2\underline{\underline{\mathbf{U}}}\cdot\hat{\mathbf{k}})e^{iL\sigma p_2}}{4\sigma p_2(p_1^2-p_2^2)(p_2^2-p_3^2)} \tag{3.82}$$

$$\mathrm{Res}(\mathcal{F}_2(p_3)) = \frac{-L\underline{\underline{\mathbf{N}}}(p_3\underline{\underline{\mathbf{U}}}\cdot\hat{\mathbf{k}})e^{iL\sigma p_3}}{4\sigma p_3(p_1^2-p_3^2)(p_2^2-p_3^2)}. \tag{3.83}$$

Similarly, for the functions $\mathcal{F}_3(k)$ and $\mathcal{F}_4(k)$ we use a semi–circle in the lower half plane as the contour, calculating the residue of $\mathcal{F}_3(k)$ at $-p_1$, $-p_2$, $-p_3$ and 0 but the residue of $\mathcal{F}_4(k)$ only at $-p_1$, $-p_2$, $-p_3$. These residues are given by

$$\mathrm{Res}(\mathcal{F}_3(-p_1)) = \frac{i\underline{\underline{\mathbf{N}}}(p_1\underline{\underline{\mathbf{U}}}\cdot\hat{\mathbf{k}})e^{iL\sigma p_1}}{4\sigma p_1^2(p_1^2-p_2^2)(p_1^2-p_3^2)} \tag{3.84}$$

$$\mathrm{Res}(\mathcal{F}_3(-p_2)) = \frac{-i\underline{\underline{\mathbf{N}}}(p_2\underline{\underline{\mathbf{U}}}\cdot\hat{\mathbf{k}})e^{iL\sigma p_2}}{4\sigma p_2^2(p_1^2-p_2^2)(p_2^2-p_3^2)} \tag{3.85}$$

$$\mathrm{Res}(\mathcal{F}_3(-p_3)) = \frac{i\underline{\underline{\mathbf{N}}}(p_3\underline{\underline{\mathbf{U}}}\cdot\hat{\mathbf{k}})e^{iL\sigma p_3}}{4\sigma p_3^2(p_1^2-p_3^2)(p_2^2-p_3^2)} \tag{3.86}$$

$$\mathrm{Res}(\mathcal{F}_3(0)) = \frac{-i\underline{\underline{\mathbf{N}}}(\mathbf{0})}{2\sigma p_1^2p_2^2p_3^2} \tag{3.87}$$

$$\mathrm{Res}(\mathcal{F}_4(-p_1)) = \frac{L\underline{\underline{\mathbf{N}}}(p_1\underline{\underline{\mathbf{U}}}\cdot\hat{\mathbf{k}})e^{iL\sigma p_1}}{4\sigma p_1(p_1^2-p_2^2)(p_1^2-p_3^2)} \tag{3.88}$$

$$\mathrm{Res}(\mathcal{F}_4(-p_2)) = \frac{-L\underline{\underline{\mathbf{N}}}(p_2\underline{\underline{\mathbf{U}}}\cdot\hat{\mathbf{k}})e^{iL\sigma p_2}}{4\sigma p_2(p_1^2-p_2^2)(p_2^2-p_3^2)} \tag{3.89}$$

$$\mathrm{Res}(\mathcal{F}_4(-p_3)) = \frac{L\underline{\underline{\mathbf{N}}}(p_3\underline{\underline{\mathbf{U}}}\cdot\hat{\mathbf{k}})e^{iL\sigma p_3}}{4\sigma p_3(p_1^2-p_3^2)(p_2^2-p_3^2)}. \tag{3.90}$$

The values of the residues provided by the pole at zero, are halved as the pole lies on both contours. We sum the residues in the following way because each residue has to be evaluated by moving anti–clockwise around the contour.

$$\begin{aligned}\text{Residue} \;=\; & \mathrm{Res}(\mathcal{F}_1(p_1)) + \mathrm{Res}(\mathcal{F}_1(p_2)) + \mathrm{Res}(\mathcal{F}_1(p_3)) + \frac{1}{2}\mathrm{Res}(\mathcal{F}_1(0)) + \\ & \mathrm{Res}(\mathcal{F}_2(p_1)) + \mathrm{Res}(\mathcal{F}_2(p_2)) + \mathrm{Res}(\mathcal{F}_2(p_3)) - \\ & \mathrm{Res}(\mathcal{F}_3(-p_1)) - \mathrm{Res}(\mathcal{F}_3(-p_2)) - \mathrm{Res}(\mathcal{F}_3(-p_3)) - \frac{1}{2}\mathrm{Res}(\mathcal{F}_3(0)) - \\ & \mathrm{Res}(\mathcal{F}_4(-p_1)) - \mathrm{Res}(\mathcal{F}_4(-p_2)) - \mathrm{Res}(\mathcal{F}_4(-p_3)).\end{aligned} \tag{3.91}$$

Thus, by this application of the Cauchy residue theorem [39], the SPFT estimates

are delivered as

$$C_{lmpq}^{(spft)} = C_{lmpq}^{(ocm)} + \frac{\omega^2 \rho^{(ocm)} f^{(1)} f^{(2)} \left(\xi_{lmrs}^{(2)} - \xi_{lmrs}^{(1)}\right)\left(\xi_{tupq}^{(2)} - \xi_{tupq}^{(1)}\right)}{4\pi i} \times \int_{\phi=0}^{2\pi}\int_{\theta=0}^{\pi} d\phi\, d\theta\, \frac{k_t \sin\theta \left\{k_s \left[\underline{\underline{\mathbf{a}}}^{-1}(\hat{\mathbf{k}})\right]_{rv} + k_r \left[\underline{\underline{\mathbf{a}}}^{-1}(\hat{\mathbf{k}})\right]_{sv}\right\}}{(k\sigma)^2 \det\left[\underline{\underline{\mathbf{a}}}(\hat{\mathbf{k}})\right]} \left[\underline{\underline{\mathbf{b}}}(\hat{\mathbf{k}})\right]_{vu}, \tag{3.92}$$

and

$$\rho_{mp}^{(spft)} = \rho^{(ocm)}\delta_{mp} - \frac{\omega^2 f^{(1)} f^{(2)} \left(\rho^{(2)} - \rho^{(1)}\right)^2}{2\pi i} \times \int_{\phi=0}^{2\pi}\int_{\theta=0}^{\pi} d\phi\, d\theta\, \frac{\sin\theta}{\det\left[\underline{\underline{\mathbf{a}}}(\hat{\mathbf{k}})\right]} \left[\underline{\underline{\mathbf{b}}}(\hat{\mathbf{k}})\right]_{mp}, \tag{3.93}$$

where the residue is given by

$$\begin{aligned}\underline{\underline{\mathbf{b}}}(\hat{\mathbf{k}}) = \frac{1}{2i}\Bigg[& \frac{e^{iL\sigma p_1}\underline{\underline{\mathbf{N}}}(p_1\underline{\underline{\mathbf{U}}}\cdot\hat{\mathbf{k}})}{\sigma p_1^2(p_1^2-p_2^2)(p_1^2-p_3^2)}\left(1 - iL\sigma p_1\right) - \\ & \frac{e^{iL\sigma p_2}\underline{\underline{\mathbf{N}}}(p_2\underline{\underline{\mathbf{U}}}\cdot\hat{\mathbf{k}})}{\sigma p_2^2(p_1^2-p_2^2)(p_2^2-p_3^2)}\left(1 - iL\sigma p_2\right) + \\ & \frac{e^{iL\sigma p_3}\underline{\underline{\mathbf{N}}}(p_3\underline{\underline{\mathbf{U}}}\cdot\hat{\mathbf{k}})}{\sigma p_3^2(p_2^2-p_3^2)(p_1^2-p_3^2)}\left(1 - iL\sigma p_3\right) - \frac{\underline{\underline{\mathbf{N}}}(\mathbf{0})}{\sigma p_1^2 p_2^2 p_3^2}\Bigg].\end{aligned} \tag{3.94}$$

The integrals in (3.92) and (3.93) are readily evaluated by standard numerical methods [40].

Significantly, the SPFT estimates $C_{lmpq}^{(spft)}$ and $\rho_{mp}^{(spft)}$ are complex–valued even when the corresponding quantities for the component materials, i.e., $C_{lmpq}^{(\ell)}$ and $\rho^{(\ell)}$ $(\ell = 1, 2)$, are real–valued. This reflects the fact that the SPFT takes into account losses due to scattering. We note that for [33]

(i) the time–averaged strain energy density to be positive–valued, we require $\mathrm{Re}\,\underline{\underline{\mathbf{C}}}_{6\times6}^{(spft)}$ to be positive–definite; and

(ii) the time–averaged dissipated energy density to be positive–valued, we require $-\mathrm{Im}\,\underline{\underline{\mathbf{C}}}_{6\times6}^{(spft)}$ to be positive–semi–definite,

where $\underline{\underline{\mathbf{C}}}_{6\times6}^{(spft)}$ is the 6×6 matrix with components $\left[\underline{\underline{\mathbf{C}}}_{6\times6}^{(spft)}\right]_{st} = \left[\underline{\underline{\mathbf{C}}}^{(spft)}\right]_{st}$ $(s, t \in$

$\{1, 2, \ldots, 6\}$) and $\underline{\underline{\mathbf{C}}}^{(spft)}$ is the 9×9 matrix equivalent to the SPFT stiffness tensor $C^{(spft)}_{lmpq}$.

A complex–valued anisotropic density, as delivered by (3.93), is not without precedent [41]; see Milton [42] for a discussion on this issue.

The regime of validity of (3.92) and (3.93) have also been derived by Zhuck and Lakhtakia [14]. If we consider the average fluctuations in density and stiffness tensor values between the component and composite materials to be given by χ_ρ and χ_C respectively, then (3.92) and (3.93) hold if

$$\begin{aligned}(\omega L)^2 \left(\frac{\chi_C}{\overline{C}}\right)^2 \frac{\overline{\rho}}{\overline{C}} &\ll 1 \\ (\omega L)^2 \left(\frac{\chi_\rho}{\overline{\rho}}\right)^2 \frac{\overline{\rho}}{\overline{C}} &\ll 1\end{aligned}$$

where $\overline{C}$ and $\overline{\rho}$ are the average stiffness tensor entries and average density values of the two component materials.

3.3 The Mori–Tanaka estimate and Hashin–Shtrikman bounds

In order to provide a baseline for the SPFT estimate of the HCM stiffness tensor, the corresponding results provided by the Mori–Tanaka mean–field formalism [20] were also computed. The Mori–Tanaka estimate of the 9×9 stiffness matrix of the HCM may be written as [43]

$$\underline{\underline{\mathbf{C}}}^{(MT)} = \left[f^{(1)}\underline{\underline{\mathbf{C}}}^{(1)} + f^{(2)}\underline{\underline{\mathbf{C}}}^{(2)} \cdot \underline{\underline{\mathbf{B}}}^{MT} \right] \cdot \left[f^{(1)}\underline{\underline{\boldsymbol{\tau}}} + f^{(2)}\underline{\underline{\mathbf{B}}}^{MT} \right]^{\dagger}, \tag{3.95}$$

where

$$\underline{\underline{\mathbf{B}}}^{MT} = \left[\underline{\underline{\boldsymbol{\tau}}} + \underline{\underline{\mathbf{S}}}^{(esh)} \cdot \left(\underline{\underline{\mathbf{C}}}^{(1)}\right)^{\dagger} \cdot \left(\underline{\underline{\mathbf{C}}}^{(2)} - \underline{\underline{\mathbf{C}}}^{(1)}\right) \right]^{\dagger}, \tag{3.96}$$

and $\underline{\underline{\mathbf{S}}}^{(esh)}$ is the 9×9 Eshelby matrix [44].

3.3.1 Eshelby tensor/matrix

If the component materials are orthotropic and the inclusion particles spherical (i.e., $a = b = c$), then the tensor counterpart of the 9×9 Eshelby matrix is given as [45]

$$S_{ijkl}^{(esh)} = \frac{1}{8\pi} C_{mnkl}^{(1)} \int_{-1}^{+1} d\zeta_3 \int_0^{2\pi} d\omega \ \left[F_{imjn}^{(esh)}(\overline{\vartheta}) + F_{jmin}^{(esh)}(\overline{\vartheta}) \right], \tag{3.97}$$

wherein

$$\left.\begin{array}{l} F_{ijkl}^{(esh)}(\overline{\vartheta}) = \dfrac{\overline{\vartheta}_k \overline{\vartheta}_l N_{ij}}{\varepsilon_{mnl} \mathcal{K}_{m1} \mathcal{K}_{n2} \mathcal{K}_{l3}}, \quad \mathcal{N}_{ij}(\overline{\vartheta}) = \dfrac{1}{2} \varepsilon_{ikl} \varepsilon_{jmn} \mathcal{K}_{km} \mathcal{K}_{ln}, \quad \mathcal{K}_{ik} = C_{ijkl}^{(1)} \overline{\vartheta}_j \overline{\vartheta}_i \\ \overline{\vartheta}_1 = \dfrac{\zeta_1}{a}, \quad \overline{\vartheta}_2 = \dfrac{\zeta_2}{b}, \quad \overline{\vartheta}_3 = \dfrac{\zeta_3}{c} \\ \zeta_1 = (1 - \zeta_3^2)^{1/2} \cos(\omega), \quad \zeta_2 = (1 - \zeta_3^2)^{1/2} \sin(\omega), \quad \zeta_3 = \zeta_3 \end{array}\right\}, \tag{3.98}$$

with ϵ_{ijk} being the Levi–Civita symbol. The integrals in (3.97) can be evaluated using standard numerical methods [40].

If the component materials are isotropic and the ellipsoidal inclusion particles described by the shape matrix $\underline{\underline{\mathbf{U}}}$, then the Eshelby matrix has the form represented in (3.5) with distinct components given as [43]

$$\left[\underline{\underline{\mathbf{S}}}^{(esh)} \right]_{11} = \frac{3a^2 I_{\alpha\alpha} + \left(1 - 2\nu^{(1)}\right) I_\alpha}{8\pi \left(1 - \nu^{(1)}\right)}, \tag{3.99}$$

$$\left[\underline{\underline{\mathbf{S}}}^{(esh)} \right]_{12} = \frac{3b^2 I_{\alpha\beta} - \left(1 - 2\nu^{(1)}\right) I_\alpha}{8\pi \left(1 - \nu^{(1)}\right)}, \tag{3.100}$$

$$\left[\underline{\underline{\mathbf{S}}}^{(esh)} \right]_{13} = \frac{3c^2 I_{\alpha\gamma} - \left(1 - 2\nu^{(1)}\right) I_\alpha}{8\pi \left(1 - \nu^{(1)}\right)}, \tag{3.101}$$

$$\left[\underline{\underline{\mathbf{S}}}^{(esh)} \right]_{21} = \frac{3a^2 I_{\alpha\beta} - \left(1 - 2\nu^{(1)}\right) I_\beta}{8\pi \left(1 - \nu^{(1)}\right)}, \tag{3.102}$$

$$\left[\underline{\underline{\mathbf{S}}}^{(esh)}\right]_{22} = \frac{3b^2 I_{\beta\beta} + \left(1-2\nu^{(1)}\right) I_\beta}{8\pi\left(1-\nu^{(1)}\right)}, \tag{3.103}$$

$$\left[\underline{\underline{\mathbf{S}}}^{(esh)}\right]_{23} = \frac{3c^2 I_{\beta\gamma} + \left(1-2\nu^{(1)}\right) I_\beta}{8\pi\left(1-\nu^{(1)}\right)}, \tag{3.104}$$

$$\left[\underline{\underline{\mathbf{S}}}^{(esh)}\right]_{31} = \frac{3a^2 I_{\alpha\gamma} - \left(1-2\nu^{(1)}\right) I_\gamma}{8\pi\left(1-\nu^{(1)}\right)}, \tag{3.105}$$

$$\left[\underline{\underline{\mathbf{S}}}^{(esh)}\right]_{32} = \frac{3b^2 I_{\beta\gamma} - \left(1-2\nu^{(1)}\right) I_\gamma}{8\pi\left(1-\nu^{(1)}\right)}, \tag{3.106}$$

$$\left[\underline{\underline{\mathbf{S}}}^{(esh)}\right]_{33} = \frac{3c^2 I_{\gamma\gamma} + \left(1-2\nu^{(1)}\right) I_\gamma}{8\pi\left(1-\nu^{(1)}\right)}, \tag{3.107}$$

$$\left[\underline{\underline{\mathbf{S}}}^{(esh)}\right]_{44} = \frac{3(b^2+c^2) I_{\beta\gamma} + \left(1-2\nu^{(1)}\right)\left(I_\beta + I_\gamma\right)}{16\pi\left(1-\nu^{(1)}\right)}, \tag{3.108}$$

$$\left[\underline{\underline{\mathbf{S}}}^{(esh)}\right]_{55} = \frac{3(a^2+c^2) I_{\alpha\gamma} + \left(1-2\nu^{(1)}\right)\left(I_\alpha + I_\gamma\right)}{16\pi\left(1-\nu^{(1)}\right)}, \tag{3.109}$$

$$\left[\underline{\underline{\mathbf{S}}}^{(esh)}\right]_{66} = \frac{3(a^2+b^2) I_{\alpha\beta} + \left(1-2\nu^{(1)}\right)\left(I_\alpha + I_\beta\right)}{16\pi\left(1-\nu^{(1)}\right)}, \tag{3.110}$$

where $\nu^{(1)} = \dfrac{\lambda^{(1)}}{2\left(\lambda^{(1)}+\mu^{(1)}\right)}$ is the Poisson ratio of component material '1'. For

the case $a > b > c$ we have

$$\left.\begin{aligned}
I_\alpha &= \frac{4\pi abc}{(a^2-b^2)(a^2-c^2)^{1/2}}\,[\,F^{\sim}(\theta^{\sim},k^{\sim})-E^{\sim}(\theta^{\sim},k^{\sim})] \\
I_\gamma &= \frac{4\pi abc}{(b^2-c^2)(a^2-c^2)^{1/2}}\left[\,\frac{b}{ac}(a^2-c^2)^{1/2}-E^{\sim}(\theta^{\sim},k^{\sim})\right] \\
I_\beta &= 4\pi-(I_\alpha+I_\gamma), \qquad I_{\alpha\beta}=\frac{I_\alpha-I_\beta}{3(b^2-a^2)}, \\
I_{\alpha\gamma} &= \frac{I_\alpha-I_\gamma}{3(c^2-a^2)}, \qquad I_{\beta\gamma}=\frac{I_\beta-I_\gamma}{3(c^2-b^2)} \\
I_{\alpha\alpha} &= \frac{4\pi}{3a^2}-(I_{\alpha\beta}+I_{\alpha\gamma}), \qquad I_{\beta\beta}=\frac{4\pi}{3b^2}-(I_{\alpha\beta}+I_{\beta\gamma}), \\
I_{\gamma\gamma} &= \tfrac{4\pi}{3c^2}-(I_{\alpha\gamma}+I_{\beta\gamma})
\end{aligned}\right\}, \tag{3.111}$$

with the elliptic integrals given by

$$\left.\begin{aligned}
E^{\sim}(\theta^{\sim},k^{\sim}) &= \int_0^{\theta^{\sim}} d\phi\;(1-[k^{\sim}]^2\sin^2\phi)^{1/2} \\
F^{\sim}(\theta^{\sim},k^{\sim}) &= \int_0^{\theta^{\sim}} d\phi(1-[k^{\sim}]^2\sin^2\phi)^{-1/2}
\end{aligned}\right\}, \tag{3.112}$$

wherein

$$\theta^{\sim}=\sin^{-1}\frac{(a^2-c^2)^{1/2}}{a}, \qquad k^{\sim}=\frac{(a^2-b^2)^{1/2}}{(a^2-c^2)^{1/2}}. \tag{3.113}$$

3.3.2 The Hashin–Shtrikman bounds

The well known Hashin-Shtrikman (HS) bounds [2, 15] are bounds on $\kappa^{(hcm)}$ and $\mu^{(hcm)}$. The upper HS bounds are given by

$$\mu^{(HS\,upper)} \le f^{(1)}\mu^{(1)}+f^{(2)}\mu^{(2)}-\frac{f^{(1)}f^{(2)}\left(\mu^{(1)}-\mu^{(2)}\right)^2}{f^{(1)}\mu^{(2)}+f^{(2)}\mu^{(1)}+\frac{\mu^{(2)}\left(9\kappa^{(2)}+8\mu^{(2)}\right)}{\left[6\left(\kappa^{(2)}+2\mu^{(2)}\right)\right]}} \tag{3.114}$$

$$\kappa^{(HS\,upper)} \le f^{(1)}\kappa^{(1)}+f^{(2)}\kappa^{(2)}-\frac{f^{(1)}f^{(2)}\left(\kappa^{(1)}-\kappa^{(2)}\right)^2}{f^{(1)}\kappa^{(2)}+f^{(2)}\kappa^{(1)}+4\mu^{(2)}/3} \tag{3.115}$$

with $\kappa^{(\ell)}=\lambda^{(\ell)}+2\mu^{(\ell)}/3$ for $\ell=(1,\,2)$. With the lower HS bounds given by

$$\mu^{(HS\,lower)} \ge f^{(1)}\mu^{(1)}+f^{(2)}\mu^{(2)}-\frac{f^{(1)}f^{(2)}\left(\mu^{(1)}-\mu^{(2)}\right)^2}{f^{(1)}\mu^{(2)}+f^{(2)}\mu^{(1)}+\frac{\mu^{(1)}\left(9\kappa^{(1)}+8\mu^{(1)}\right)}{\left[6\left(\kappa^{(1)}+2\mu^{(1)}\right)\right]}} \tag{3.116}$$

and

$$\kappa^{(HS\,lower)} \geq f^{(1)}\kappa^{(1)} + f^{(2)}\kappa^{(2)} - \frac{f^{(1)}f^{(2)}\left(\kappa^{(1)} - \kappa^{(2)}\right)^2}{f^{(1)}\kappa^{(2)} + f^{(2)}\kappa^{(1)} + 4\mu^{(1)}/3}. \tag{3.117}$$

As a further check on the validity of our results, for $\underline{\underline{\mathbf{C}}}^{(ocm)}$ with $\underline{\underline{\mathbf{C}}}^{(1,2)}$ isotropic, we compare $\mu^{(HS\,lower)}$ and $\mu^{(HS\,upper)}$ with $\left[\underline{\underline{\mathbf{C}}}^{(ocm)}\right]_{44}$ along with comparing $\left[\underline{\underline{\mathbf{C}}}^{(ocm)}\right]_{11}$ to $\left\{\kappa^{(HS\,lower)} + \frac{4}{3}\mu^{(HS\,lower)}\right\}$ and $\left\{\kappa^{(HS\,upper)} + \frac{4}{3}\mu^{(HS\,upper)}\right\}$.

3.4 Numerical results

In this section, we present the 9×9 stiffness matrix of the HCM, namely $\underline{\underline{\mathbf{C}}}^{(hcm)}$, as estimated by the lowest–order SPFT (i.e., $hcm = ocm$), the second–order SPFT (i.e., $hcm = spft$) and the Mori–Tanaka mean–field formalism (i.e., $hcm = MT$). The matrix $\underline{\underline{\mathbf{C}}}^{(hcm)}$ generally has the orthotropic form represented in (3.13) with $\ell = hcm$. We also present the second–order SPFT density tensor $\rho_{mp}^{(spft)}$; numerical results for the lowest–order SPFT density $\rho^{(ocm)}$ need not be presented here as that quantity is simply the volume average of the densities of the component materials. For all second–order SPFT computations, we selected $\omega = 2\pi \times 10^6$ s^{-1}. Throughout the results we construct the composite by randomly distributing particles of component material '2' in a matrix of component material '1'.

3.4.1 Isotropic component materials distributed as oriented ellipsoidal particles

Let us begin by considering the scenario in which the component materials are both isotropic. The component material '1' is taken to be acetal (i.e., $\lambda^{(1)} = \lambda^{(ace)}$, $\mu^{(1)} = \mu^{(ace)}$ and $\rho^{(1)} = \rho^{(ace)}$), and component material '2' to be glass (i.e., $\lambda^{(2)} = \lambda^{(gla)}$, $\mu^{(2)} = \mu^{(gla)}$ and $\rho^{(2)} = \rho^{(gla)}$). The Lamé constants and densities for these two materials are as follows [46, 47]:

$$\left.\begin{array}{lll} \lambda^{(ace)} = 2.68\ \mathrm{GPa}, & \mu^{(ace)} = 1.15\ \mathrm{GPa}, & \rho^{(ace)} = 1.43 \times 10^3\ \mathrm{kg\,m^{-3}} \\ \lambda^{(gla)} = 21.73\ \mathrm{GPa}, & \mu^{(gla)} = 29.2\ \mathrm{GPa}, & \rho^{(gla)} = 2.23 \times 10^3\ \mathrm{kg\,m^{-3}} \end{array}\right\}. \tag{3.118}$$

The eccentricities of the ellipsoidal inclusion particles are specified by the parameters $\{a, b, c\}$, per (3.8) and (3.9).

In Fig. 3.1 the components of the HCM stiffness matrix $\underline{\underline{\mathbf{C}}}^{(hcm)}$, as computed using the lowest–order SPFT and the Mori–Tanaka formalism, are plotted as functions of volume fraction $f^{(2)}$ for the case $a = b = c$. Since the HCM is isotropic in this case, only the components $\left[\underline{\underline{\mathbf{C}}}^{(hcm)}\right]_{11} \equiv \lambda^{(hcm)} + 2\mu^{(hcm)}$, $\left[\underline{\underline{\mathbf{C}}}^{(hcm)}\right]_{12} \equiv \lambda^{(hcm)}$ and $\left[\underline{\underline{\mathbf{C}}}^{(hcm)}\right]_{44} \equiv \mu^{(hcm)}$ are presented, per (3.14) with $\ell = hcm$. Notice that the following limits necessarily apply for both the SPFT and Mori–Tanaka estimates:

$$\lim_{f^{(2)}\to 0} \underline{\underline{\mathbf{C}}}^{(hcm)} = \underline{\underline{\mathbf{C}}}^{(1)}, \qquad \lim_{f^{(2)}\to 1} \underline{\underline{\mathbf{C}}}^{(hcm)} = \underline{\underline{\mathbf{C}}}^{(2)}. \tag{3.119}$$

It is apparent from Fig. 3.1 that, while the lowest–order SPFT and the Mori–Tanaka estimates are qualitatively similar, the Mori–Tanaka estimates display a greater deviation from the naive HCM estimate $f^{(1)}\left[\underline{\underline{\mathbf{C}}}^{(1)}\right]_{pq} + f^{(2)}\left[\underline{\underline{\mathbf{C}}}^{(2)}\right]_{pq}$ for mid–range values of $f^{(2)}$. For further comparison in this isotropic scenario, the familiar variational bounds on $\left[\underline{\underline{\mathbf{C}}}^{(hcm)}\right]_{11}$ and $\left[\underline{\underline{\mathbf{C}}}^{(hcm)}\right]_{44}$ established by Hashin and Shtrikman, §3.3.2 [2, 15], are also presented in Fig. 3.1: the lower Hashin–Shtrikman bound coincides with the Mori–Tanaka estimate and the lowest–order SPFT estimate lies within the upper and lower Hashin–Shtrikman bounds for all values of $f^{(2)}$.

The corresponding lowest–order SPFT and Mori–Tanaka estimates for the orthotropic HCM arising from the distribution of ellipsoidal inclusion particles described by $\{a/c = 5,\ b/c = 1.5\}$ are presented in Fig. 3.2. The degree of orthotropy exhibited by the HCM can be gauged by relative differences in the values of $\left[\underline{\underline{\mathbf{C}}}^{(hcm)}\right]_{pq}$ for $pq \in \{11, 22, 33\}$; and similarly by relative differences in $\left[\underline{\underline{\mathbf{C}}}^{(hcm)}\right]_{pq}$ for $pq \in \{44, 55, 66\}$ and by relative differences in $\left[\underline{\underline{\mathbf{C}}}^{(hcm)}\right]_{pq}$ for $pq \in \{12, 13, 23\}$. These relative differences are greatest for mid–range values of the volume fraction $f^{(2)}$.

The orthotropic nature of the HCM is accentuated by using more eccentrically–shaped inclusion particles. This is illustrated by Fig. 3.3, which shows results computed for the same scenario as for Fig. 3.2 but with ellipsoidal particles described by $\{a/c = 10,\ b/c = 2\}$. A comparison of Figs. 3.1–3.3 reveals that differences be-

tween the estimates of the lowest–order SPFT and the Mori–Tanaka mean–field formalism increase as the orthotropic nature of the HCM is accentuated.

Now let us turn to the second–order SPFT estimates of the HCM constitutive parameters. We considered these quantities as functions of $\bar{k}L$, where

$$\bar{k} = \frac{\omega}{4}\left(\sqrt{\frac{\rho^{(1)}}{\lambda^{(1)}+2\mu^{(1)}}}+\sqrt{\frac{\rho^{(1)}}{\mu^{(1)}}}+\sqrt{\frac{\rho^{(2)}}{\lambda^{(2)}+2\mu^{(2)}}}+\sqrt{\frac{\rho^{(2)}}{\mu^{(2)}}}\right) \tag{3.120}$$

is an approximate wavenumber calculated as the average of the shear and longitudinal wavenumbers in the component materials, and L is the correlation length associated with the two–point covariance function (3.12). Fig. 3.4 shows the real and imaginary parts of the components of $\underline{\underline{\tilde{\mathbf{C}}}}^{(spft)} = \underline{\underline{\mathbf{C}}}^{(spft)} - \underline{\underline{\mathbf{C}}}^{(ocm)}$ plotted against $\bar{k}L$ for $f^{(2)} = 0.5$. The values of the shape parameters $\{a,\, b,\, c\}$ correspond to those used in the calculations for Figs. 3.1–3.3. Notice that

$$\lim_{L\to 0} \underline{\underline{\mathbf{C}}}^{(spft)} = \underline{\underline{\mathbf{C}}}^{(ocm)} \tag{3.121}$$

and

$$\left|\left[\underline{\underline{\tilde{\mathbf{C}}}}^{(spft)}\right]_{pq}\right| \ll \left|\left[\underline{\underline{\mathbf{C}}}^{(ocm)}\right]_{pq}\right| \tag{3.122}$$

for all values of the indexes p and q. Furthermore, for the particular example considered here, the magnitude of $\left[\underline{\underline{\tilde{\mathbf{C}}}}^{(spft)}\right]_{pq}$ generally decreases as the inclusion particles become more eccentric in shape.

A very striking feature of the second–order SPFT estimates presented in Fig. 3.4 is that

$$\text{Im}\,\left[\underline{\underline{\mathbf{C}}}^{(spft)}\right]_{pq} \neq 0, \tag{3.123}$$

whereas $\text{Im}\,\left[\underline{\underline{\mathbf{C}}}^{(1,2)}\right]_{pq} = \text{Im}\,\left[\underline{\underline{\mathbf{C}}}^{(ocm)}\right]_{pq} = 0$. Furthermore, the magnitude of $\text{Im}\,\left[\underline{\underline{\mathbf{C}}}^{(spft)}\right]_{pq}$ grows steadily as the correlation length increases. These observations may be interpreted in terms of losses due to scattering as follows. For all reported calculations, $\text{Re}\,\underline{\underline{\mathbf{C}}}^{(spft)}_{6\times 6}$ is positive–definite and $-\text{Im}\,\underline{\underline{\mathbf{C}}}^{(spft)}_{6\times 6}$ is positive–semi–definite, which together imply that the associated time–averaged strain energy and dissipated energy densities are positive–valued [33], as discussed

in §3.2.4. Accordingly, the emergence of nonzero imaginary parts of $\left[\underline{\underline{\mathbf{C}}}^{(spft)}\right]_{pq}$ indicates that the HCM has acquired a dissipative nature, despite the component materials being nondissipative. The dissipation must be a scattering loss, because the second–order SPFT accommodates interactions between spatially–distinct scattering centres via the two–point covariance function (3.12). As the correlation length increases, the number of scattering particles that can mutually interact also increases, thereby increasing the scattering loss per unit volume.

Lastly in this subsection, the real and imaginary parts of the second–order SPFT density tensor $\tilde{\rho}_{pq}^{(spft)} = \rho_{pq}^{(spft)} - \rho^{(ocm)}$ are plotted as functions of $\bar{k}L$ in Fig. 3.5. Only the $p = q$ components are presented, as the $p \neq q$ components are negligibly small. The density tensor exhibits characteristics similar to those of the corresponding stiffness tensor insofar as

$$\lim_{L \to 0} \rho_{pq}^{(spft)} = \rho^{(ocm)} \tag{3.124}$$

and

$$\left| \tilde{\rho}_{pq}^{(spft)} \right| \ll \left| \rho^{(ocm)} \right| \tag{3.125}$$

for all values of the indexes p and q. Also, $|\tilde{\rho}_{pq}^{(spft)}|$ generally decreases as the shape of the inclusion particles deviates further from spherical.

3.4.2 Orthotropic component materials distributed as spheres

Let us now explore the scenario wherein the component materials are orthotropic perturbations of the isotropic component materials considered in §3.4.1. In the notation of (3.13), we choose

$$\left.\begin{aligned} \underline{\underline{\mathcal{M}}}^{(1)} &= \begin{pmatrix} \wp^{(ace)}\,(1+\varsigma) & \lambda^{(ace)}\,(1-\varsigma) & \lambda^{(ace)}\,(1+2\varsigma) \\ \lambda^{(ace)}\,(1-\varsigma) & \wp^{(ace)}\left(1-\frac{1}{4}\varsigma\right) & \lambda^{(ace)}\left(1+\frac{1}{4}\varsigma\right) \\ \lambda^{(ace)}\,(1+2\varsigma) & \lambda^{(ace)}\left(1+\frac{1}{4}\varsigma\right) & \wp^{(ace)}\,(1-2\varsigma) \end{pmatrix} \\ \underline{\underline{\mathcal{D}}}^{(1)} &= \begin{pmatrix} \left(\mu^{(ace)}\right)(1-\varsigma) & 0 & 0 \\ 0 & \mu^{(ace)}\left(1-\frac{1}{2}\varsigma\right) & 0 \\ 0 & 0 & \mu^{(ace)}\left(1-\frac{2}{3}\varsigma\right) \end{pmatrix} \end{aligned}\right\} \tag{3.126}$$

and

$$\left.\begin{array}{l} \underline{\underline{\mathcal{M}}}^{(2)} = \begin{pmatrix} \wp^{(gla)}\,(1+2\varsigma) & \lambda^{(gla)}\,(1-2\varsigma) & \lambda^{(gla)}\left(1+\frac{1}{2}\varsigma\right) \\ \lambda^{(gla)}\,(1-2\varsigma) & \wp^{(gla)}\left(1+\frac{1}{3}\varsigma\right) & \lambda^{(gla)}\left(1-\frac{1}{3}\varsigma\right) \\ \lambda^{(gla)}\left(1+\frac{1}{2}\varsigma\right) & \lambda^{(gla)}\left(1-\frac{1}{3}\varsigma\right) & \wp^{(gla)}\left(1-\frac{1}{2}\varsigma\right) \end{pmatrix} \\ \underline{\underline{\mathcal{D}}}^{(2)} = \begin{pmatrix} \left(\mu^{(gla)}\right)\left(1-\frac{3}{2}\varsigma\right) & 0 & 0 \\ 0 & \mu^{(gla)}\left(1-\frac{4}{5}\varsigma\right) & 0 \\ 0 & 0 & \mu^{(gla)}\left(1-\frac{2}{3}\varsigma\right) \end{pmatrix} \end{array}\right\}, \tag{3.127}$$

where the real–valued scalar ς controls the degree of orthotropy and $\wp^{(\ell)} = \lambda^{(\ell)} + 2\mu^{(\ell)}$ for $\ell =$ gla, ace. As in §3.4.1, the densities of the component materials are taken to be $\rho^{(1)} = \rho^{(ace)}$ and $\rho^{(2)} = \rho^{(gla)}$. Component material '2' is distributed as spherical inclusion particles (i.e., $a = b = c$).

The lowest–order SPFT and Mori–Tanaka estimates for the HCM arising from orthotropic component materials characterized by $\varsigma = 0.05$ and $\varsigma = 0.1$ are presented in Fig. 3.6 and 3.7, respectively. The plots for $\varsigma = 0$, for which case the HCM is isotropic, are the ones displayed in Fig. 3.1. The degree of orthotropy exhibited by the HCM clearly increases as the value of ς increases, as do differences between the estimates of the lowest–order SPFT and the Mori–Tanaka mean–field formalism. In a manner resembling the scenario considered in §3.4.1, the lowest–order SPFT and the Mori–Tanaka estimates are qualitatively similar, but the Mori–Tanaka estimates display a greater deviation from the naive HCM estimate $f^{(1)}\left[\underline{\underline{\mathbf{C}}}^{(1)}\right]_{pq} + f^{(2)}\left[\underline{\underline{\mathbf{C}}}^{(2)}\right]_{pq}$ for mid–range values of $f^{(2)}$, at all values of ς.

The degree of orthotropy exhibited by the HCM clearly increases as the value of ς increases, and differences between the estimates of the lowest–order SPFT and the Mori–Tanaka mean–field formalism also vary as ς increases. To explore this matter further, the associated ratios

$$\frac{\left[\underline{\underline{\mathbf{C}}}^{(hcm)}\right]_{11}}{\left[\underline{\underline{\mathbf{C}}}^{(hcm)}\right]_{33}}, \quad \frac{\left[\underline{\underline{\mathbf{C}}}^{(hcm)}\right]_{12}}{\left[\underline{\underline{\mathbf{C}}}^{(hcm)}\right]_{23}} \quad \text{and} \quad \frac{\left[\underline{\underline{\mathbf{C}}}^{(hcm)}\right]_{44}}{\left[\underline{\underline{\mathbf{C}}}^{(hcm)}\right]_{66}}$$

are plotted against $f^{(2)}$ for $\varsigma = 0.05$ and 0.1, in Fig. 3.8. The three different pat-

terns are portrayed in the three plots: for $\left[\underline{\underline{\mathbf{C}}}^{(hcm)}\right]_{11}/\left[\underline{\underline{\mathbf{C}}}^{(hcm)}\right]_{33}$ differences between the lowest–order SPFT and the Mori–Tanaka estimates are larger for when the HCM is more orthotropic; the reverse is the case for $\left[\underline{\underline{\mathbf{C}}}^{(hcm)}\right]_{12}/\left[\underline{\underline{\mathbf{C}}}^{(hcm)}\right]_{23}$, while for $\left[\underline{\underline{\mathbf{C}}}^{(hcm)}\right]_{44}/\left[\underline{\underline{\mathbf{C}}}^{(hcm)}\right]_{66}$ there is no noticeable difference between the lowest–order SPFT and Mori–Tanaka estimates as the degree of HCM orthotropy is increased.

Next we focus on the second–order SPFT estimate of the HCM stiffness tensor. The real and imaginary parts of the components of $\underline{\underline{\tilde{\mathbf{C}}}}^{(spft)} = \underline{\underline{\mathbf{C}}}^{(spft)} - \underline{\underline{\mathbf{C}}}^{(ocm)}$ are graphed against $\bar{k}L$ in Fig. 3.9. The volume fraction is fixed at $f^{(2)} = 0.5$. The values of the orthotropy parameter ς are 0, 0.05 and 0.1, in correspondence with the calculations of Figs. 3.1, 3.6 and 3.7. As we observed in §3.4.1, the magnitude of the components of $\underline{\underline{\tilde{\mathbf{C}}}}^{(spft)}$ generally decrease as the HCM becomes more orthotropic. Also, the second–order SPFT estimate $\underline{\underline{\mathbf{C}}}^{(spft)}$ has components with nonzero imaginary parts, which implies that the HCM is dissipative even though the component materials are nondissipative. Furthermore, the HCM becomes increasingly dissipative as the correlation length increases, this dissipation being attributable to scattering losses.

Finally, the real and imaginary parts of the second–order SPFT density tensor $\tilde{\rho}_{pq}^{(spft)} = \rho_{pq}^{(spft)} - \rho^{(ocm)}$ are plotted as functions of $\bar{k}L$ in Fig. 3.10. As previously, §3.4.1, the components for $p \neq q$ are negligibly small so only the $p = q$ components are provided here. The density plots resemble those of the corresponding stiffness tensor; i.e., the components $\tilde{\rho}_{pp}^{(spft)}$ are much smaller than $\rho^{(ocm)}$ and they increase rapidly from zero as L increases. The magnitudes of $\tilde{\rho}_{pp}^{(spft)}$ are smallest when the orthotropy parameter describing the component materials is greatest. Apparent contradictions abound in homogenization theory [1], but for the SPFT as with many other formalisms the ultimate test of their validity is against a battery of experimental tests which, as far as we are aware, do not exist at present.

3.5 Closing remarks

The elastodynamic SPFT has been further developed, in order to undertake numerical studies based on a specific choice of two–point covariance function. From

our theoretical considerations in §3.2 and our representative numerical studies in §3.4, the following conclusions were drawn:

- The lowest–order SPFT estimate of the HCM stiffness tensor is qualitatively similar to that provided by the Mori–Tanaka mean–field formalism.

- Differences between the estimates of the lowest–order SPFT and the Mori–Tanaka mean–field formalism are greatest for mid–range values of the volume fraction.

- Differences between the estimates of the lowest–order SPFT and the Mori–Tanaka mean–field formalism vary as the HCM becomes more orthotropic. The degree of orthotropy of the HCM may be increased by increasing either the degree of orthotropy of component materials or the degree of eccentricity (nonsphericity) of the inclusion particles.

- The second–order SPFT provides a correction to the quasi–static lowest–order estimates of the HCM stiffness tensor and density.

- The correction provided by second–order SPFT, though relatively small in magnitude, is highly significant as it indicates effective dissipation due to scattering loss.

- Differences between the second–order and lowest–order SPFT estimates of the HCM constitutive parameters diminish as the HCM becomes more orthotropic.

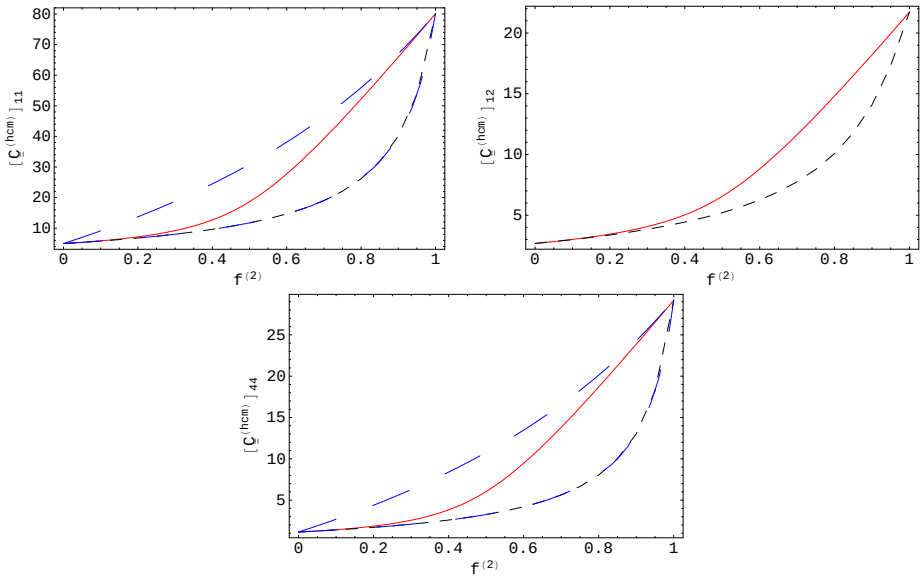

Figure 3.1: Plots of $\left[\underline{\underline{\mathbf{C}}}^{(hcm)}\right]_{11}$, $\left[\underline{\underline{\mathbf{C}}}^{(hcm)}\right]_{12}$ and $\left[\underline{\underline{\mathbf{C}}}^{(hcm)}\right]_{44}$ (in GPa) as estimated using the lowest–order SPFT (i.e., $hcm = ocm$) (red, solid curves) and the Mori–Tanaka mean–field formalism (i.e., $hcm = MT$) (black, dashed curves), against the volume fraction of component material '2'. Also plotted are the upper and lower Hashin–Shtrikman bounds (blue, long dashed curves) for $\left[\underline{\underline{\mathbf{C}}}^{(hcm)}\right]_{11}$ and $\left[\underline{\underline{\mathbf{C}}}^{(hcm)}\right]_{44}$; the lower Hashin–Shtrikman bounds coincide with the Mori–Tanaka estimates. Component material '1' is acetal and component material '2' is glass, as specified in (3.118). The component materials are distributed as spheres (i.e., $a = b = c$).

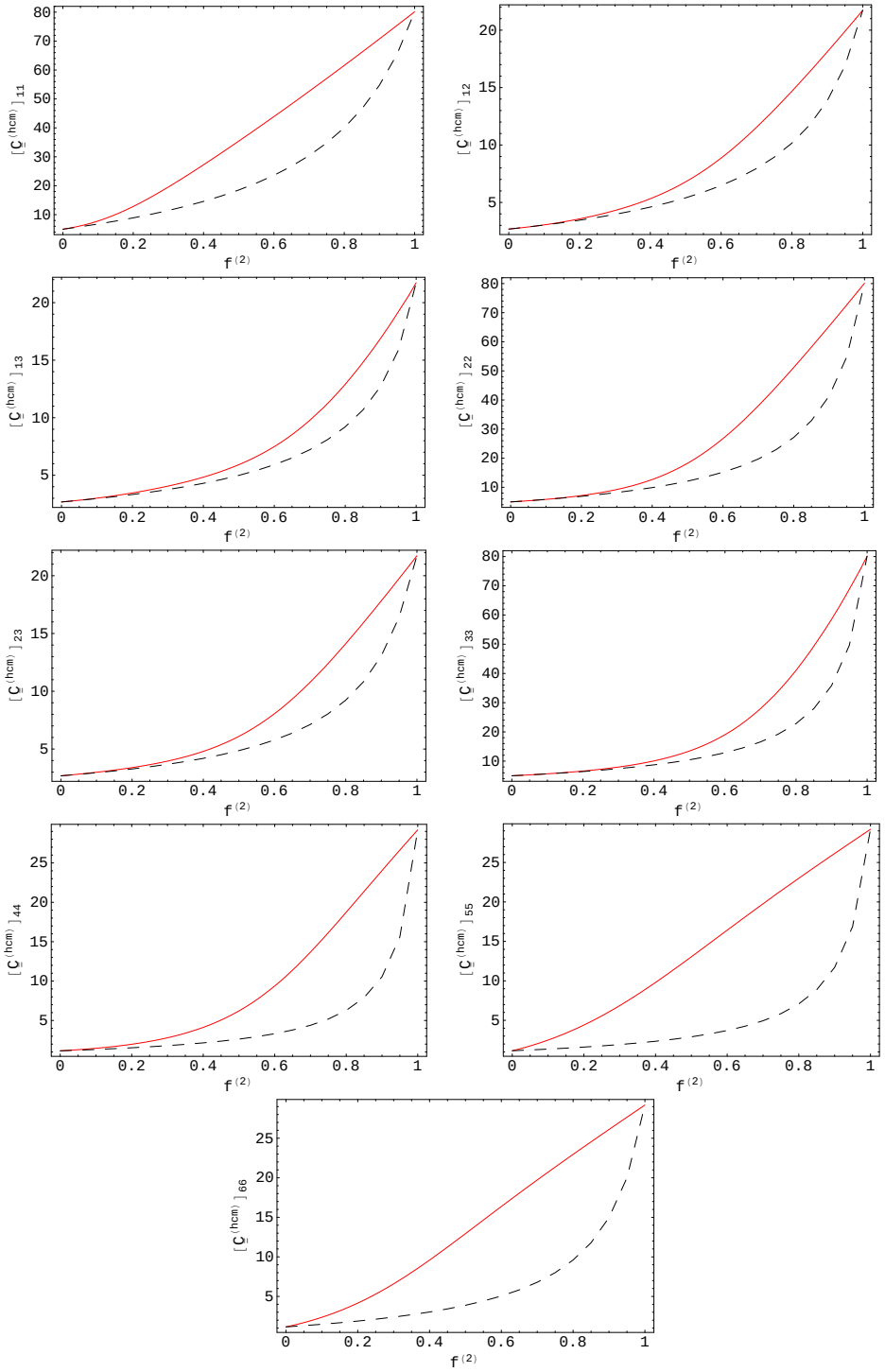

Figure 3.2: Plots of $\left[\underline{\underline{\mathbf{C}}}^{(hcm)}\right]_{rs}$, with $rs \in \{11, 12, 13, 22, 23, 33, 44, 55, 66\}$ (in GPa) as estimated using the lowest–order SPFT (i.e., $hcm = ocm$) (red, solid curves) and the Mori–Tanaka mean–field formalism (i.e., $hcm = MT$) (black, dashed curves), against the volume fraction of component material '2'. Component material '1' is acetal and component material '2' is glass, as specified in (3.118). The component materials are distributed as ellipsoids with $a/c = 5$ and $b/c = 1.5$.

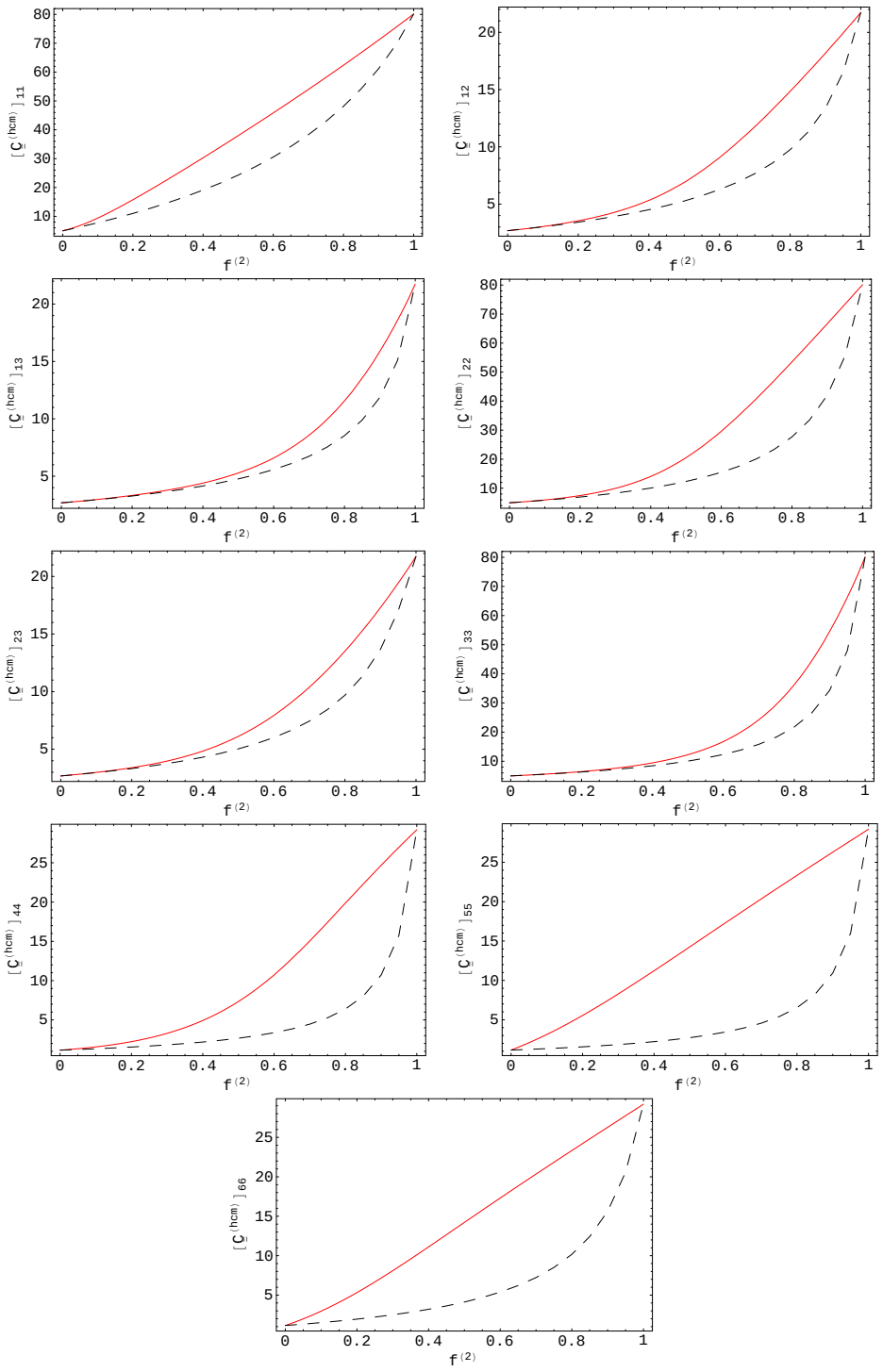

Figure 3.3: As Fig. 3.2 but for ellipsoidal component particles specified by $a/c = 10$ and $b/c = 2$.

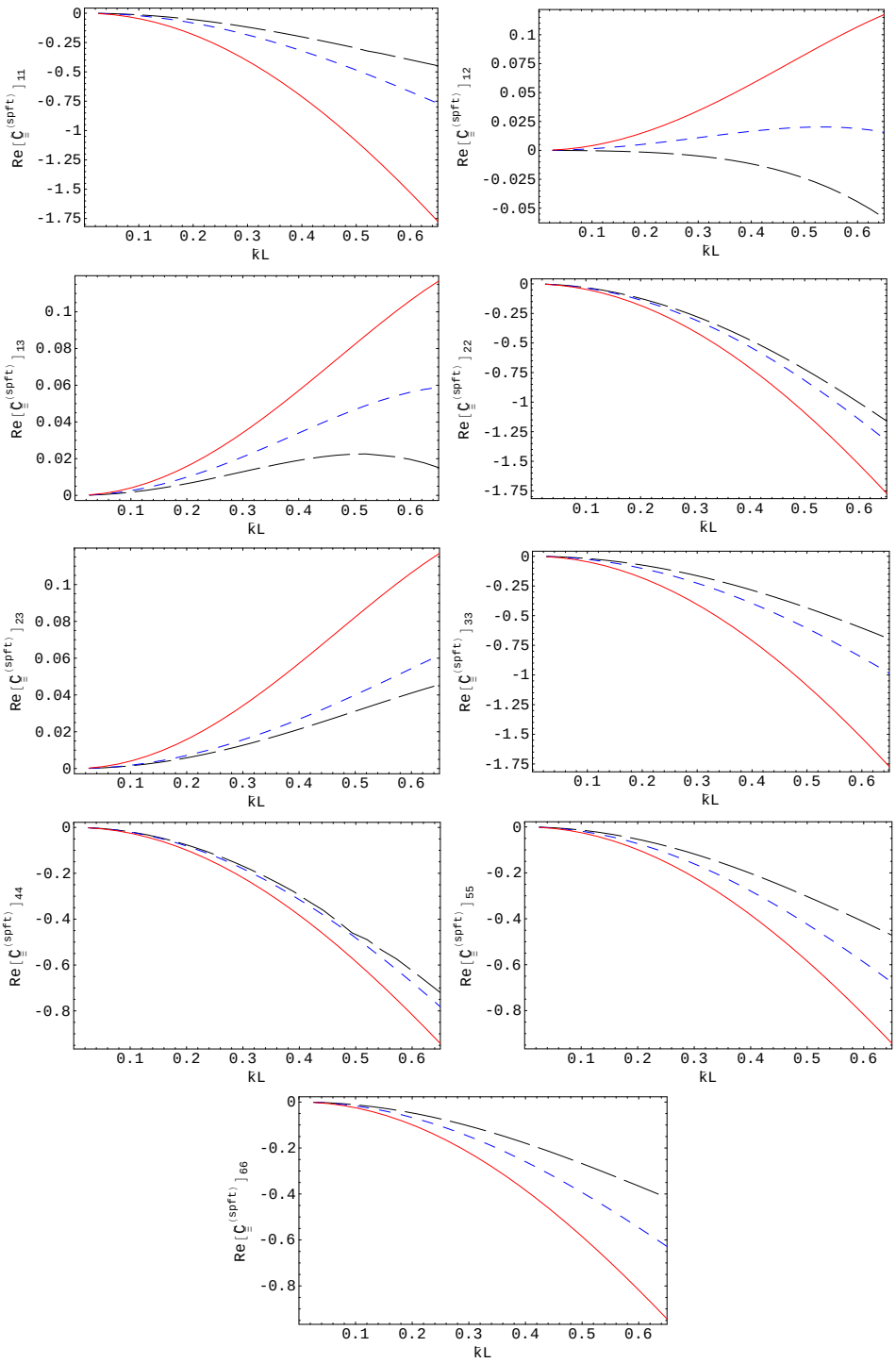

Figure 3.4: The real and imaginary parts of the components of $\underline{\underline{\tilde{\mathbf{C}}}}^{(spft)} = \underline{\underline{\mathbf{C}}}^{(spft)} - \underline{\underline{\mathbf{C}}}^{(ocm)}$ (in GPa), plotted as functions of $\bar{k}L$, for $f^{(2)} = 0.5$. Component material '1' is acetal and component material '2' is glass, as specified in (3.118). The component materials are distributed as (i) spheres (i.e., $a = b = c$) (red, solid curves), or (ii) ellipsoids with shape parameters $\{a/c = 5,\ b/c = 1.5\}$ (blue, short–dashed curves), or (iii) ellipsoids with shape parameters $\{a/c = 10,\ b/c = 2\}$ (black, long–dashed curves).

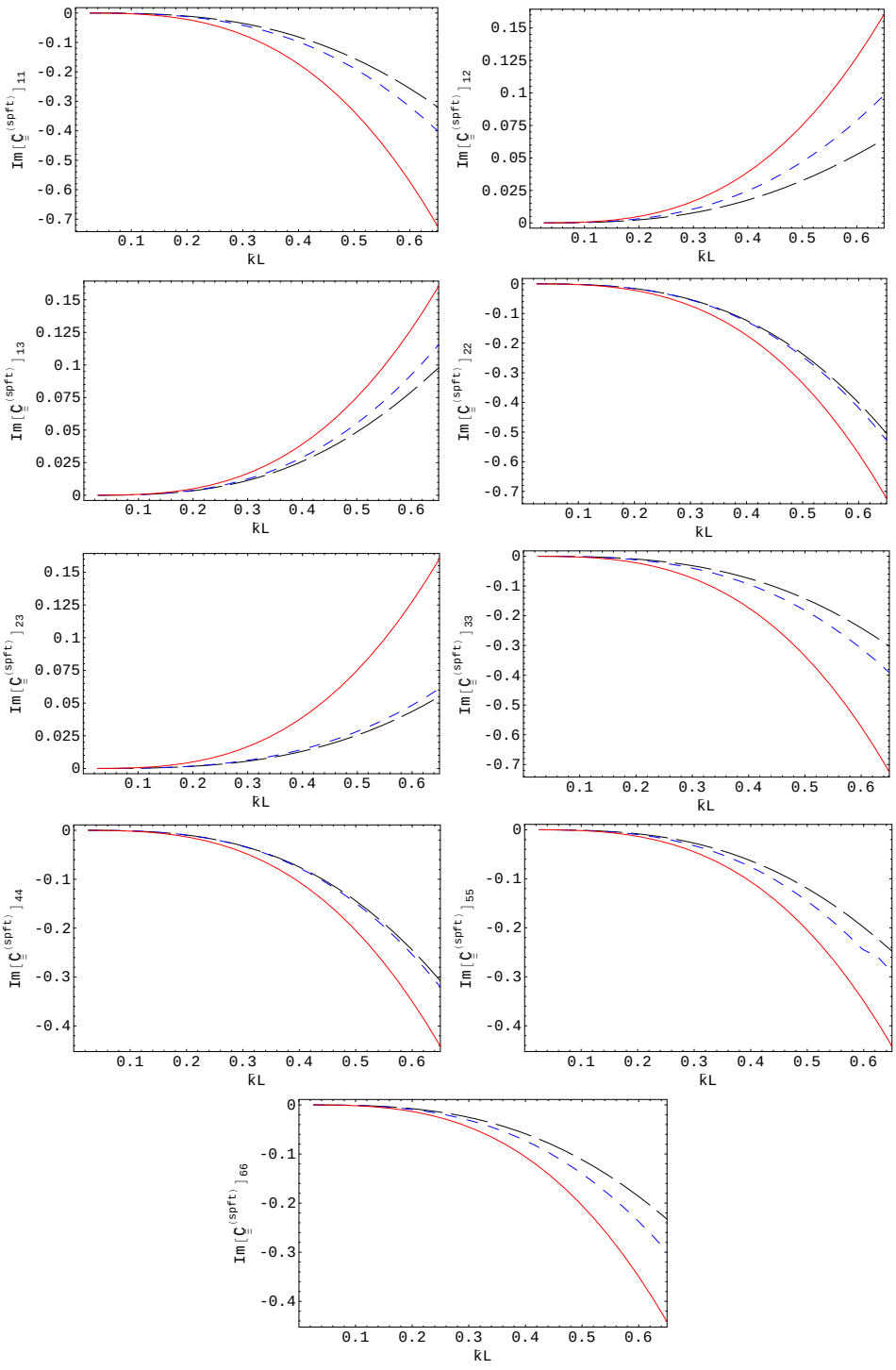

Figure 3.4: Continued.

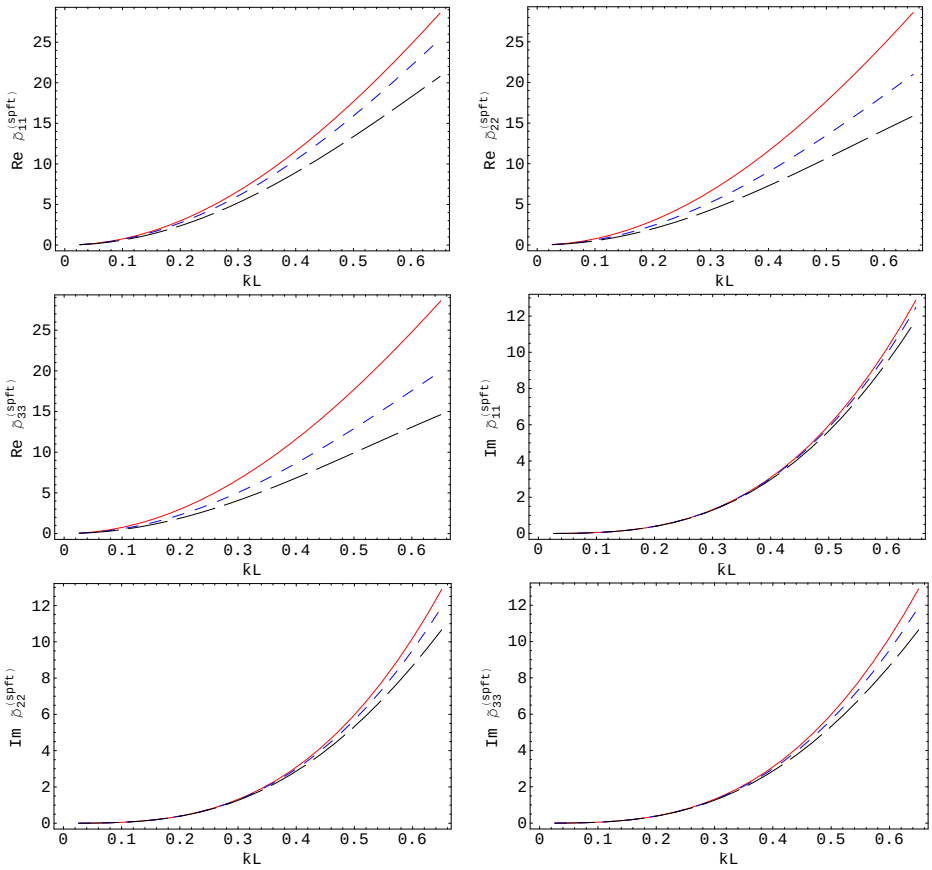

Figure 3.5: As Fig. 3.4 but the quantities plotted are the real and imaginary parts of the excess of the second–order SPFT density tensor over the density of the comparison material, i.e., $\tilde{\rho}_{rr}^{(spft)} = \rho_{rr}^{(spft)} - \rho^{(ocm)}$, $(r \in \{1, 2, 3\})$, in $\mathrm{kg\,m^{-3}}$.

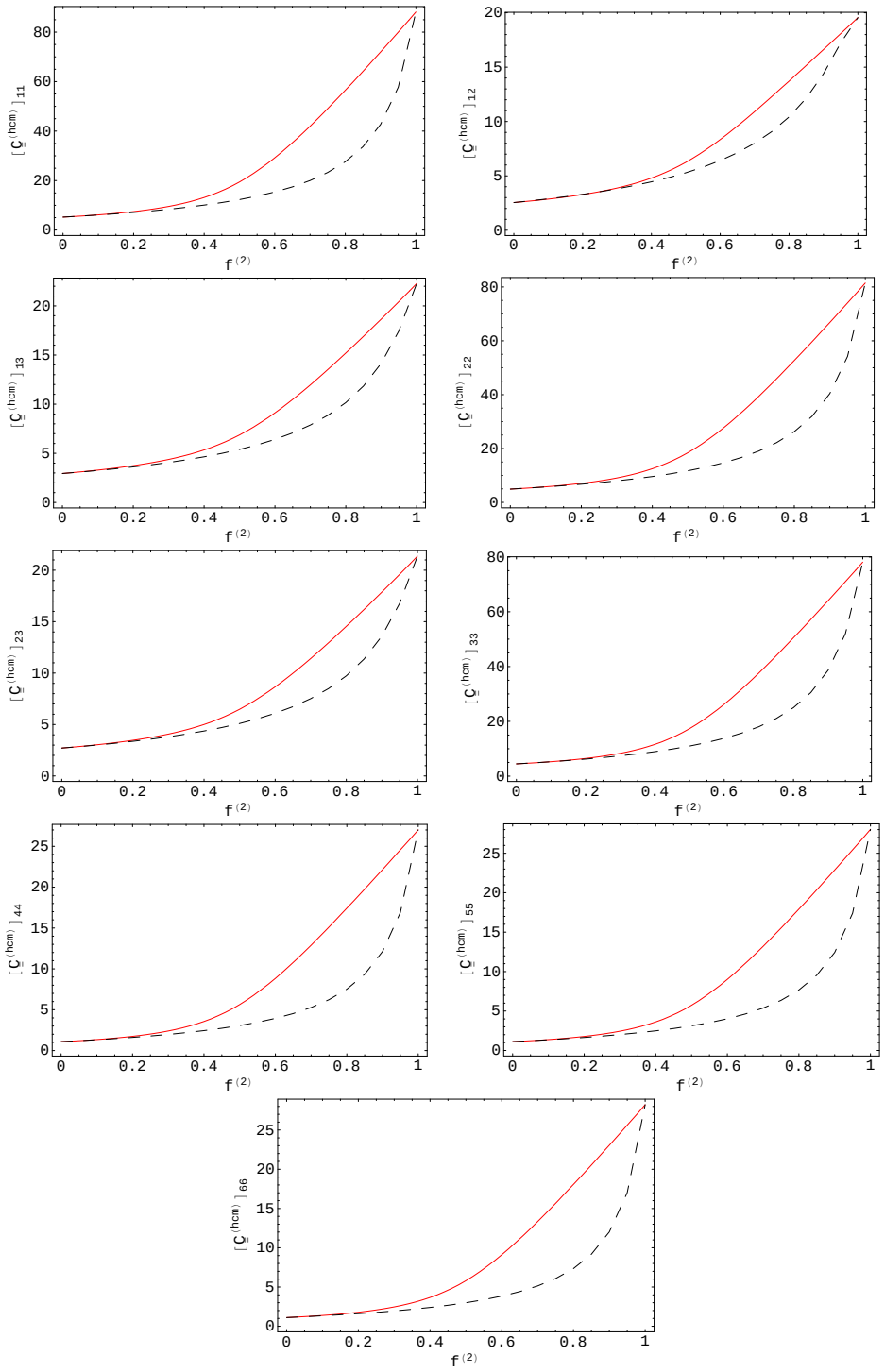

Figure 3.6: Plots of $\left[\underline{\underline{\mathbf{C}}}^{(hcm)}\right]_{rs}$, with $rs \in \{11, 12, 13, 22, 23, 33, 44, 55, 66\}$ (in GPa) as estimated using the lowest–order SPFT (i.e., $hcm = ocm$) (red, solid curves) and the Mori–Tanaka mean–field formalism (i.e., $hcm = MT$) (black, dashed curves), against the volume fraction of component material '2'. The component materials are distributed as spheres. Their constitutive parameters are specified by (3.126) and (3.127), with the orthotropy parameter $\varsigma = 0.05$.

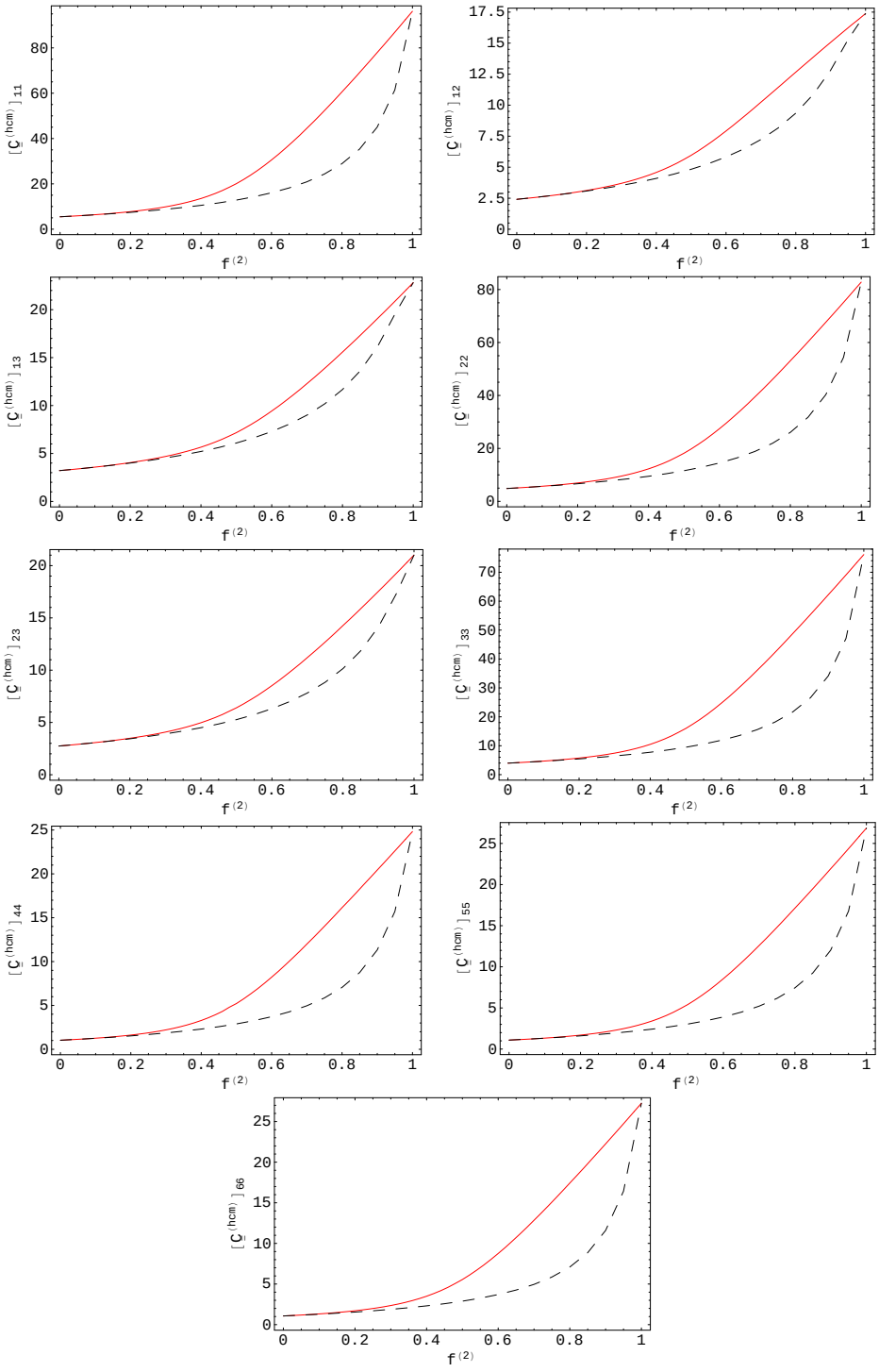

Figure 3.7: As Fig. 3.6 but with orthotropy parameter $\varsigma = 0.1$.

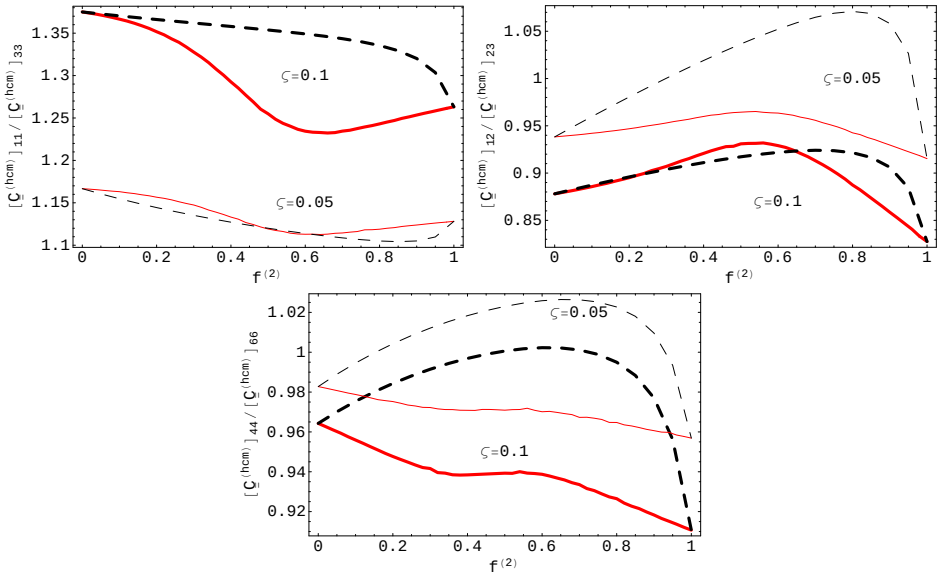

Figure 3.8: Plot of $\left[\underline{\underline{\mathbf{C}}}^{(hcm)}\right]_{11} / \left[\underline{\underline{\mathbf{C}}}^{(hcm)}\right]_{33}$, $\left[\underline{\underline{\mathbf{C}}}^{(hcm)}\right]_{12} / \left[\underline{\underline{\mathbf{C}}}^{(hcm)}\right]_{23}$ and $\left[\underline{\underline{\mathbf{C}}}^{(hcm)}\right]_{44} / \left[\underline{\underline{\mathbf{C}}}^{(hcm)}\right]_{66}$ (in GPa) as estimated using the lowest–order SPFT (i.e., $hcm = ocm$) (red, solid curves), the Mori–Tanaka mean–field formalism (i.e., $hcm = MT$) (black, dashed curves) against the volume fraction of component material '2'. Component material '1' is acetal and component material '2' is glass, as specified in (3.118). The component materials are distributed as spheres with the orthotropy parameter $\varsigma = 0.05$ (thin curves) and $\varsigma = 0.1$ (thick curves).

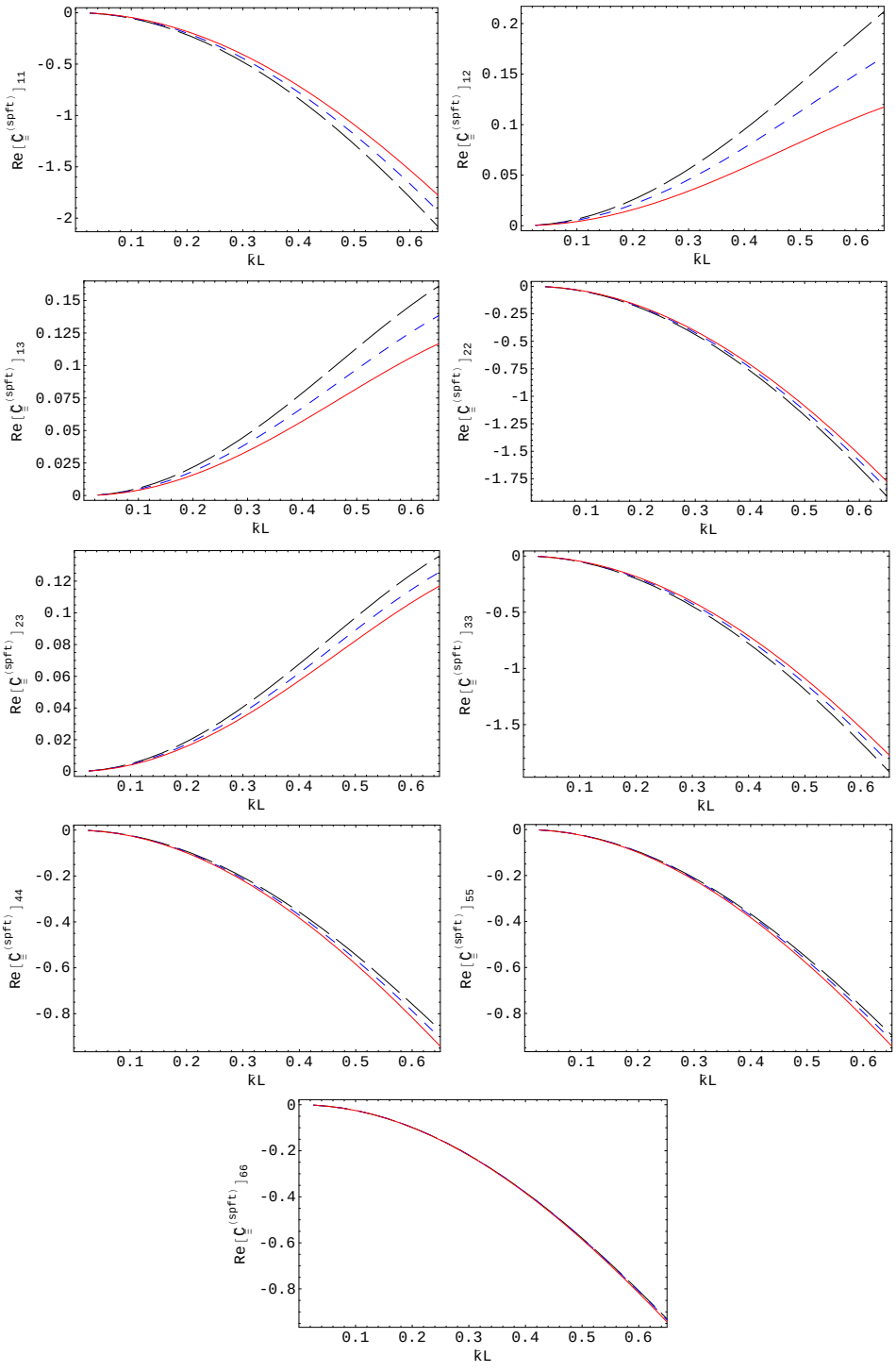

Figure 3.9: The real and imaginary parts of the components of $\underline{\underline{\tilde{\mathbf{C}}}}^{(spft)} = \underline{\underline{\mathbf{C}}}^{(spft)} - \underline{\underline{\mathbf{C}}}^{(ocm)}$ (in GPa) plotted as functions of $\bar{k}L$, for $f^{(2)} = 0.5$. The component materials are distributed as spheres. Their constitutive parameters are specified by (3.126) and (3.127), with the orthotropy parameter $\varsigma = 0$ (red, solid curves), $\varsigma = 0.05$ (blue, short-dashed curves) and $\varsigma = 0.1$ (black, long-dashed curves).

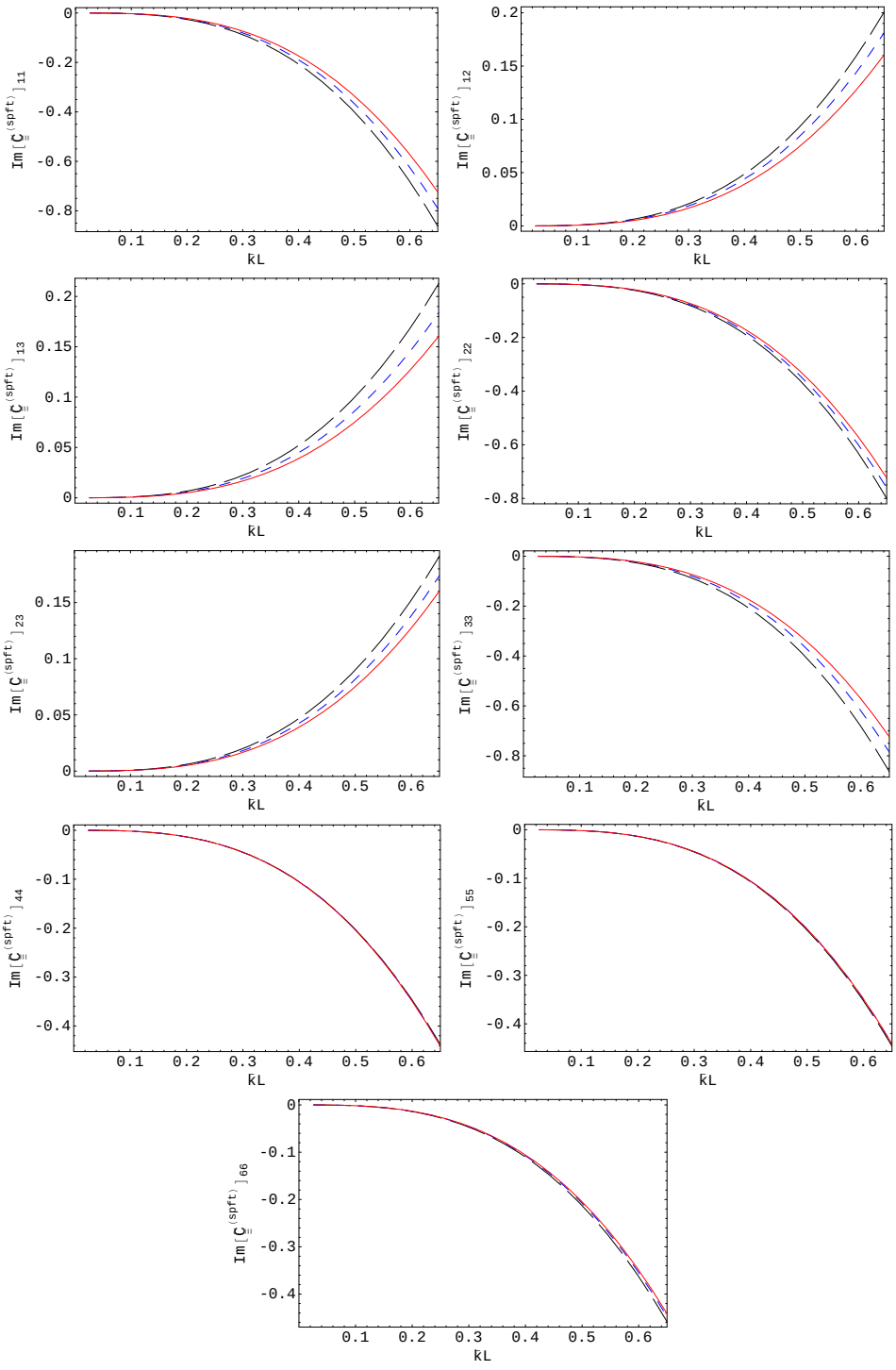

Figure 3.9: Continued.

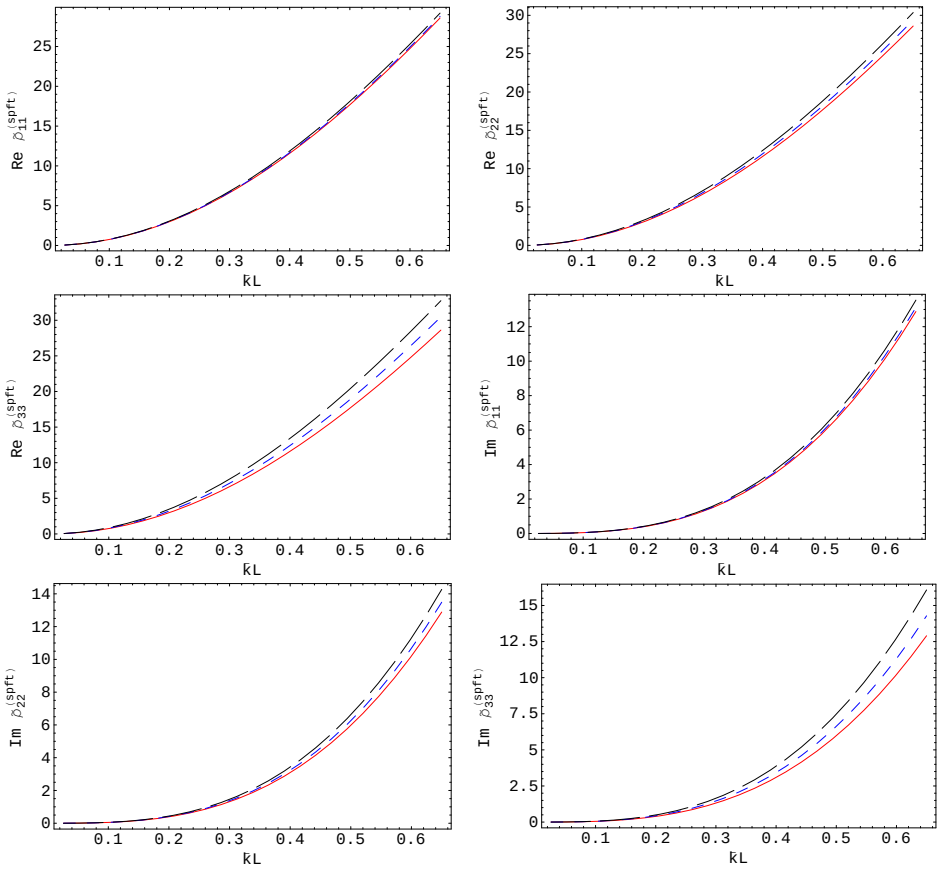

Figure 3.10: As Fig. 3.9 but the quantities plotted are the real and imaginary parts of the excess of the second–order SPFT density tensor over the density of the comparison material, i.e., $\tilde{\rho}_{rr}^{(spft)} = \rho_{rr}^{(spft)} - \rho^{(ocm)}$, $(r \in \{1, 2, 3\})$, in $\mathrm{kg\,m^{-3}}$.

Chapter 4

Derivation of Piezoelectric SPFT

4.1 Introduction

In this chapter we derive the piezoelectric SPFT estimate. The process followed is to extend the elastodynamic SPFT, developed by Zhuck and Lakhtakia [14]. We begin by converting the two constitutive piezoelectric equations to a single extended constitutive equation [48]. This allows the formulation of an equation of motion analogous to the elastodynamic equation of motion and enables us to use the methods of Zhuck and Lakhtakia [14].

We begin with the constitutive relations in piezoelectrics

$$\begin{aligned} \sigma_{lm}^{(\ell)}(\mathbf{r}) &= C_{lmpq}^{(\ell)} S_{pq}^{(\ell)}(\mathbf{r}) - e_{qlm}^{(\ell)} E_q^{(\ell)}(\mathbf{r}), \\ D_l^{(\ell)}(\mathbf{r}) &= e_{lpq}^{(\ell)} S_{pq}^{(\ell)}(\mathbf{r}) + \epsilon_{lq}^{(\ell)} E_q^{(\ell)}(\mathbf{r}), \end{aligned} \tag{4.1}$$

where $\sigma_{lm}^{(\ell)}(\mathbf{r})$, $S_{pq}^{(\ell)}(\mathbf{r})$, $E_q^{(\ell)}(\mathbf{r})$ and $D_l^{(\ell)}(\mathbf{r})$ are the stress, strain, electric field and electric displacement tensors of material 'ℓ' respectively. $C_{lmpq}^{(\ell)}$, $e_{qlm}^{(\ell)}$ and $\epsilon_{lq}^{(\ell)}$ are the elastic stiffness, piezoelectric and permittivity tensors with symmetries

$$\left.\begin{aligned} C_{lmpq}^{(\ell)} = C_{mlpq}^{(\ell)} = C_{lmqp}^{(\ell)} = C_{pqlm}^{(\ell)} \\ e_{qlm}^{(\ell)} = e_{qml}^{(\ell)} \\ \epsilon_{lq}^{(\ell)} = \epsilon_{ql}^{(\ell)} \end{aligned}\right\}. \tag{4.2}$$

We can combine these tensors into the extended stiffness

$$\breve{C}^{(\ell)}_{lMPq} = \begin{cases} C^{(\ell)}_{lmpq} & M = m = 1,2,3;\ P = p = 1,2,3 \\ e^{(\ell)}_{qlm} & M = m = 1,2,3;\ P = 4 \\ -e^{(\ell)}_{lpq} & M = 4;\ P = p = 1,2,3 \\ \epsilon^{(\ell)}_{lq} & M, P = 4 \end{cases}, \tag{4.3}$$

where the lowercase subscripts range from 1 to 3 and the uppercase subscripts from 1 to 4. Similarly, we define the extended density as

$$\breve{\rho}^{(\ell)}_{MP} = \begin{cases} \rho^{(\ell)} & M = P = 1,2,3 \\ 0 & \text{otherwise} \end{cases}, \tag{4.4}$$

where $\rho^{(\ell)}$ is the density of material 'ℓ'. The extended stiffness and extended density are not tensors but they allow us to rewrite the constitutive equations as a single constitutive equation

$$\breve{\sigma}^{(\ell)}_{lM}(\mathbf{r}) = \breve{C}^{(\ell)}_{lMPq}\breve{S}^{(\ell)}_{Pq}(\mathbf{r}) \tag{4.5}$$

where

$$\breve{\sigma}^{(\ell)}_{iJ}(\mathbf{r}) = \begin{cases} \sigma^{(\ell)}_{ij}(\mathbf{r}) & J = 1,2,3 \\ D^{(\ell)}_{i}(\mathbf{r}) & J = 4 \end{cases} \tag{4.6}$$

and

$$\breve{S}^{(\ell)}_{Ij}(\mathbf{r}) = \begin{cases} S^{(\ell)}_{ij}(\mathbf{r}) = \frac{1}{2}(\partial_j u^{(\ell)}_i(\mathbf{r}) + \partial_i u^{(\ell)}_j(\mathbf{r})) & I = 1,2,3 \\ E^{(\ell)}_j(\mathbf{r}) = -\partial_j \varphi(\mathbf{r})^{(\ell)} & I = 4 \end{cases} \tag{4.7}$$

are the extended stress and strain respectively, with $u^{(\ell)}_i$ the displacement tensor and $\varphi^{(\ell)}$ the electric potential of material 'ℓ'.

To establish the piezoelectric SPFT we follow the methods of Zhuck and Lakhtakia [14] by considering a composite made up of several component materials and introducing effective constitutive operators (ECOs) which eventually become the SPFT estimates in the spatially–transformed Fourier domain. The introduction of an orthorhombic comparison material (OCM) follows and this is compared with the composite. We then renormalize the solutions to the synthe-

sized equation of motion, which allows strong fluctuations in component materials to be examined. Effective perturbation operators (EPOs) are then introduced and we find the ECOs in terms of these EPOs through algebraic equations in the spatially–transformed Fourier domain. A second–order approximation is then used to find the EPOs and thus the ECOs. Finally, all secular terms are removed to ensure convergence when strong fluctuations in the component materials are present.

4.1.1 Notation

In this chapter matrices are denoted by double underlining and bold font, whereas vectors are in bold font with no underlining. The extended symbols are represented in normal font with their components indicated by subscripts and/or superscripts. All lowercase indexes range from 1 to 3 and the uppercase indexes from 1 to 4. For use later on, we note that the pqth entry of a matrix $\underline{\underline{\mathbf{A}}}$ is written as $\big[\underline{\underline{\mathbf{A}}}\big]_{pq}$, while the pth entry of a vector $\mathbf{b}$ is written as $[\,\mathbf{b}\,]_p$. Accordingly, the matrix entry $\big[\underline{\underline{\mathbf{A}}}\cdot\underline{\underline{\mathbf{B}}}\big]_{pr}=\big[\underline{\underline{\mathbf{A}}}\big]_{pq}\big[\underline{\underline{\mathbf{B}}}\big]_{qr}$, the vector entry $\big[\underline{\underline{\mathbf{A}}}\cdot\mathbf{b}\big]_p=\big[\underline{\underline{\mathbf{A}}}\big]_{pq}\big[\mathbf{b}\big]_q$, and the scalar $\mathbf{a}\cdot\mathbf{b}=[\mathbf{a}]_p\,[\mathbf{b}]_p$. The adjoint, determinant, inverse, trace and transpose of a matrix $\underline{\underline{\mathbf{A}}}$ are denoted by $\mathrm{adj}\,\big(\underline{\underline{\mathbf{A}}}\big)$, $\det\big(\underline{\underline{\mathbf{A}}}\big)$, $\underline{\underline{\mathbf{A}}}^{-1}$, $\mathrm{tr}\,\big(\underline{\underline{\mathbf{A}}}\big)$ and $\underline{\underline{\mathbf{A}}}^T$, respectively. The $n\times n$ null matrix is written as $\underline{\underline{\mathbf{0}}}_{n\times n}$.

4.2 Effective constitutive relations

Now we have the constitutive equation, (4.5), we can begin our analysis. We follow the same method as Zhuck and Lakhtakia by considering a composite occupying all space with extended stiffness $\breve{C}_{lMPq}(\mathbf{r})$ and extended density $\breve{\rho}_{MP}(\mathbf{r})$. This composite is considered to be a random mixture of more than one component material and its extended stiffness symbol can, for example, be expressed as

$$\breve{C}_{lMPq}(\mathbf{r})=\sum_{\ell=1}^{n}\breve{C}^{(\ell)}_{lMPq}\Phi^{(\ell)}(\mathbf{r}) \tag{4.8}$$

for composite consisting of n component materials with $\Phi^{(\ell)}(\mathbf{r})$ the characteristic function of material 'ℓ'. We consider the piezoelectric equation of motion, which

is an extended version of the elastic equation of motion (3.1) [49]. Assuming an $e^{-i\omega t}$ time dependence we have

$$\partial_l \breve{\sigma}_{lM}(\mathbf{r}) + \omega^2 \breve{\rho}_{MP}(\mathbf{r}) \breve{u}_P(\mathbf{r}) = -\breve{F}_M(\mathbf{r}). \tag{4.9}$$

Herein, $\breve{u}_P(\mathbf{r})$ and $\breve{F}_M(\mathbf{r})$ are the extended displacement and extended force of the composite respectively, given by

$$\breve{u}_I(\mathbf{r}) = \begin{cases} u_i(\mathbf{r}) & I = 1,2,3 \\ \varphi(\mathbf{r}) & I = 4 \end{cases} \tag{4.10}$$

and

$$\breve{F}_J(\mathbf{r}) = \begin{cases} F_j(\mathbf{r}) & J = 1,2,3 \\ -q & J = 4 \end{cases}, \tag{4.11}$$

with $u_i(\mathbf{r})$, $\varphi(\mathbf{r})$, $F_j(\mathbf{r})$ and q the elastic displacement tensor, electric potential, body force tensor and the charge respectively.

Following Zhuck and Lakhtakia we define effective constitutive relations by

$$\langle \breve{C}_{lMPq}(\mathbf{r}) \breve{S}_{Pq}(\mathbf{r}) \rangle \equiv \breve{C}^{(eco)}_{lMPq}(\mathbf{r}) * \langle \breve{S}_{Pq}(\mathbf{r}) \rangle + \beta^{(eco)}_{lMP}(\mathbf{r}) * \langle \breve{u}_P(\mathbf{r}) \rangle, \tag{4.12}$$

$$\langle \breve{\rho}_{MP}(\mathbf{r}) \breve{u}_P(\mathbf{r}) \rangle \equiv \varepsilon^{(eco)}_{MPq}(\mathbf{r}) * \langle \breve{S}_{Pq}(\mathbf{r}) \rangle + \breve{\rho}^{(eco)}_{MP}(\mathbf{r}) * \langle \breve{u}_P(\mathbf{r}) \rangle \tag{4.13}$$

where $\breve{C}^{(eco)}_{lMPq}(\mathbf{r})$, $\beta^{(eco)}_{lMP}(\mathbf{r})$, $\varepsilon^{(eco)}_{MPq}(\mathbf{r})$ and $\breve{\rho}^{(eco)}_{MP}(\mathbf{r})$ are the effective constitutive operators (ECOs) and $\langle \ldots \rangle$ defines the ensemble average, the average over all possible particle positions within the composite. Now the mean field equations are produced by taking the ensemble average of (4.7) and (4.9), whilst using (4.2), (4.12) and (4.13) gives

$$(\partial_l \breve{C}^{(eco)}_{lMPq}(\mathbf{r}) + \omega^2 \varepsilon^{(eco)}_{MPq})(\mathbf{r}) * \langle \breve{S}_{Pq}(\mathbf{r}) \rangle + (\omega^2 \breve{\rho}^{(eco)}_{MP}(\mathbf{r}) + \partial_l \beta^{(eco)}_{lMP}(\mathbf{r})) * \langle \breve{u}_P(\mathbf{r}) \rangle = -\breve{F}_M(\mathbf{r}) \tag{4.14}$$

and

$$\langle \breve{S}_{Pq}(\mathbf{r}) \rangle = \begin{cases} \frac{1}{2}(\partial_q \langle u_p(\mathbf{r}) \rangle + \partial_p \langle u_q(\mathbf{r}) \rangle) & P = 1,2,3 \\ -\partial_q \langle \varphi(\mathbf{r}) \rangle & P = 4 \end{cases}. \tag{4.15}$$

Now we consider the composite to be a HCM and so $\breve{C}_{lMPq}$ and $\breve{\rho}_{MP}$ are statis-

tically homogeneous and homogeneously interrelated, that is their ensemble averages are independent of spatial coordinates and their two–point second–order statistical moments depend on the difference of the two spatial coordinates [14]. As with Zhuck and Lakhtakia the ECOs are non-local due to the operations in (4.12) and (4.13), this gives us

$$\digamma(\mathbf{r}) * \daleth(\mathbf{r}) \equiv \int d^3r' \digamma(\mathbf{r}, \mathbf{r}') \daleth(\mathbf{r}') \equiv \int d^3r' \digamma(\mathbf{r} - \mathbf{r}') \daleth(\mathbf{r}'), \tag{4.16}$$

where $\digamma(\mathbf{r})$ represents any of the ECOs and $\daleth(\mathbf{r})$ is some test function. As the ECOs are shift–invariant [14], we can write

$$\digamma(\mathbf{r} - \mathbf{r}') = (2\pi)^{-3} \int d^3k \digamma(\mathbf{k}) e^{i\mathbf{k}\cdot(\mathbf{r}-\mathbf{r}')} \tag{4.17}$$

and so

$$\digamma(\mathbf{r}) * e^{i\mathbf{k}\cdot\mathbf{r}} \equiv \digamma(\mathbf{k}) e^{i\mathbf{k}\cdot\mathbf{r}} \tag{4.18}$$

where $\mathbf{k} = (k_1, k_2, k_3)$ is an unspecified wave vector. Equation (4.18) gives us the spectral counterpart $\digamma(\mathbf{k})$ of $\digamma(\mathbf{r})$, where $\digamma$ is shift–invariant [14].

From Zhuck and Lakhtakia, we have that if the extended force has the spectral form

$$\breve{F}_M(\mathbf{r}) = \breve{F}_M(\mathbf{k}) e^{i\mathbf{k}\cdot\mathbf{r}} \tag{4.19}$$

then from the mean field equations we also have

$$\langle \breve{u}_M(\mathbf{r}) \rangle = \breve{u}_M(\mathbf{k}) e^{i\mathbf{k}\cdot\mathbf{r}}, \tag{4.20}$$

$$\langle \breve{S}_{Pq}(\mathbf{r}) \rangle = \breve{S}_{Pq}(\mathbf{k}) e^{i\mathbf{k}\cdot\mathbf{r}}. \tag{4.21}$$

Now ECOs simplify such that for some function $\daleth(\mathbf{r}) = \daleth(\mathbf{k}) e^{i\mathbf{k}\cdot\mathbf{r}}$ we have

$$\digamma(\mathbf{r}) * \daleth(\mathbf{r}) = \digamma(\mathbf{k}) \daleth(\mathbf{k}) e^{i\mathbf{k}\cdot\mathbf{r}} \text{ for } \digamma = \breve{C}^{(eco)}_{lMPq}, \beta^{(eco)}_{lMP}, \varepsilon^{(eco)}_{MPq}, \breve{\rho}^{(eco)}_{MP} \tag{4.22}$$

with

$$\begin{array}{ll} \lim\limits_{\mathbf{k}\to\mathbf{0}} \breve{C}^{(eco)}_{lMPq}(\mathbf{k}) = \breve{C}^{(spft)}_{lMPq}, & \lim\limits_{\mathbf{k}\to\mathbf{0}} \beta^{(eco)}_{lMPq}(\mathbf{k}) = \beta^{(spft)}_{lMPq} \\ \lim\limits_{\mathbf{k}\to\mathbf{0}} \varepsilon^{(eco)}_{MPq}(\mathbf{k}) = \varepsilon^{(spft)}_{MPq}, & \lim\limits_{\mathbf{k}\to\mathbf{0}} \breve{\rho}^{(eco)}_{MP}(\mathbf{k}) = \breve{\rho}^{(spft)}_{MP} \end{array} \tag{4.23}$$

as the long–wavelength limits.

4.3 Comparison material

As with the elastodynamic SPFT we introduce a homogeneous comparison material. This homogeneous comparison material provides the initial ansatz for an iterative procedure that delivers a succession of SPFT estimates of the HCM constitutive parameters [14]. Accordingly, the comparison material represents the lowest–order SPFT estimate of the HCM. We take our comparison material to be orthorhombic with extended stiffness $\breve{C}^{(ocm)}_{lMPq}$ and extended density $\breve{\rho}^{(ocm)}_{MP}$. The comparison material has equation of motion

$$\breve{C}^{(ocm)}_{lMPq}\partial_l\partial_q\breve{u}^{(ocm)}_P(\mathbf{r}) + \omega^2\breve{\rho}^{(ocm)}_{MP}\breve{u}_P(\mathbf{r}) = -\breve{F}^{(ocm)}_M(\mathbf{r}). \tag{4.24}$$

and its solution is given by

$$\breve{u}^{(ocm)}_P(\mathbf{r}) = \breve{G}^{(ocm)}_{PM}(\mathbf{r}) * \breve{F}^{(ocm)}_M(\mathbf{r}). \tag{4.25}$$

In k–space we convert the Greens Function G_{PM} into the 4×4 matrix form as

$$\underline{\underline{\breve{\mathbf{G}}}}^{(ocm)}(\mathbf{k}) = \left[k^2\underline{\underline{\breve{\mathbf{a}}}}(\hat{\mathbf{k}}) - \omega^2\underline{\underline{\breve{\boldsymbol{\rho}}}}^{(ocm)}\right]^{-1}. \tag{4.26}$$

with $\underline{\underline{\breve{\boldsymbol{\rho}}}}^{(ocm)}$ being the 4×4 matrix representation of $\breve{\rho}^{(ocm)}_{MP}$ and $\underline{\underline{\breve{\mathbf{a}}}}(\hat{\mathbf{k}})$ is the 4×4 matrix with entries

$$\left[\underline{\underline{\breve{\mathbf{a}}}}(\hat{\mathbf{k}})\right]_{MP} = \frac{k_l\breve{C}^{(ocm)}_{lMPq}k_q}{k^2}. \tag{4.27}$$

with $k = \sqrt{\mathbf{k}\cdot\mathbf{k}}$ and $\hat{\mathbf{k}} = \dfrac{\mathbf{k}}{k}$. As with the elastodynamic case we can rewrite $\underline{\underline{\breve{\mathbf{G}}}}$ as

$$\underline{\underline{\breve{\mathbf{G}}}}^{(ocm)}(\mathbf{k}) = \frac{\underline{\underline{\breve{\mathbf{N}}}}(\mathbf{k})}{\breve{\Delta}(\mathbf{k})}, \tag{4.28}$$

where the 4×4 matrix function

$$\underline{\underline{\breve{\mathbf{N}}}}(\mathbf{k}) = \text{adj}\left[k^2\,\underline{\underline{\breve{\mathbf{a}}}}(\hat{\mathbf{k}}) - \omega^2\underline{\underline{\breve{\boldsymbol{\rho}}}}^{(ocm)}\right] \tag{4.29}$$

and the scalar function

$$\begin{aligned}\breve{\Delta}(\mathbf{k}) &= k^8 \det\left[\underline{\underline{\breve{\mathbf{a}}}}(\hat{\mathbf{k}})\right] - \mathrm{tr}\left\{\mathrm{adj}\left[k^2\underline{\underline{\breve{\mathbf{a}}}}(\hat{\mathbf{k}})\right]\cdot\omega^2\underline{\underline{\breve{\boldsymbol{\rho}}}}^{(ocm)}\right\} - \\ &\quad k^2\,\mathrm{tr}\left[\mathrm{adj}(\omega^2\underline{\underline{\breve{\boldsymbol{\rho}}}}^{(ocm)})\cdot\underline{\underline{\breve{\mathbf{a}}}}(\hat{\mathbf{k}})\right] + k^4\Big(\mathrm{tr}\Big\{\left[\underline{\underline{\breve{\mathbf{a}}}}(\hat{\mathbf{k}})\right]_{44}\left[\underline{\underline{\breve{\mathbf{a}}}}^{\sharp}(\hat{\mathbf{k}})\cdot\mathrm{adj}(\omega^2\underline{\underline{\breve{\boldsymbol{\rho}}}}^{\sharp})\right]\Big\} - \\ &\quad \left[\underline{\underline{\breve{\mathbf{a}}}}(\hat{\mathbf{k}})\right]_{41}\left[\underline{\underline{\breve{\mathbf{a}}}}(\hat{\mathbf{k}})\right]_{14}\left[\mathrm{adj}(\omega^2\underline{\underline{\breve{\boldsymbol{\rho}}}}^{\sharp})\right]_{11} - \left[\underline{\underline{\breve{\mathbf{a}}}}(\hat{\mathbf{k}})\right]_{42}\left[\underline{\underline{\breve{\mathbf{a}}}}(\hat{\mathbf{k}})\right]_{24}\left[\mathrm{adj}(\omega^2\underline{\underline{\breve{\boldsymbol{\rho}}}}^{\sharp})\right]_{22} - \\ &\quad \left[\underline{\underline{\breve{\mathbf{a}}}}(\hat{\mathbf{k}})\right]_{43}\left[\underline{\underline{\breve{\mathbf{a}}}}(\hat{\mathbf{k}})\right]_{34}\left[\mathrm{adj}(\omega^2\underline{\underline{\breve{\boldsymbol{\rho}}}}^{\sharp})\right]_{33}\Big), \end{aligned} \tag{4.30}$$

with the 3×3 matrices $\underline{\underline{\breve{\mathbf{a}}}}^{\sharp}$ and $\underline{\underline{\breve{\boldsymbol{\rho}}}}^{\sharp}$ having entries

$$\begin{aligned}\underline{\underline{\breve{\mathbf{a}}}}^{\sharp}(\mathbf{k}) &= \begin{pmatrix} \left[\underline{\underline{\breve{\mathbf{a}}}}(\hat{\mathbf{k}})\right]_{11} & \left[\underline{\underline{\breve{\mathbf{a}}}}(\hat{\mathbf{k}})\right]_{12} & \left[\underline{\underline{\breve{\mathbf{a}}}}(\hat{\mathbf{k}})\right]_{13} \\ \left[\underline{\underline{\breve{\mathbf{a}}}}(\hat{\mathbf{k}})\right]_{21} & \left[\underline{\underline{\breve{\mathbf{a}}}}(\hat{\mathbf{k}})\right]_{22} & \left[\underline{\underline{\breve{\mathbf{a}}}}(\hat{\mathbf{k}})\right]_{23} \\ \left[\underline{\underline{\breve{\mathbf{a}}}}(\hat{\mathbf{k}})\right]_{31} & \left[\underline{\underline{\breve{\mathbf{a}}}}(\hat{\mathbf{k}})\right]_{32} & \left[\underline{\underline{\breve{\mathbf{a}}}}(\hat{\mathbf{k}})\right]_{33} \end{pmatrix}, \\ \underline{\underline{\breve{\boldsymbol{\rho}}}}^{\sharp} &= \begin{pmatrix} \left[\underline{\underline{\breve{\boldsymbol{\rho}}}}^{(ocm)}\right]_{11} & \left[\underline{\underline{\breve{\boldsymbol{\rho}}}}^{(ocm)}\right]_{12} & \left[\underline{\underline{\breve{\boldsymbol{\rho}}}}^{(ocm)}\right]_{13} \\ \left[\underline{\underline{\breve{\boldsymbol{\rho}}}}^{(ocm)}\right]_{21} & \left[\underline{\underline{\breve{\boldsymbol{\rho}}}}^{(ocm)}\right]_{22} & \left[\underline{\underline{\breve{\boldsymbol{\rho}}}}^{(ocm)}\right]_{23} \\ \left[\underline{\underline{\breve{\boldsymbol{\rho}}}}^{(ocm)}\right]_{31} & \left[\underline{\underline{\breve{\boldsymbol{\rho}}}}^{(ocm)}\right]_{32} & \left[\underline{\underline{\breve{\boldsymbol{\rho}}}}^{(ocm)}\right]_{33} \end{pmatrix}. \end{aligned} \tag{4.31}$$

We now have the details for the OCM and for the composite considered in §4.2 described by extended stiffness $\breve{C}_{lMPq}(\mathbf{r})$ and extended density $\breve{\rho}_{MP}(\mathbf{r})$. The next step is to compare the two. As Zhuck and Lakhtakia do, we synthesize the two equations of motion

$$\breve{C}^{(ocm)}_{lMPq}\partial_l\partial_q\breve{u}_P(\mathbf{r}) + \omega^2\breve{\rho}^{(ocm)}_{MP}\breve{u}_P(\mathbf{r}) = -\breve{F}^{(ocm)}_M(\mathbf{r}) - \delta\breve{F}_M(\mathbf{r}), \tag{4.32}$$

where

$$\delta\breve{F}_M(\mathbf{r}) = \partial_l\delta\breve{C}_{lMPq}(\mathbf{r})\breve{S}_{Pq}(\mathbf{r}) + \omega^2\delta\breve{\rho}_{MP}(\mathbf{r})\breve{u}_P(\mathbf{r}), \tag{4.33}$$

$$\delta\breve{C}_{lMPq}(\mathbf{r}) = \breve{C}_{lMPq}(\mathbf{r}) - \breve{C}^{(ocm)}_{lMPq}, \tag{4.34}$$

$$\delta\breve{\rho}_{MP}(\mathbf{r}) = \breve{\rho}_{MP}(\mathbf{r}) - \breve{\rho}^{(ocm)}_{MP}. \tag{4.35}$$

This synthesized equation of motion can be solved exactly as with (4.24) to give

$$\begin{aligned}\breve{u}_J(\mathbf{r}) &= \breve{u}_J^{(ocm)}(\mathbf{r}) + \omega^2 \breve{G}_{JM}^{(ocm)}(\mathbf{r}) * [\delta\breve{\rho}_{MP}(\mathbf{r})\breve{u}_P(\mathbf{r})] + \\ &\quad H_{JlM}^{(ocm)}(\mathbf{r}) * \left[\delta\breve{C}_{lMPq}(\mathbf{r})\breve{S}_{Pq}(\mathbf{r})\right]. \end{aligned} \tag{4.36}$$

Substituting into our equation for the extended strain (4.7) we get

$$\begin{aligned}\breve{S}_{Ij}(\mathbf{r}) &= \breve{S}_{Ij}^{(ocm)}(\mathbf{r}) + \omega^2 G_{IjM}^{(ocm)}(\mathbf{r}) * [\delta\breve{\rho}_{MP}(\mathbf{r})\breve{u}_P(\mathbf{r})] + \\ &\quad \mathcal{H}_{IjlM}^{(ocm)}(\mathbf{r}) * \left[\delta\breve{C}_{lMPq}(\mathbf{r})\breve{S}_{Pq}(\mathbf{r})\right]. \end{aligned} \tag{4.37}$$

Herein we have

$$H_{JlM}^{(ocm)}(\mathbf{r}) = \partial_l \breve{G}_{JM}^{(ocm)}(\mathbf{r}) \tag{4.38}$$

$$G_{IjM}^{(ocm)}(\mathbf{r}) = \begin{cases} \frac{1}{2}\left[\partial_j \breve{G}_{iM}^{(ocm)}(\mathbf{r}) + \partial_i \breve{G}_{jM}^{(ocm)}(\mathbf{r})\right] & I = 1,2,3 \\ -\partial_j \breve{G}_{4M}^{(ocm)}(\mathbf{r}) & I = 4 \end{cases} \tag{4.39}$$

$$\mathcal{H}_{IjlM}^{(ocm)}(\mathbf{r}) = \partial_l G_{IjM}^{(ocm)}(\mathbf{r}). \tag{4.40}$$

Now we can recast $\underline{\underline{\breve{\mathbf{G}}}}^{(ocm)}(\mathbf{k})$ as

$$\underline{\underline{\breve{\mathbf{G}}}}^{(ocm)}(\mathbf{k}) = \frac{\left[\underline{\underline{\breve{\mathbf{a}}}}(\hat{\mathbf{k}})\right]^{-1}}{k^2} + \frac{\omega^2}{k^2\breve{\Delta}(\mathbf{k})}\left[\underline{\underline{\breve{\mathbf{a}}}}(\hat{\mathbf{k}})\right]^{-1} \cdot \underline{\underline{\breve{\boldsymbol{\rho}}}}^{(ocm)} \cdot \underline{\underline{\breve{\mathbf{N}}}}(\mathbf{k}). \tag{4.41}$$

Substituting this into (4.38–4.40) allows us to find the spectral counterpart of

$\mathcal{H}^{(ocm)}_{IjlM}(\mathbf{r})$ as

$$\mathcal{H}^{(ocm)}_{IjlM}(\mathbf{k}) = \begin{cases} -\dfrac{(\mathbf{k})_l}{2k^2}\left[(\mathbf{k})_j\left[\breve{\underline{\underline{\mathbf{a}}}}(\hat{\mathbf{k}})\right]^{-1}_{iM} + (\mathbf{k})_i\left[\breve{\underline{\underline{\mathbf{a}}}}(\hat{\mathbf{k}})\right]^{-1}_{jM}\right] - \\ \dfrac{\omega^2}{2k^2\breve{\Delta}(\mathbf{k})}\left[(\mathbf{k})_j\left[\breve{\underline{\underline{\mathbf{a}}}}(\hat{\mathbf{k}})\right]^{-1}_{iS} + (\mathbf{k})_i\left[\breve{\underline{\underline{\mathbf{a}}}}(\hat{\mathbf{k}})\right]^{-1}_{jS}\right]\times , \qquad I = 1,2,3 \\ (\mathbf{k})_l\left[\breve{\underline{\boldsymbol{\rho}}}^{(ocm)}\right]_{SP}\left[\breve{\underline{\underline{\mathbf{N}}}}(\mathbf{k})\right]_{PM}, \\ \\ -\dfrac{(\mathbf{k})_j(\mathbf{k})_l\left[\breve{\underline{\underline{\mathbf{a}}}}(\hat{\mathbf{k}})\right]^{-1}_{4M}}{k^2} - \\ \dfrac{\omega^2}{k^2\breve{\Delta}(\mathbf{k})}\left[(\mathbf{k})_j(\mathbf{k})_l\left[\breve{\underline{\underline{\mathbf{a}}}}(\hat{\mathbf{k}})\right]^{-1}_{4S}\left[\breve{\underline{\boldsymbol{\rho}}}^{(ocm)}\right]_{SP}\left[\breve{\underline{\underline{\mathbf{N}}}}(\mathbf{k})\right]_{PM}\right], \qquad I = 4. \end{cases} \tag{4.42}$$

Once again we follow Zhuck and Lakhtakia [14] to observe that for $1 \leq I \leq 4$ the first term of $\mathcal{H}^{(ocm)}_{IjlM}$ doesn't vanish as $k \to \infty$. Thus, we can write

$$\mathcal{H}^{(ocm)}_{IjlM}(\mathbf{r}) = \mathcal{H}'^{(ocm)}_{IjlM}(\mathbf{r}) - \breve{W}_{IjlM} \tag{4.43}$$

where $\mathcal{H}'^{(ocm)}_{IjlM}(\mathbf{r})$ is a singular integral operator associated with an infinitely small exclusion region and $\breve{W}_{IjlM}$ is a constant tensor. Both these terms are dependent on an exclusion region but their difference $\mathcal{H}^{(ocm)}_{IjlM}(\mathbf{r})$ is not [14]. However, the spectral form of $\mathcal{H}'^{(ocm)}_{IjlM}(\mathbf{r})$ can be written as [14]

$$\mathcal{H}'^{(ocm)}_{IjlM}(\mathbf{k}) = \mathcal{H}^{(ocm)}_{IjlM}(\mathbf{k}) + \breve{W}_{IjlM} \tag{4.44}$$

where $\breve{W}_{IjlM}$ is an extended version of the elastodynamic renormalization tensor W_{rstu} independent of $\mathbf{k}$. We make this rearrangement because it removes any importance of an exclusion region and the exact form of $\mathcal{H}'^{(ocm)}_{IjlM}(\mathbf{r})$ plays no further role in the analysis [14].

Finally in this section we seek to renormalize (4.36) and (4.37). We introduce

$$\breve{\varpi}_{Ij}(\mathbf{r}) = \breve{S}_{Ij}(\mathbf{r}) + \breve{W}_{IjlM}\delta\breve{C}_{lMPq}(\mathbf{r})\breve{S}_{Pq}(\mathbf{r}) \tag{4.45}$$

and $\breve{\eta}_{PqSt}$ such that

$$\breve{S}_{Pq}(\mathbf{r}) = \breve{\eta}_{PqSt}\breve{\varpi}_{St}(\mathbf{r}). \tag{4.46}$$

This allows (4.37) to be rewritten as

$$\breve{\varpi}_{Ij}(\mathbf{r}) = \breve{S}^{(ocm)}_{Ij}(\mathbf{r}) + \omega^2 G^{(ocm)}_{IjM}(\mathbf{r}) * [\delta\breve{\rho}_{MP}(\mathbf{r})\breve{u}_P(\mathbf{r})] + \mathcal{H}'^{(ocm)}_{IjlM}(\mathbf{r}) * \left[\breve{\xi}_{lMPq}(\mathbf{r})\breve{\varpi}_{Pq}(\mathbf{r})\right] \tag{4.47}$$

where

$$\breve{\xi}_{lMPq}(\mathbf{r}) = \delta\breve{C}_{lMSt}(\mathbf{r})\breve{\eta}_{StPq} \tag{4.48}$$

is considered to be an extension of a random perturbation tensor associated with fluctuations of the component materials within the disordered composite [14]. Similarly we have

$$\breve{u}_J(\mathbf{r}) = \breve{u}^{(ocm)}_J(\mathbf{r}) + \omega^2 \breve{G}^{(ocm)}_{JM}(\mathbf{r}) * [\delta\breve{\rho}_{MP}(\mathbf{r})\breve{u}_P(\mathbf{r})] + H^{(ocm)}_{JlM}(\mathbf{r}) * \left[\breve{\xi}_{lMPq}(\mathbf{r})\breve{\varpi}_{Pq}(\mathbf{r})\right]. \tag{4.49}$$

These renormalized equations contain the extended stiffness and extended density of both the disordered composite and the OCM. We now seek the optimal choice of $\breve{W}_{IjlM}$.

4.4 Effective perturbation operators

We can rewrite (4.47) and (4.49) as

$$\psi(\mathbf{r}) = \psi^{(ocm)}(\mathbf{r}) + \Upsilon^{(ocm)}(\mathbf{r})\Pi(\mathbf{r}) * \psi(\mathbf{r}). \tag{4.50}$$

where

$$\psi(\mathbf{r}) = \begin{pmatrix} \breve{\varpi}_{Ij}(\mathbf{r}) \\ \breve{u}_J(\mathbf{r}) \end{pmatrix}, \quad \psi^{(ocm)}(\mathbf{r}) = \begin{pmatrix} \breve{S}^{(ocm)}_{Ij}(\mathbf{r}) \\ \breve{u}^{(ocm)}_J(\mathbf{r}) \end{pmatrix}, \tag{4.51}$$

$$\Upsilon^{(ocm)}(\mathbf{r}) = \begin{pmatrix} \mathcal{H}'^{(ocm)}_{IjlM}(\mathbf{r}) & \omega^2 G^{(ocm)}_{IjM}(\mathbf{r}) \\ H^{(ocm)}_{JlM}(\mathbf{r}) & \omega^2 \breve{G}^{(ocm)}_{JM}(\mathbf{r}) \end{pmatrix}, \quad \Pi(\mathbf{r}) = \begin{pmatrix} \breve{\xi}_{lMPq}(\mathbf{r}) & 0 \\ 0 & \delta\breve{\rho}_{MP}(\mathbf{r}) \end{pmatrix}. \tag{4.52}$$

Now the solution to (4.50) is given by

$$\psi(\mathbf{r}) = \left(1 - \Upsilon^{(ocm)}(\mathbf{r})\Pi(\mathbf{r})\right)^{-1} * \psi^{(ocm)}(\mathbf{r}) \tag{4.53}$$

and we recreate equations (2.47)–(2.50) from Zhuck and Lakhtakia [14] to show that from

$$\langle\psi(\mathbf{r})\rangle = \langle\left(1-\Upsilon^{(ocm)}(\mathbf{r})\Pi(\mathbf{r})\right)^{-1}\rangle * \psi^{(ocm)}(\mathbf{r}) \tag{4.54}$$

$$\langle\Pi(\mathbf{r})\psi(\mathbf{r})\rangle = \langle\Pi(\mathbf{r})\left(1-\Upsilon^{(ocm)}(\mathbf{r})\Pi(\mathbf{r})\right)^{-1}\rangle * \psi^{(ocm)}(\mathbf{r}) \tag{4.55}$$

we have the deterministic operator

$$\Pi^{(e)}(\mathbf{r}) = \langle\Pi(\mathbf{r})\left(1-\Upsilon^{(ocm)}(\mathbf{r})\Pi(\mathbf{r})\right)^{-1}\rangle\langle\left(1-\Upsilon^{(ocm)}(\mathbf{r})\Pi(\mathbf{r})\right)^{-1}\rangle^{-1} \tag{4.56}$$

satisfying

$$\langle\Pi(\mathbf{r})\psi(\mathbf{r})\rangle = \Pi^{(e)}(\mathbf{r}) * \langle\psi(\mathbf{r})\rangle. \tag{4.57}$$

Equivalently we have

$$\langle\breve{\xi}_{lMPq}(\mathbf{r})\breve{\varpi}_{Pq}(\mathbf{r})\rangle = a^{(epo)}_{lMPq}(\mathbf{r}) * \langle\breve{\varpi}_{Pq}(\mathbf{r})\rangle + b^{(epo)}_{lMP}(\mathbf{r}) * \langle\breve{u}_{P}(\mathbf{r})\rangle \tag{4.58}$$

$$\langle\delta\breve{\rho}_{MP}(\mathbf{r})\breve{u}_{P}(\mathbf{r})\rangle = v^{(epo)}_{MPq}(\mathbf{r}) * \langle\breve{\varpi}_{Pq}(\mathbf{r})\rangle + w^{(epo)}_{MP}(\mathbf{r}) * \langle\breve{u}_{P}(\mathbf{r})\rangle. \tag{4.59}$$

where $a^{(epo)}_{lMPq}(\mathbf{r})$, $b^{(epo)}_{lMP}(\mathbf{r})$, $v^{(epo)}_{MPq}(\mathbf{r})$ and $w^{(epo)}_{MP}(\mathbf{r})$ are the effective perturbation operators (EPOs).

Our aim is to find the ECOs, to do this we suppose we have found the solution to (4.56) and we know what the EPOs are. Combining (4.12), (4.13), (4.45), (4.46) and (4.48) gives us equations we can compare with (4.58) and (4.59):

$$\begin{aligned}\langle\breve{\varpi}_{Ij}(\mathbf{r})\rangle = {} & \langle\breve{S}_{Ij}(\mathbf{r})\rangle + \breve{W}_{IjlM}\left[\breve{C}^{(eco)}_{lMPq}(\mathbf{r}) - \breve{C}^{(ocm)}_{lMPq}\right] * \langle\breve{S}_{Pq}(\mathbf{r})\rangle + \\ & \breve{W}_{IjlM}\beta^{(eco)}_{lMP}(\mathbf{r}) * \langle\breve{u}_{P}(\mathbf{r})\rangle,\end{aligned} \tag{4.60}$$

$$\langle\breve{\xi}_{lMPq}(\mathbf{r})\breve{\varpi}_{Pq}(\mathbf{r})\rangle = \left[\breve{C}^{(eco)}_{lMPq}(\mathbf{r}) - \breve{C}^{(ocm)}_{lMPq}\right] * \langle\breve{S}_{Pq}(\mathbf{r})\rangle + \beta^{(eco)}_{lMP}(\mathbf{r}) * \langle\breve{u}_{P}(\mathbf{r})\rangle, \tag{4.61}$$

$$\langle\delta\breve{\rho}_{MP}(\mathbf{r})\breve{u}_{P}(\mathbf{r})\rangle = \varepsilon^{(eco)}_{MPq}(\mathbf{r}) * \langle\breve{S}_{Pq}(\mathbf{r})\rangle + \left[\breve{\rho}^{(eco)}_{MP}(\mathbf{r}) - \breve{\rho}^{(ocm)}_{MP}\right] * \langle\breve{u}_{P}(\mathbf{r})\rangle. \tag{4.62}$$

Following this we substitute (4.60) into (4.58) and (4.59) to produce

$$\begin{aligned}\langle\breve{\xi}_{lMPq}(\mathbf{r})\breve{\varpi}_{Pq}(\mathbf{r})\rangle &= a^{(epo)}_{lMPq}(\mathbf{r}) * \Big[\breve{W}_{PqrS}(\breve{C}^{(eco)}_{rSTu}(\mathbf{r}) - \breve{C}^{(ocm)}_{rSTu}) * \langle\breve{S}_{Tu}(\mathbf{r})\rangle + \\ &\quad \langle\breve{S}_{Pq}(\mathbf{r})\rangle + \breve{W}_{PqrS}\beta^{(eco)}_{rST}(\mathbf{r}) * \langle\breve{u}_{T}(\mathbf{r})\rangle\Big] + \\ &\quad b^{(epo)}_{lMP}(\mathbf{r}) * \langle\breve{u}_{P}(\mathbf{r})\rangle \qquad (4.63)\\ \langle\delta\breve{\rho}_{MP}(\mathbf{r})\breve{u}_{P}(\mathbf{r})\rangle &= v^{(epo)}_{MPq}(\mathbf{r}) * \Big[\breve{W}_{PqrS}(\breve{C}^{(eco)}_{rSTu}(\mathbf{r}) - \breve{C}^{(ocm)}_{rSTu}) * \langle\breve{S}_{Tu}(\mathbf{r})\rangle + \\ &\quad \langle\breve{S}_{Pq}(\mathbf{r})\rangle + \breve{W}_{PqrS}\beta^{(eco)}_{rST}(\mathbf{r}) * \langle\breve{u}_{T}(\mathbf{r})\rangle\Big] + \\ &\quad w^{(epo)}_{MP}(\mathbf{r}) * \langle\breve{u}_{P}(\mathbf{r})\rangle. \qquad (4.64)\end{aligned}$$

Rearranging gives us

$$\begin{aligned}\langle\breve{\xi}_{lMPq}(\mathbf{r})\breve{\varpi}_{Pq}(\mathbf{r})\rangle &= \Big[a^{(epo)}_{lMPq}(\mathbf{r}) + a^{(epo)}_{lMRs}(\mathbf{r}) * \breve{W}_{RstU}(\breve{C}^{(eco)}_{tUPq}(\mathbf{r}) - \breve{C}^{(ocm)}_{tUPq})\Big] * \\ &\quad \langle\breve{S}_{Pq}(\mathbf{r})\rangle + \Big[b^{(epo)}_{lMP}(\mathbf{r}) + a^{(epo)}_{lMRs}(\mathbf{r}) * \\ &\quad \breve{W}_{RstU}\beta^{(eco)}_{tUP}(\mathbf{r})\Big] * \langle\breve{u}_{P}(\mathbf{r})\rangle \qquad (4.65)\\ \langle\delta\breve{\rho}_{MP}(\mathbf{r})\breve{u}_{P}(\mathbf{r})\rangle &= \Big[v^{(epo)}_{MPq}(\mathbf{r}) + v^{(epo)}_{MRs}(\mathbf{r}) * \breve{W}_{RstU}(\breve{C}^{(eco)}_{tUPq}(\mathbf{r}) - \breve{C}^{(ocm)}_{tUPq})\Big] * \\ &\quad \langle\breve{S}_{Pq}(\mathbf{r})\rangle + \Big[w^{(epo)}_{MP}(\mathbf{r}) + v^{(epo)}_{MRs}(\mathbf{r}) * \\ &\quad \breve{W}_{RstU}\beta^{(eco)}_{tUP}(\mathbf{r})\Big] * \langle\breve{u}_{P}(\mathbf{r})\rangle. \qquad (4.66)\end{aligned}$$

Comparing these with (4.61) and (4.62) gives us

$$\breve{C}^{(eco)}_{lMPq}(\mathbf{r}) - \breve{C}^{(ocm)}_{lMPq} = a^{(epo)}_{lMPq}(\mathbf{r}) + a^{(epo)}_{lMRs}(\mathbf{r}) * \breve{W}_{RstU}\left(\breve{C}^{(eco)}_{tUPq}(\mathbf{r}) - \breve{C}^{(ocm)}_{tUPq}\right) \qquad (4.67)$$

$$\beta^{(eco)}_{lMP}(\mathbf{r}) = b^{(epo)}_{lMP}(\mathbf{r}) + a^{(epo)}_{lMRs}(\mathbf{r}) * \breve{W}_{RstU}\beta^{(eco)}_{tUP}(\mathbf{r}) \qquad (4.68)$$

$$\varepsilon^{(eco)}_{MPq}(\mathbf{r}) = v^{(epo)}_{MPq}(\mathbf{r}) + v^{(epo)}_{MRs}(\mathbf{r}) * \breve{W}_{RstU}\left(\breve{C}^{(eco)}_{tUPq}(\mathbf{r}) - \breve{C}^{(ocm)}_{tUPq}\right) \qquad (4.69)$$

$$\breve{\rho}^{(eco)}_{MP}(\mathbf{r}) - \breve{\rho}^{(ocm)}_{MP} = w^{(epo)}_{MP}(\mathbf{r}) + v^{(epo)}_{MRs}(\mathbf{r}) * \breve{W}_{RstU}\beta^{(eco)}_{tUP}(\mathbf{r}) \qquad (4.70)$$

which reduce to algebraic relations in the k-domain

$$\breve{C}^{(eco)}_{lMPq}(\mathbf{k}) - \breve{C}^{(ocm)}_{lMPq} = a^{(epo)}_{lMPq}(\mathbf{k}) + a^{(epo)}_{lMRs}(\mathbf{k})\breve{W}_{RstU}\left(\breve{C}^{(eco)}_{tUPq}(\mathbf{k}) - \breve{C}^{(ocm)}_{tUPq}\right) \tag{4.71}$$

$$\beta^{(eco)}_{lMP}(\mathbf{k}) = b^{(epo)}_{lMP}(\mathbf{k}) + a^{(epo)}_{lMRs}(\mathbf{k})\breve{W}_{RstU}\beta^{(eco)}_{tUP}(\mathbf{k}) \tag{4.72}$$

$$\varepsilon^{(eco)}_{MPq}(\mathbf{k}) = v^{(epo)}_{MPq}(\mathbf{k}) + v^{(epo)}_{MRs}(\mathbf{k})\breve{W}_{RstU}\left(\breve{C}^{(eco)}_{tUPq}(\mathbf{k}) - \breve{C}^{(ocm)}_{tUPq}\right) \tag{4.73}$$

$$\breve{\rho}^{(eco)}_{MP}(\mathbf{k}) - \breve{\rho}^{(ocm)}_{MP} = w^{(epo)}_{MP}(\mathbf{k}) + v^{(epo)}_{MRs}(\mathbf{k})\breve{W}_{RstU}\beta^{(eco)}_{tUP}(\mathbf{k}). \tag{4.74}$$

We now have the ECOs expressed in terms of the EPOs and the final step is to find $\Pi^{(e)}(\mathbf{r})$, giving us the EPOs explicitly.

4.5 Second–order approximation

Following Zhuck and Lakhtakia [14] we expand $\Pi^{(e)}$ as

$$\Pi^{(e)}(\mathbf{r}) = \sum_{n=1}^{\infty} \Pi_n(\mathbf{r}) \tag{4.75}$$

where

$$\Pi_1(\mathbf{r}) = \langle \Pi(\mathbf{r}) \rangle, \tag{4.76}$$

$$\Pi_n(\mathbf{r}) = \langle \Pi(\mathbf{r}) \left(\Upsilon^{(ocm)}(\mathbf{r}) \Pi(\mathbf{r}) \right)^{n-1} \rangle - \sum_{m=1}^{n-1} \Pi_m(\mathbf{r}) \langle \left(\Upsilon^{(ocm)}(\mathbf{r}) \Pi(\mathbf{r}) \right)^{n-m} \rangle, \; n = 2, 3, 4, \ldots \tag{4.77}$$

Now the second–order approximation is given by [14, 50]

$$\Pi^{(e)}(\mathbf{r}) \approx \Pi_1(\mathbf{r}) + \Pi_2(\mathbf{r}) \tag{4.78}$$

$$\approx \langle \Pi(\mathbf{r}) \rangle + \langle \Pi(\mathbf{r}) \; \Upsilon^{(ocm)}(\mathbf{r}) \; \Pi(\mathbf{r}) \rangle + \langle \Pi(\mathbf{r}) \rangle \Upsilon^{(ocm)}(\mathbf{r}) \langle \Pi(\mathbf{r}) \rangle \tag{4.79}$$

which can be expanded to give the EPOs as

$$
\begin{aligned}
a^{(epo)}_{lMPq}(\mathbf{r}) &= \langle \breve{\xi}_{lMPq}(\mathbf{r})\rangle + \mathcal{H}'^{(ocm)}_{RstU}(\mathbf{r})\mathcal{B}^{lMRs}_{tUPq}(\mathbf{r}-\mathbf{r}') && (4.80)\\
\beta^{(epo)}_{lMP}(\mathbf{r}) &= \omega^2 G^{(ocm)}_{RsU}(\mathbf{r})\mathcal{B}^{lMRs}_{UP}(\mathbf{r}-\mathbf{r}') && (4.81)\\
v^{(epo)}_{MPq}(\mathbf{r}) &= \mathcal{B}^{sTPq}_{MR}(\mathbf{r}'-\mathbf{r})H^{(ocm)}_{RsT}(\mathbf{r}) && (4.82)\\
w^{(epo)}_{MP}(\mathbf{r}) &= \omega^2 \mathcal{B}_{MSUP}(\mathbf{r}-\mathbf{r}')\breve{G}^{(ocm)}_{SU}(\mathbf{r}) && (4.83)
\end{aligned}
$$

where

$$
\begin{aligned}
\mathcal{B}^{lMRs}_{tUPq}(\mathbf{r}-\mathbf{r}') &= \langle \breve{\xi}_{lMRs}(\mathbf{r})\breve{\xi}_{tUPq}(\mathbf{r}')\rangle - \langle \breve{\xi}_{lMRs}(\mathbf{r})\rangle\langle \breve{\xi}_{tUPq}(\mathbf{r}')\rangle && (4.84)\\
\mathcal{B}^{lMRs}_{UP}(\mathbf{r}-\mathbf{r}') &= \langle \breve{\xi}_{lMRs}(\mathbf{r})\delta\breve{\rho}_{UP}(\mathbf{r}')\rangle - \langle \breve{\xi}_{lMRs}(\mathbf{r})\rangle\langle \delta\breve{\rho}_{UP}(\mathbf{r}')\rangle && (4.85)\\
\mathcal{B}_{RSUP}(\mathbf{r}-\mathbf{r}') &= \langle \delta\breve{\rho}_{RS}(\mathbf{r})\delta\breve{\rho}_{UP}(\mathbf{r}')\rangle - \langle \delta\breve{\rho}_{RS}(\mathbf{r})\rangle\langle \delta\breve{\rho}_{UP}(\mathbf{r}')\rangle && (4.86)
\end{aligned}
$$

are the correlation functions. Now let us solve for $\breve{C}^{(spft)}_{lMPq}$. An approximate solution to (4.67) can be found by replacing the term in parenthesis by the entire right–hand side, in the manner of a Born series, as per

$$
\begin{aligned}
\breve{C}^{(eco)}_{lMPq}(\mathbf{r}) - \breve{C}^{(ocm)}_{lMPq} &= a^{(epo)}_{lMPq}(\mathbf{r}) + a^{(epo)}_{lMRs}(\mathbf{r}) * \breve{W}_{RstU}\Big[a^{(epo)}_{tUPq}(\mathbf{r}) + \\
&\quad a^{(epo)}_{tUAb}(\mathbf{r}) * \breve{W}_{AblM}\left(\breve{C}^{(eco)}_{lMPq}(\mathbf{r}) - \breve{C}^{(ocm)}_{lMPq}\right)\Big] \\
&\approx a^{(epo)}_{lMPq}(\mathbf{r}) + a^{(epo)}_{lMRs}(\mathbf{r}) * \breve{W}_{RstU} a^{(epo)}_{tUPq}(\mathbf{r}) && (4.87)
\end{aligned}
$$

where only the leading order term in $\breve{W}_{RstU}$ in the series has been retained. Now

$$
\mathcal{H}'^{(ocm)}_{RstU}(\mathbf{r}) = \mathcal{H}^{(ocm)}_{RstU}(\mathbf{r}) + \breve{W}_{RstU} = \partial_s \mathcal{G}^{(ocm)}_{RtU}(\mathbf{r}) + \breve{W}_{RstU}. \qquad (4.88)
$$

This allows us to write (4.87) as

$$\begin{aligned}
\breve{C}^{(eco)}_{lMPq}(\mathbf{r}) - \breve{C}^{(ocm)}_{lMPq} &= \langle\breve{\xi}_{lMPq}(\mathbf{r})\rangle + \mathcal{H}'^{(ocm)}_{RstU}(\mathbf{r})\mathcal{B}^{lMRs}_{tUPq}(\mathbf{r}-\mathbf{r}') + \\
&\quad \left[\langle\breve{\xi}_{lMRs}(\mathbf{r})\rangle + \mathcal{H}'^{(ocm)}_{PqaB}(\mathbf{r})\mathcal{B}^{lMPq}_{aBRs}(\mathbf{r}-\mathbf{r}')\right] * \qquad (4.89)\\
&\quad \breve{W}_{RstU}\left[\langle\breve{\xi}_{tUPq}(\mathbf{r})\rangle + \mathcal{H}'^{(ocm)}_{CdaB}(\mathbf{r})\mathcal{B}^{tUCd}_{aBPq}(\mathbf{r}-\mathbf{r}')\right] \\
&\approx \langle\breve{\xi}_{lMPq}(\mathbf{r})\rangle + \mathcal{H}'^{(ocm)}_{RstU}(\mathbf{r})\mathcal{B}^{lMRs}_{tUPq}(\mathbf{r}-\mathbf{r}') + \\
&\quad \left[\langle\breve{\xi}_{lMRs}(\mathbf{r})\rangle + \mathcal{H}^{(ocm)}_{PqaB}(\mathbf{r})\mathcal{B}^{lMPq}_{aBRs}(\mathbf{r}-\mathbf{r}')\right] * \qquad (4.90)\\
&\quad \breve{W}_{RstU}\left[\langle\breve{\xi}_{tUPq}(\mathbf{r})\rangle + \mathcal{H}^{(ocm)}_{CdaB}(\mathbf{r})\mathcal{B}^{tUCd}_{abPq}(\mathbf{r}-\mathbf{r}')\right],
\end{aligned}$$

again retaining only the leading order term in W_{RstU}. Now using (4.88) we have

$$\begin{aligned}
\breve{C}^{(eco)}_{lMPq}(\mathbf{r}) - \breve{C}^{(ocm)}_{lMPq} &= \langle\breve{\xi}_{lMPq}(\mathbf{r})\rangle + \mathcal{H}'^{(ocm)}_{RstU}(\mathbf{r})\mathcal{B}^{lMRs}_{tUPq}(\mathbf{r}-\mathbf{r}') + \\
&\quad \left(\langle\breve{\xi}_{lMRs}(\mathbf{r})\rangle + \partial_q G'^{(ocm)}_{PaB}(\mathbf{r})\mathcal{B}^{lMPq}_{aBRs}(\mathbf{r}-\mathbf{r}')\right) * \qquad (4.91)\\
&\quad \breve{W}_{RstU}\left(\langle\breve{\xi}_{tUPq}(\mathbf{r})\rangle + \partial_d G'^{(ocm)}_{CaB}(\mathbf{r})\mathcal{B}^{tUCd}_{aBPq}(\mathbf{r}-\mathbf{r}')\right) \\
&= \langle\breve{\xi}_{lMPq}(\mathbf{r})\rangle + \mathcal{H}'^{(ocm)}_{RstU}(\mathbf{r})\mathcal{B}^{lMRs}_{tUPq}(\mathbf{r}-\mathbf{r}') + \\
&\quad \left(\langle\breve{\xi}_{lMRs}(\mathbf{r})\rangle * \breve{W}_{RstU}\langle\breve{\xi}_{tUPq}(\mathbf{r})\rangle\right) + \qquad (4.92)\\
&\quad 2\left(\partial_q G'^{(ocm)}_{PaB}(\mathbf{r}) * \langle\breve{\xi}_{lMRs}(\mathbf{r})\rangle\breve{W}_{RstU}\mathcal{B}^{lMPq}_{aBRs}(\mathbf{r}-\mathbf{r}')\right) + \\
&\quad \Big(\partial_q G'^{(ocm)}_{PaB}(\mathbf{r}) * \mathcal{B}^{lMPq}_{aBRs}(\mathbf{r}-\mathbf{r}')\breve{W}_{RstU}\partial_d G'^{(ocm)}_{CaB}(\mathbf{r}) \times \\
&\quad \mathcal{B}^{tUCd}_{aBpq}(\mathbf{r}-\mathbf{r}')\Big).
\end{aligned}$$

Taking the spatial Fourier transform of (4.91) gives

$$\begin{aligned}
\breve{C}^{(eco)}_{lMPq}(\mathbf{k}) - \breve{C}^{(ocm)}_{lMPq}\,\delta(\mathbf{k}) &= \langle\breve{\xi}_{lMPq}(\mathbf{r})\rangle\delta(\mathbf{k}) + \mathcal{H}'^{(ocm)}_{RstU}(\mathbf{k}) * \breve{B}^{lMRs}_{tUPq}(\mathbf{k}) + \\
&\quad \left(\langle\breve{\xi}_{lMRs}(\mathbf{r})\rangle\breve{W}_{RstU}\langle\breve{\xi}_{tUPq}(\mathbf{r})\rangle\right)\delta(\mathbf{k}) + \\
&\quad i\,[\mathbf{k}]_q\, G'^{(ocm)}_{PaB}(\mathbf{k}) \times \\
&\quad \Bigg[F.T.\left\{2\langle\breve{\xi}_{lMRs}(\mathbf{r})\rangle\breve{W}_{RstU}\mathcal{B}^{lMPq}_{aBRs}(\mathbf{r}-\mathbf{r}')\right\} + \\
&\quad F.T.\Big\{\mathcal{B}^{lMPq}_{aBRs}(\mathbf{r}-\mathbf{r}')\breve{W}_{RstU}\partial_d G'^{(ocm)}_{CaB}(\mathbf{r}) \times \\
&\quad \mathcal{B}^{tUCd}_{aBPq}(\mathbf{r}-\mathbf{r}')\Big\}\Bigg], \qquad (4.93)
\end{aligned}$$

where $F.T.$ denotes the spatial Fourier transform. This yields

$$\breve{C}^{(spft)}_{lMPq} \approx \breve{C}^{(ocm)}_{lMPq} + \langle\breve{\xi}_{lMPq}(\mathbf{r})\rangle + \langle\breve{\xi}_{lMRs}(\mathbf{r})\rangle\breve{W}_{RstU}\langle\breve{\xi}_{tUPq}(\mathbf{r})\rangle + \int d^3k'\mathcal{H}'^{(ocm)}_{RstU}(\mathbf{k}')\breve{B}^{lMRs}_{tUPq}(\mathbf{k}') \tag{4.94}$$

in the limit $\mathbf{k}\rightarrow\mathbf{0}$. Performing the same process with (4.68), (4.69) and (4.70) gives

$$\beta^{(spft)}_{lMP} \approx \omega^2\int d^3k'\breve{B}^{lMRs}_{UP}(\mathbf{k}')\tilde{G}^{(ocm)}_{RsU}(\mathbf{k}'), \tag{4.95}$$

$$\varepsilon^{(spft)}_{MPq} \approx \int d^3k'\breve{B}^{tUPq}_{MR}(-\mathbf{k}')\tilde{H}^{(ocm)}_{RtU}(\mathbf{k}'), \tag{4.96}$$

$$\breve{\rho}^{(spft)}_{MP} \approx \breve{\rho}^{(ocm)}_{MP} + \langle\delta\breve{\rho}_{MP}(\mathbf{r})\rangle + \omega^2\int d^3k'\breve{B}_{MSUP}(\mathbf{k}')\tilde{G}^{(ocm)}_{SU}(\mathbf{k}'). \tag{4.97}$$

In the above we have $\breve{B}^{lMRs}_{tUPq}(\mathbf{k})$, $\breve{B}^{lMRs}_{UP}(\mathbf{k})$ and $\breve{B}_{MSUP}(\mathbf{k})$ as the Fourier transforms of $\mathcal{B}^{lMRs}_{tUPq}(\mathbf{r}-\mathbf{r}')$, $\mathcal{B}^{lMRs}_{UP}(\mathbf{r}-\mathbf{r}')$ and $\mathcal{B}_{MSUP}(\mathbf{r}-\mathbf{r}')$ given by, for example,

$$\breve{B}^{lMRs}_{tUPq} = \frac{1}{2\pi^3}\int d^3r\mathcal{B}^{lMRs}_{tUPq}(\mathbf{r}-\mathbf{r}')e^{(-i\mathbf{k}\cdot(\mathbf{r}-\mathbf{r}'))}. \tag{4.98}$$

Finally, we assume that $\mathcal{B}^{lMRs}_{UP}(\mathbf{r}-\mathbf{r}')$ is even giving $\breve{B}^{lMRs}_{UP}(\mathbf{k})$ as an odd function and so we follow Zhuck and Lakhtakia [14] and observe that, as $\underline{\underline{\breve{\mathbf{G}}}}^{(ocm)}$ is an even function of $\mathbf{k}$, the integrands of (4.95) and (4.96) are odd. This gives us $\beta^{(spft)}_{lMP}=0$ and $\varepsilon^{(spft)}_{MPq}=0$ in the second–order approximation.

4.6 Strong–property–fluctuations

The expressions for $\breve{C}^{(spft)}_{lMPq}$ and $\breve{\rho}^{(spft)}_{MP}$, (4.94) and (4.97), can be further simplified if all secular terms are removed. This requires us to have [14, 51]

$$\langle\breve{\xi}_{lMPq}(\mathbf{r})\rangle = \langle\delta\breve{\rho}_{MP}(\mathbf{r})\rangle = 0 \tag{4.99}$$

which in turn means we must have

$$\langle\breve{\rho}_{MP}(\mathbf{r})\rangle = \breve{\rho}^{(ocm)}_{MP} \tag{4.100}$$

and we define $\breve{W}_{RstU}$ to be the solution of

$$\breve{W}_{rstU}\int d^3k\breve{B}^{lMrs}_{tUPq}(\mathbf{k}) = \int d^3k\breve{B}^{lMrs}_{tUPq}(\mathbf{k})\frac{(\mathbf{k})_t}{2k^2}\left[(\mathbf{k})_s\left[\underline{\underline{\breve{\mathbf{a}}}}(\hat{\mathbf{k}})\right]^{-1}_{rU}+(\mathbf{k})_r\left[\underline{\underline{\breve{\mathbf{a}}}}(\hat{\mathbf{k}})\right]^{-1}_{sU}\right] \quad \mathrm{R}=\mathrm{r}=1,2,3 \tag{4.101}$$

$$\breve{W}_{4stU}\int d^3k\breve{B}^{lM4s}_{tUPq}(\mathbf{k}) = \int d^3k\breve{B}^{lM4s}_{tUPq}(\mathbf{k})\frac{(\mathbf{k})_t(\mathbf{k})_s\left[\underline{\underline{\breve{\mathbf{a}}}}(\hat{\mathbf{k}})\right]^{-1}_{4U}}{k^2}, \quad \mathrm{R}=4. \tag{4.102}$$

This gives us our final equations for $\breve{C}^{(spft)}_{lMPq}$ and $\breve{\rho}^{(spft)}_{MP}$ as

$$\begin{aligned}\breve{C}^{(spft)}_{lMPq} \approx\ & \breve{C}^{(ocm)}_{lMPq}-\frac{\omega^2}{2}\int d^3k\breve{B}^{lMrs}_{tUPq}(\mathbf{k})\frac{(\mathbf{k})_t}{k^2}\left[(\mathbf{k})_s\left[\underline{\underline{\breve{\mathbf{a}}}}(\hat{\mathbf{k}})\right]^{-1}_{rX}+(\mathbf{k})_r\left[\underline{\underline{\breve{\mathbf{a}}}}(\hat{\mathbf{k}})\right]^{-1}_{sX}\right]\times \\ & \left[\underline{\underline{\breve{\boldsymbol{\rho}}}}^{(ocm)}\right]_{XY}\cdot\left[\underline{\underline{\breve{\mathbf{G}}}}(\mathbf{k})\right]_{YU}- \\ & \frac{\omega^2}{2}\int d^3k\breve{B}^{lM4s}_{tUPq}(\mathbf{k})\frac{(\mathbf{k})_t}{k^2}(\mathbf{k})_s\left[\underline{\underline{\breve{\mathbf{a}}}}(\hat{\mathbf{k}})\right]^{-1}_{4X}\cdot\left[\underline{\underline{\breve{\boldsymbol{\rho}}}}^{(ocm)}\right]_{XY}\cdot\left[\underline{\underline{\breve{\mathbf{G}}}}(\mathbf{k})\right]_{YU},\end{aligned} \tag{4.103}$$

$$\breve{\rho}^{(spft)}_{MP} \approx \breve{\rho}^{(ocm)}_{MP}+\omega^2\int d^3kB_{MSUP}(\mathbf{k})\left[\underline{\underline{\breve{\mathbf{G}}}}(\mathbf{k})\right]_{SU}. \tag{4.104}$$

These results allow strong fluctuations, provided the size of the particles are sufficiently small [14]. It is of interest to note that the conditions (4.99) and (4.100) also set $\langle\Pi(\mathbf{r})\rangle = 0$ and therefore makes the first–order approximation equal to the zeroth–order approximation, or OCM estimate.

4.7 Closing remarks

The theory for the piezoelectric SPFT has been developed following the same methods as used by Zhuck and Lakhtakia [14] the elastodynamic SPFT. The next step is to produce numerical results. This will be done in the next chapter by simplifying (4.103) and (4.104) such that they can be evaluated numerically.

Chapter 5

Implementation of the Piezoelectric SPFT

5.1 Theory

5.1.1 Introduction

In this chapter we take the theory derived in Chapter 4 and establish the linear, second–order SPFT appropriate to orthorhombic $mm2$ piezoelectric HCMs, arising from two homogenous component materials with randomly distributed but identically oriented ellipsoidal particles of one in a matrix of the second. As with the elastodynamic SPFT we also derive the implementation of a two–point covariance function which characterizes the distributions of the component materials and simplify equations (4.103) and (4.104) in order to evaluate them numerically. A representative numerical example is used to illustrate the developments and results are compared to the well–established Mori–Tanaka mean–field formalism [20, 48, 52].

5.1.2 Preliminaries

The constitutive relations for piezoelectric materials have been outlined in §4.1. We develop the SPFT in the frequency domain. Accordingly the complex–valued representations of the stress, strain and electromagnetic fields have an implicit

$\exp(-i\omega t)$ dependency on time t, with ω being the angular frequency and $i = \sqrt{-1}$. The possibility of dissipative behaviour is thereby accommodated via the imaginary parts of complex–valued constitutive parameters.

In developing the piezoelectric SPFT, it is expedient to express the constitutive relations (4.5) in matrix–vector form as

$$\breve{\boldsymbol{\sigma}}^{(\ell)} = \breve{\underline{\underline{\mathbf{C}}}}^{(\ell)} \cdot \breve{\mathbf{S}}^{(\ell)}, \tag{5.1}$$

wherein $\breve{\boldsymbol{\sigma}}$ and $\breve{\mathbf{S}}$ are column 12–vectors representing the extended stress and extended strain symbols, respectively, and $\breve{\underline{\underline{\mathbf{C}}}}$ is a 12×12 matrix which represents the extended stiffness symbol. The conversion from extended symbol notation to matrix or vector notation is given in §5.1.3. Here, and hereafter, matrices are denoted by double underlining and bold font, whereas vectors are in bold font with no underlining. For use later on, we note that the pqth entry of a matrix $\underline{\underline{\mathbf{A}}}$ is written as $\big[\underline{\underline{\mathbf{A}}}\big]_{pq}$, while the pth entry of a vector $\mathbf{b}$ is written as $[\mathbf{b}]_p$. Accordingly, the matrix entry $\big[\underline{\underline{\mathbf{A}}} \cdot \underline{\underline{\mathbf{B}}}\big]_{pr} = \big[\underline{\underline{\mathbf{A}}}\big]_{pq}\big[\underline{\underline{\mathbf{B}}}\big]_{qr}$, the vector entry $\big[\underline{\underline{\mathbf{A}}} \cdot \mathbf{b}\big]_p = \big[\underline{\underline{\mathbf{A}}}\big]_{pq}[\mathbf{b}]_q$, and the scalar $\mathbf{a} \cdot \mathbf{b} = [\mathbf{a}]_p[\mathbf{b}]_p$. The adjoint, determinant, inverse, trace and transpose of a matrix $\underline{\underline{\mathbf{A}}}$ are denoted by $\text{adj}\,\big(\underline{\underline{\mathbf{A}}}\big)$, $\det\big(\underline{\underline{\mathbf{A}}}\big)$, $\underline{\underline{\mathbf{A}}}^{-1}$, $\text{tr}\,\big(\underline{\underline{\mathbf{A}}}\big)$ and $\underline{\underline{\mathbf{A}}}^{T}$, respectively. The $n \times n$ null matrix is written as $\underline{\underline{\mathbf{0}}}_{n\times n}$.

Our concern in this chapter is with orthorhombic $mm2$ piezoelectric materials [53, 54]. For this symmetry class, the extended stiffness matrix for material 'ℓ' has the block matrix form

$$\breve{\underline{\underline{\mathbf{C}}}}^{(\ell)} = \begin{pmatrix} \underline{\underline{\mathbf{C}}}^{(\ell)} & -\underline{\underline{\mathbf{e}}}^{(\ell)T} \\ \underline{\underline{\mathbf{e}}}^{(\ell)} & \underline{\underline{\boldsymbol{\epsilon}}}^{(\ell)} \end{pmatrix}, \tag{5.2}$$

where the 9×9 stiffness matrix $\underline{\underline{\mathbf{C}}}^{(\ell)}$ may be expressed as

$$\underline{\underline{\mathbf{C}}}^{(\ell)} = \begin{pmatrix} \underline{\underline{\mathcal{M}}}^{(\ell)} & \underline{\underline{\mathbf{0}}}_{3\times3} & \underline{\underline{\mathbf{0}}}_{3\times3} \\ \underline{\underline{\mathbf{0}}}_{3\times3} & \underline{\underline{\mathcal{D}}}^{(\ell)} & \underline{\underline{\mathcal{D}}}^{(\ell)} \\ \underline{\underline{\mathbf{0}}}_{3\times3} & \underline{\underline{\mathcal{D}}}^{(\ell)} & \underline{\underline{\mathcal{D}}}^{(\ell)} \end{pmatrix}, \tag{5.3}$$

with the 3×3 symmetric matrix components

$$\underline{\underline{\mathcal{M}}}^{(\ell)} = \begin{pmatrix} C_{11}^{(\ell)} & C_{12}^{(\ell)} & C_{13}^{(\ell)} \\ C_{12}^{(\ell)} & C_{22}^{(\ell)} & C_{23}^{(\ell)} \\ C_{13}^{(\ell)} & C_{23}^{(\ell)} & C_{33}^{(\ell)} \end{pmatrix}, \qquad \underline{\underline{\mathcal{D}}}^{(\ell)} = \begin{pmatrix} C_{44}^{(\ell)} & 0 & 0 \\ 0 & C_{55}^{(\ell)} & 0 \\ 0 & 0 & C_{66}^{(\ell)} \end{pmatrix}; \tag{5.4}$$

while the 9×3 piezoelectric matrix $\underline{\underline{\mathbf{e}}}^{(\ell)}$ may be expressed as

$$\underline{\underline{\mathbf{e}}}^{(\ell)} = \begin{pmatrix} 0 & 0 & 0 & 0 & e_{15}^{(\ell)} & 0 & 0 & e_{15}^{(\ell)} & 0 \\ 0 & 0 & 0 & e_{24}^{(\ell)} & 0 & 0 & e_{24}^{(\ell)} & 0 & 0 \\ e_{31}^{(\ell)} & e_{32}^{(\ell)} & e_{33}^{(\ell)} & 0 & 0 & 0 & 0 & 0 & 0 \end{pmatrix} \tag{5.5}$$

and the 3×3 dielectric matrix $\underline{\underline{\boldsymbol{\epsilon}}}^{(\ell)}$ as

$$\underline{\underline{\boldsymbol{\epsilon}}}^{(\ell)} = \begin{pmatrix} \epsilon_{11}^{(\ell)} & 0 & 0 \\ 0 & \epsilon_{22}^{(\ell)} & 0 \\ 0 & 0 & \epsilon_{33}^{(\ell)} \end{pmatrix}. \tag{5.6}$$

5.1.3 Tensor/extended symbol to matrix correspondence

The extended symbol $\breve{A}_{aMPq}$ ($a, q \in \{1,2,3\}$, $M, P \in \{1,2,3,4\}$) may be conveniently represented by the 12×12 matrix with entries $\left[\underline{\underline{\breve{\mathbf{A}}}}\right]_{\gamma o}$ ($\gamma, o \in [1,12]$), upon replacing the index pair aM with γ and the index pair Pq with o. For the most

general 12×12 matrix encountered in this thesis, which has the form

$$\underline{\underline{\breve{\mathbf{A}}}} = \begin{pmatrix} A_{1,1} & A_{1,2} & A_{1,3} & 0 & 0 & 0 & 0 & 0 & 0 & 0 & 0 & A_{1,12} \\ A_{2,1} & A_{2,2} & A_{2,3} & 0 & 0 & 0 & 0 & 0 & 0 & 0 & 0 & A_{2,12} \\ A_{3,1} & A_{3,2} & A_{3,3} & 0 & 0 & 0 & 0 & 0 & 0 & 0 & 0 & A_{3,12} \\ 0 & 0 & 0 & A_{4,4} & 0 & 0 & A_{4,4} & 0 & 0 & 0 & A_{4,11} & 0 \\ 0 & 0 & 0 & 0 & A_{5,5} & 0 & 0 & A_{5,5} & 0 & A_{5,10} & 0 & 0 \\ 0 & 0 & 0 & 0 & 0 & A_{6,6} & 0 & 0 & A_{6,6} & 0 & 0 & 0 \\ 0 & 0 & 0 & A_{4,4} & 0 & 0 & A_{4,4} & 0 & 0 & 0 & A_{4,11} & 0 \\ 0 & 0 & 0 & 0 & A_{5,5} & 0 & 0 & A_{5,5} & 0 & A_{5,10} & 0 & 0 \\ 0 & 0 & 0 & 0 & 0 & A_{6,6} & 0 & 0 & A_{6,6} & 0 & 0 & 0 \\ 0 & 0 & 0 & 0 & A_{10,5} & 0 & 0 & A_{10,5} & 0 & A_{10,10} & 0 & 0 \\ 0 & 0 & 0 & A_{11,4} & 0 & 0 & A_{11,4} & 0 & 0 & 0 & A_{11,11} & 0 \\ A_{12,1} & A_{12,2} & A_{12,3} & 0 & 0 & 0 & 0 & 0 & 0 & 0 & 0 & A_{12,12} \end{pmatrix}, \tag{5.7}$$

the correspondence between the extended symbol indexes and the matrix indexes is provided in Table 5.1. The scheme presented in Table 5.1 also relates the extended symbol $\breve{t}_{aM}$ to the corresponding column 12–vector entries $\left[\breve{\mathbf{t}}\right]_{\gamma}$.

aM or Pq	γ or o	aM or Pq	γ or o
11	1	23 or 32	7
22	2	13 or 31	8
33	3	12 or 21	9
23 or 32	4	14 or 41	10
13 or 31	5	24 or 42	11
12 or 21	6	34 or 43	12

Table 5.1: Conversion between extended symbol and matrix notation.

We introduce the matrix $\underline{\underline{\breve{\mathbf{A}}}}^{\ddagger}$ which plays a role similar to the matrix inverse insofar as

$$\underline{\underline{\breve{\mathbf{A}}}}^{\ddagger} \cdot \underline{\underline{\breve{\mathbf{A}}}} = \underline{\underline{\breve{\mathbf{A}}}} \cdot \underline{\underline{\breve{\mathbf{A}}}}^{\ddagger} = \underline{\underline{\breve{\boldsymbol{\tau}}}}. \tag{5.8}$$

Herein,

$$\underline{\underline{\breve{\boldsymbol{\tau}}}} = \begin{pmatrix} \underline{\underline{\mathbf{I}}} & \underline{\underline{\mathbf{0}}}_{3\times3} & \underline{\underline{\mathbf{0}}}_{3\times3} & \underline{\underline{\mathbf{0}}}_{3\times3} \\ \underline{\underline{\mathbf{0}}}_{3\times3} & \frac{1}{2}\underline{\underline{\mathbf{I}}} & \frac{1}{2}\underline{\underline{\mathbf{I}}} & \underline{\underline{\mathbf{0}}}_{3\times3} \\ \underline{\underline{\mathbf{0}}}_{3\times3} & \frac{1}{2}\underline{\underline{\mathbf{I}}} & \frac{1}{2}\underline{\underline{\mathbf{I}}} & \underline{\underline{\mathbf{0}}}_{3\times3} \\ \underline{\underline{\mathbf{0}}}_{3\times3} & \underline{\underline{\mathbf{0}}}_{3\times3} & \underline{\underline{\mathbf{0}}}_{3\times3} & \underline{\underline{\mathbf{I}}} \end{pmatrix} \tag{5.9}$$

is the 12×12 matrix representation of the extended identity symbol, with $\underline{\underline{\mathbf{I}}}$ being the 3×3 identity matrix, and we have

$$\underline{\underline{\breve{\mathbf{A}}}} \cdot \underline{\underline{\breve{\boldsymbol{\tau}}}} = \underline{\underline{\breve{\boldsymbol{\tau}}}} \cdot \underline{\underline{\breve{\mathbf{A}}}} = \underline{\underline{\breve{\mathbf{A}}}}. \tag{5.10}$$

The matrix $\underline{\underline{\breve{\mathbf{A}}}}^{\ddagger}$ has the form

$$\underline{\underline{\breve{\mathbf{A}}}}^{\ddagger} = \begin{pmatrix} \ddagger_{1,1} & \ddagger_{1,2} & \ddagger_{1,3} & 0 & 0 & 0 & 0 & 0 & 0 & 0 & 0 & \ddagger_{1,12} \\ \ddagger_{2,1} & \ddagger_{2,2} & \ddagger_{2,3} & 0 & 0 & 0 & 0 & 0 & 0 & 0 & 0 & \ddagger_{2,12} \\ \ddagger_{3,1} & \ddagger_{3,2} & \ddagger_{3,3} & 0 & 0 & 0 & 0 & 0 & 0 & 0 & 0 & \ddagger_{3,12} \\ 0 & 0 & 0 & \frac{\ddagger_{4,4}}{2} & 0 & 0 & \frac{\ddagger_{4,4}}{2} & 0 & 0 & 0 & \ddagger_{4,11} & 0 \\ 0 & 0 & 0 & 0 & \frac{\ddagger_{5,5}}{2} & 0 & 0 & \frac{\ddagger_{5,5}}{2} & 0 & \ddagger_{5,10} & 0 & 0 \\ 0 & 0 & 0 & 0 & 0 & \frac{\ddagger_{6,6}}{2} & 0 & 0 & \frac{\ddagger_{6,6}}{2} & 0 & 0 & 0 \\ 0 & 0 & 0 & \frac{\ddagger_{4,4}}{2} & 0 & 0 & \frac{\ddagger_{4,4}}{2} & 0 & 0 & 0 & \ddagger_{4,11} & 0 \\ 0 & 0 & 0 & 0 & \frac{\ddagger_{5,5}}{2} & 0 & 0 & \frac{\ddagger_{5,5}}{2} & 0 & \ddagger_{5,10} & 0 & 0 \\ 0 & 0 & 0 & 0 & 0 & \frac{\ddagger_{6,6}}{2} & 0 & 0 & \frac{\ddagger_{6,6}}{2} & 0 & 0 & 0 \\ 0 & 0 & 0 & 0 & \ddagger_{10,5} & 0 & 0 & \ddagger_{10,5} & 0 & \ddagger_{10,10} & 0 & 0 \\ 0 & 0 & 0 & \ddagger_{11,4} & 0 & 0 & \ddagger_{11,4} & 0 & 0 & 0 & \ddagger_{11,11} & 0 \\ \ddagger_{12,1} & \ddagger_{12,2} & \ddagger_{12,3} & 0 & 0 & 0 & 0 & 0 & 0 & 0 & 0 & \ddagger_{12,12} \end{pmatrix}, \tag{5.11}$$

with entries

$$
\begin{aligned}
\ddagger_{1,1} &= (-A_{12,3}A_{2,2}A_{3,12} + A_{12,2}A_{2,3}A_{3,12} + A_{12,3}A_{2,12}A_{3,2} - A_{12,12}A_{2,3}A_{3,2} - \\
&\quad A_{12,2}A_{2,12}A_{3,3} + A_{12,12}A_{2,2}A_{3,3})/\Lambda, && (5.12)\\
\ddagger_{1,2} &= (A_{1,2}A_{12,3}A_{3,12} - A_{12,2}A_{1,3}A_{3,12} - A_{1,12}A_{12,3}A_{3,2} + A_{12,12}A_{1,3}A_{3,2} - \\
&\quad A_{1,2}A_{12,12}A_{3,3} + A_{1,12}A_{12,2}A_{3,3})/\Lambda, && (5.13)\\
\ddagger_{1,3} &= (-A_{1,2}A_{12,3}A_{2,12} + A_{12,2}A_{1,3}A_{2,12} + A_{1,12}A_{12,3}A_{2,2} - A_{12,12}A_{1,3}A_{2,2} + \\
&\quad A_{1,2}A_{12,12}A_{2,3} - A_{1,12}A_{12,2}A_{2,3})/\Lambda, && (5.14)\\
\ddagger_{2,1} &= (-A_{12,3}A_{2,12}A_{3,1} + A_{12,12}A_{2,3}A_{3,1} + A_{12,3}A_{2,1}A_{3,12} - A_{12,1}A_{2,3}A_{3,12} - \\
&\quad A_{12,12}A_{2,1}A_{3,3} + A_{12,1}A_{2,12}A_{3,3})/\Lambda, && (5.15)\\
\ddagger_{2,2} &= (A_{1,12}A_{12,3}A_{3,1} - A_{12,12}A_{1,3}A_{3,1} - A_{1,1}A_{12,3}A_{3,12} + A_{12,1}A_{1,3}A_{3,12} - \\
&\quad A_{1,12}A_{12,1}A_{3,3} + A_{1,1}A_{12,12}A_{3,3})/\Lambda, && (5.16)\\
\ddagger_{2,3} &= (-A_{1,12}A_{12,3}A_{2,1} + A_{12,12}A_{1,3}A_{2,1} + A_{1,1}A_{12,3}A_{2,12} - A_{12,1}A_{1,3}A_{2,12} + \\
&\quad A_{1,12}A_{12,1}A_{2,3} - A_{1,1}A_{12,12}A_{2,3})/\Lambda, && (5.17)\\
\ddagger_{3,1} &= (A_{12,2}A_{2,12}A_{3,1} - A_{12,12}A_{2,2}A_{3,1} - A_{12,2}A_{2,1}A_{3,12} + A_{12,1}A_{2,2}A_{3,12} + \\
&\quad A_{12,12}A_{2,1}A_{3,2} - A_{12,1}A_{2,12}A_{3,2})/\Lambda, && (5.18)\\
\ddagger_{3,2} &= (A_{1,2}A_{12,12}A_{3,1} - A_{1,12}A_{12,2}A_{3,1} - A_{1,2}A_{12,1}A_{3,12} + A_{1,1}A_{12,2}A_{3,12} + \\
&\quad A_{1,12}A_{12,1}A_{3,2} - A_{1,1}A_{12,12}A_{3,2})/\Lambda, && (5.19)\\
\ddagger_{3,3} &= (-A_{1,2}A_{12,12}A_{2,1} + A_{1,12}A_{12,2}A_{2,1} + A_{1,2}A_{12,1}A_{2,12} - A_{1,1}A_{12,2}A_{2,12} - \\
&\quad A_{1,12}A_{12,1}A_{2,2} + A_{1,1}A_{12,12}A_{2,2})/\Lambda, && (5.20)\\
\ddagger_{4,4} &= \frac{A_{11,11}}{2(A_{11,11}A_{4,4} - A_{4,11}A_{11,4})}, && (5.21)\\
\ddagger_{5,5} &= \frac{A_{10,10}}{2(A_{10,10}A_{5,5} - A_{5,10}A_{10,5})}, && (5.22)\\
\ddagger_{6,6} &= \frac{1}{2A_{6,6}}, && (5.23)\\
\ddagger_{10,10} &= \frac{A_{5,5}}{(A_{10,10}A_{5,5} - A_{10,5}A_{5,10})}, && (5.24)\\
\ddagger_{11,11} &= \frac{A_{4,4}}{(A_{11,11}A_{4,4} - A_{11,4}A_{4,11})}, && (5.25)\\
\ddagger_{12,12} &= (-A_{1,3}A_{2,2}A_{3,1} + A_{1,2}A_{2,3}A_{3,1} + A_{1,3}A_{2,1}A_{3,2} - A_{1,1}A_{2,3}A_{3,2} - \\
&\quad A_{1,2}A_{2,1}A_{3,3} + A_{1,1}A_{2,2}A_{3,3})/\Lambda, && (5.26)
\end{aligned}
$$

$$
\begin{aligned}
\ddagger_{1,12} &= (A_{1,3}A_{2,2}A_{3,12} - A_{1,2}A_{2,3}A_{3,12} - A_{1,3}A_{2,12}A_{3,2} + A_{1,12}A_{2,3}A_{3,2} + \\
&\quad A_{1,2}A_{2,12}A_{3,3} - A_{1,12}A_{2,2}A_{3,3})/\Lambda, && (5.27)\\
\ddagger_{2,12} &= (A_{1,3}A_{2,12}A_{3,1} - A_{1,12}A_{2,3}A_{3,1} - A_{1,3}A_{2,1}A_{3,12} + A_{1,1}A_{2,3}A_{3,12} + \\
&\quad A_{1,12}A_{2,1}A_{3,3} - A_{1,1}A_{2,12}A_{3,3})/\Lambda, && (5.28)\\
\ddagger_{3,12} &= (-A_{1,2}A_{2,12}A_{3,1} + A_{1,12}A_{2,2}A_{3,1} + A_{1,2}A_{2,1}A_{3,12} - A_{1,1}A_{2,2}A_{3,12} - \\
&\quad A_{1,12}A_{2,1}A_{3,2} + A_{1,1}A_{2,12}A_{3,2})/\Lambda, && (5.29)\\
\ddagger_{4,11} &= \frac{A_{4,11}}{2(A_{11,4}A_{4,11} - A_{11,11}A_{4,4})}, && (5.30)\\
\ddagger_{5,10} &= \frac{A_{5,10}}{2(A_{5,10}A_{10,5} - A_{10,10}A_{5,5})}, && (5.31)\\
\ddagger_{12,1} &= (A_{12,3}A_{2,2}A_{3,1} - A_{12,2}A_{2,3}A_{3,1} - A_{12,3}A_{2,1}A_{3,2} + A_{12,1}A_{2,3}A_{3,2} + \\
&\quad A_{12,2}A_{2,1}A_{3,3} - A_{12,1}A_{2,2}A_{3,3})/\Lambda, && (5.32)\\
\ddagger_{12,2} &= (-A_{1,2}A_{12,3}A_{3,1} + A_{12,2}A_{1,3}A_{3,1} + A_{1,1}A_{12,3}A_{3,2} - A_{12,1}A_{1,3}A_{3,2} + \\
&\quad A_{1,2}A_{12,1}A_{3,3} - A_{1,1}A_{12,2}A_{3,3})/\Lambda, && (5.33)\\
\ddagger_{12,3} &= (A_{1,2}A_{12,3}A_{2,1} - A_{12,2}A_{1,3}A_{2,1} - A_{1,1}A_{12,3}A_{2,2} + A_{12,1}A_{1,3}A_{2,2} - \\
&\quad A_{1,2}A_{12,1}A_{2,3} + A_{1,1}A_{12,2}A_{2,3})/\Lambda, && (5.34)\\
\ddagger_{11,4} &= \frac{A_{11,4}}{2(A_{11,4}A_{4,11} - A_{11,11}A_{4,4})}, && (5.35)\\
\ddagger_{10,5} &= \frac{A_{10,5}}{2(A_{10,5}A_{5,10} - A_{10,10}A_{5,5})}, && (5.36)\\
& && (5.37)
\end{aligned}
$$

where the scalar

$$
\begin{aligned}
\Lambda &= A_{1,12}A_{12,3}A_{2,2}A_{3,1} - A_{12,12}A_{1,3}A_{2,2}A_{3,1} - A_{1,1}A_{12,3}A_{2,2}A_{3,12} + \\
&\quad A_{12,1}A_{1,3}A_{2,2}A_{3,12} - A_{1,12}A_{12,3}A_{2,1}A_{3,2} + A_{12,12}A_{1,3}A_{2,1}A_{3,2} + \\
&\quad A_{1,1}A_{12,3}A_{2,12}A_{3,2} - A_{12,1}A_{1,3}A_{2,12}A_{3,2} + A_{1,12}A_{12,1}A_{2,3}A_{3,2} - \\
&\quad A_{1,1}A_{12,12}A_{2,3}A_{3,2} - A_{1,12}A_{12,1}A_{2,2}A_{3,3} + A_{1,1}A_{12,12}A_{2,2}A_{3,3} + \\
&\quad A_{12,2}\Big(A_{1,3}A_{2,12}A_{3,1} - A_{1,12}A_{2,3}A_{3,1} - A_{1,3}A_{2,1}A_{3,12} + A_{1,1}A_{2,3}A_{3,12} + \\
&\quad A_{1,12}A_{2,1}A_{3,3} - A_{1,1}A_{2,12}A_{3,3}\Big) + A_{1,2}\Big(- A_{12,3}A_{2,12}A_{3,1} + A_{12,12}A_{2,3}A_{3,1} + \\
&\quad A_{12,3}A_{2,1}A_{3,12} - A_{12,1}A_{2,3}A_{3,12} - A_{12,12}A_{2,1}A_{3,3} + A_{12,1}A_{2,12}A_{3,3}\Big). && (5.38)
\end{aligned}
$$

5.1.4 Component materials

We consider the homogenization of a composite comprising two component materials, labeled as component material '1' and component material '2'. In general, both components are homogeneous, orthorhombic $mm2$ piezoelectric materials, characterized by the stiffness tensors $C^{(\ell)}_{abmn}$, piezoelectric tensors $e^{(\ell)}_{nab}$, dielectric tensors $\epsilon^{(\ell)}_{an}$ and densities $\rho^{(\ell)}$ $(\ell = 1, 2)$. In conformity with the notational practices introduced in §4.1 and §5.1.2, the component materials are also described by the extended stiffness symbols $\breve{C}^{(\ell)}_{aBMn}$ (and their 12×12 matrix equivalents $\underline{\underline{\breve{\mathbf{C}}}}^{(\ell)}$) and extended density symbols $\breve{\rho}^{(\ell)}_{BM}$ (and their 4×4 matrix equivalents $\underline{\underline{\breve{\boldsymbol{\rho}}}}^{(\ell)}$).

The inclusion particles are parameterized by (3.8) and (3.9) and the distributional statistics are described in §3.1.4. The composite has an extended stiffness symbol of the form (4.8) with $n = 2$.

5.1.5 Comparison material

We now introduce a comparison material, which in consonance with the component materials, is taken to be an orthorhombic $mm2$ piezoelectric material, in general. The piezoelectric constitutive properties of this orthorhombic comparison material (OCM) are encapsulated by its extended stiffness symbol $\breve{C}^{(ocm)}_{lMPq}$ (and its 12×12 matrix equivalent $\underline{\underline{\breve{\mathbf{C}}}}^{(ocm)}$) and extended density symbol $\breve{\rho}^{(ocm)}_{MP}$ (and its 4×4 matrix equivalent $\underline{\underline{\breve{\boldsymbol{\rho}}}}^{(ocm)}$), as described in §4.3.

In this section we derive the equations for $\underline{\underline{\breve{\mathbf{C}}}}^{(ocm)}$ and $\underline{\underline{\breve{\boldsymbol{\rho}}}}^{(ocm)}$. We begin with equations (4.99) and (4.100) which explicitly are

$$\langle \breve{\xi}_{lMPq}(\mathbf{r}) \rangle = \langle \Phi^{(1)}(\mathbf{r})\, \breve{\xi}^{(1)}_{lMPq} + \Phi^{(2)}(\mathbf{r})\, \breve{\xi}^{(2)}_{lMPq} \rangle = 0, \tag{5.39}$$

$$\langle \delta\breve{\rho}_{MP}(\mathbf{r}) \rangle = \langle \Phi^{(1)}(\mathbf{r}) \left[\breve{\rho}^{(1)} - \breve{\rho}^{(ocm)} \right]_{MP} + \Phi^{(2)}(\mathbf{r}) \left[\breve{\rho}^{(2)} - \breve{\rho}^{(ocm)} \right]_{MP} \rangle = 0 \tag{5.40}$$

and are necessary to remove all secular terms. In equation (5.39), the quantities

$$\breve{\xi}^{(\ell)}_{lMPq} = \left(\breve{C}^{(\ell)}_{lMSt} - \breve{C}^{(ocm)}_{lMSt} \right) \breve{\eta}^{(\ell)}_{StPq}, \qquad (\ell = 1, 2), \tag{5.41}$$

where $\breve{\eta}^{(\ell)}_{StPq}$ is given implicitly through

$$\breve{S}^{(\ell)}_{Pq}(\mathbf{r}) = \breve{\eta}^{(\ell)}_{PqSt}\breve{\varpi}^{(\ell)}_{St}(\mathbf{r}), \tag{5.42}$$

$$\breve{\varpi}^{(\ell)}_{Tj}(\mathbf{r}) = \breve{S}^{(\ell)}_{Tj}(\mathbf{r}) + \breve{W}_{TjlM}\left(\breve{C}^{(\ell)}_{lMPq} - \breve{C}^{(ocm)}_{lMPq}\right)\breve{S}^{(\ell)}_{Pq}(\mathbf{r}), \tag{5.43}$$

which have been reproduced from (4.45), (4.46) and (4.48). The extended renormalization symbol is given by

$$\breve{W}_{PstU} = \begin{cases} \dfrac{1}{8\pi}\displaystyle\int_0^{2\pi} d\phi \int_0^{\pi} d\theta\, \dfrac{\sin\theta}{(\underline{\underline{\mathbf{U}}}^{-1}\cdot\hat{\mathbf{k}})\cdot(\underline{\underline{\mathbf{U}}}^{-1}\cdot\hat{\mathbf{k}})}\times \\ (\underline{\underline{\mathbf{U}}}^{-1}\cdot\hat{\mathbf{k}})_t\Big\{(\underline{\underline{\mathbf{U}}}^{-1}\cdot\hat{\mathbf{k}})_s\big[\,\underline{\underline{\breve{\mathbf{a}}}}^{-1}(\underline{\underline{\mathbf{U}}}^{-1}\cdot\hat{\mathbf{k}})\,\big]_{pU} + \\ \qquad (\underline{\underline{\mathbf{U}}}^{-1}\cdot\hat{\mathbf{k}})_p\big[\,\underline{\underline{\breve{\mathbf{a}}}}^{-1}(\underline{\underline{\mathbf{U}}}^{-1}\cdot\hat{\mathbf{k}})\,\big]_{sU}\Big\}, & \mathrm{P} = \mathrm{p} = 1,\,2,\,3 \\ \\ \dfrac{1}{8\pi}\displaystyle\int_0^{2\pi} d\phi \int_0^{\pi} d\theta \sin\theta\times \\ \dfrac{(\underline{\underline{\mathbf{U}}}^{-1}\cdot\hat{\mathbf{k}})_t(\underline{\underline{\mathbf{U}}}^{-1}\cdot\hat{\mathbf{k}})_s\big[\,\underline{\underline{\breve{\mathbf{a}}}}^{-1}(\underline{\underline{\mathbf{U}}}^{-1}\cdot\hat{\mathbf{k}})\,\big]_{pU}}{(\underline{\underline{\mathbf{U}}}^{-1}\cdot\hat{\mathbf{k}})\cdot(\underline{\underline{\mathbf{U}}}^{-1}\cdot\hat{\mathbf{k}})}, & \mathrm{P} = 4 \end{cases}, \tag{5.44}$$

which is an extended version of the elastodynamic case, (3.29), as indeed is all the piezoelectric theory.

Upon substituting equations (5.41)–(5.43) into equation (5.39), exploiting $\langle\mathbf{\Phi}^{(\ell)}(\mathbf{r})\rangle = f^{(\ell)}$, and after algebraic manipulations identical to those in the elastodynamic SPFT, §3.2.2, we obtain

$$f^{(1)}\left[\left(\underline{\underline{\breve{\mathbf{C}}}}^{(1)} - \underline{\underline{\breve{\mathbf{C}}}}^{(ocm)}\right)^{\ddagger} + \underline{\underline{\breve{\mathbf{W}}}}\right]^{\ddagger} + f^{(2)}\left[\left(\underline{\underline{\breve{\mathbf{C}}}}^{(2)} - \underline{\underline{\breve{\mathbf{C}}}}^{(ocm)}\right)^{\ddagger} + \underline{\underline{\breve{\mathbf{W}}}}\right]^{\ddagger} = \underline{\mathbf{0}}_{12\times 12}, \tag{5.45}$$

wherein the 12×12 matrix equivalent of $\breve{W}_{PstU}$ (namely, $\underline{\underline{\breve{\mathbf{W}}}}$) has been introduced. The OCM stiffness extended matrix may be extracted, in exactly the same manner as the elastodynamic case, §3.2.2, from (5.45) as

$$\underline{\underline{\breve{\mathbf{C}}}}^{(ocm)} = \underline{\underline{\breve{\mathbf{C}}}}^{(1)} + f^{(2)}\left[\underline{\underline{\breve{\boldsymbol{\tau}}}} + (\underline{\underline{\breve{\mathbf{C}}}}^{(2)} - \underline{\underline{\breve{\mathbf{C}}}}^{(ocm)})\cdot\underline{\underline{\breve{\mathbf{W}}}}\right]^{\ddagger}\cdot\left(\underline{\underline{\breve{\mathbf{C}}}}^{(1)} - \underline{\underline{\breve{\mathbf{C}}}}^{(2)}\right), \tag{5.46}$$

where $\underline{\underline{\breve{\boldsymbol{\tau}}}}$ is the 12×12 matrix representation of the extended identity $\breve{\tau}_{rSTu} = \breve{\tau}_{RstU}$. By standard numerical procedures, such as the Jacobi method [37], the

nonlinear relation (5.46) is solved for $\breve{\underline{\underline{\mathbf{C}}}}^{(ocm)}$. The iteration method used in the piezoelectric SPFT is the equivalent of (3.46), with the elastic matrices replaced by the appropriate piezoelectric extension.

Exactly as in the elastodynamic case, §3.2.2, and from (5.40) we have the extended density of the OCM as the volume average of the extended densities of the component materials '1' and '2'; i.e.,

$$\breve{\underline{\underline{\boldsymbol{\rho}}}}^{(ocm)} = f^{(1)}\breve{\underline{\underline{\boldsymbol{\rho}}}}^{(1)} + f^{(2)}\breve{\underline{\underline{\boldsymbol{\rho}}}}^{(2)}. \tag{5.47}$$

5.1.6 Second-order SPFT

The second–order[1] estimates of the HCM extended stiffness and density symbols, (4.103) and (4.104), may be expressed in terms of three–dimensional integrals as

$$\begin{aligned}\breve{C}^{(spft)}_{lMPq} &= \breve{C}^{(ocm)}_{lMPq} - \frac{\omega^2}{2}\int d^3k\ \frac{k_t}{k^2}\,\breve{B}^{lMrs}_{tUPq}(\mathbf{k})\left[\breve{\underline{\underline{\boldsymbol{\rho}}}}^{(ocm)}\right]_{XY}\left[\breve{\underline{\underline{\mathbf{G}}}}^{(ocm)}(\mathbf{k})\right]_{YU}\times \\ &\quad \left\{k_s\left[\breve{\underline{\underline{\mathbf{a}}}}^{-1}(\hat{\mathbf{k}})\right]_{rX} + k_r\left[\breve{\underline{\underline{\mathbf{a}}}}^{-1}(\hat{\mathbf{k}})\right]_{sX}\right\} - \\ &\quad \frac{\omega^2}{2}\int d^3k\ \frac{k_t}{k^2}\,\breve{B}^{lM4s}_{tUPq}(\mathbf{k})\left[\breve{\underline{\underline{\boldsymbol{\rho}}}}^{(ocm)}\right]_{XY}\left[\breve{\underline{\underline{\mathbf{G}}}}^{(ocm)}(\mathbf{k})\right]_{YU}\left\{k_s\left[\breve{\underline{\underline{\mathbf{a}}}}^{-1}(\hat{\mathbf{k}})\right]_{4X}\right\}\end{aligned} \tag{5.48}$$

and

$$\breve{\rho}^{(spft)}_{MP} = \breve{\rho}^{(ocm)}_{MP} + \omega^2\int d^3k\ \breve{B}_{MSUP}(\mathbf{k})\left[\breve{\underline{\underline{\mathbf{G}}}}^{(ocm)}(\mathbf{k})\right]_{SU}. \tag{5.49}$$

The symbols $\breve{B}^{lMRs}_{tUPq}(\mathbf{k})$ and $\breve{B}_{MSUP}(\mathbf{k})$ represent the spectral covariance functions, which from (4.84), (4.86), (4.98) and utilizing (4.99), (4.100), are given by

$$\left.\begin{aligned}\breve{B}^{lMNs}_{tUPq}(\mathbf{k}) &= \frac{\left(\breve{\xi}^{(2)}_{lMNs} - \breve{\xi}^{(1)}_{lMNs}\right)\left(\breve{\xi}^{(2)}_{tUPq} - \breve{\xi}^{(1)}_{tUPq}\right)}{8\pi^3}\int d^3R\ \Gamma(\mathbf{R})\,\exp\left(-i\mathbf{k}\cdot\mathbf{R}\right) \\ \breve{B}_{MSUP}(\mathbf{k}) &= \frac{\left(\breve{\rho}^{(2)}_{MS} - \breve{\rho}^{(1)}_{MS}\right)\left(\breve{\rho}^{(2)}_{UP} - \breve{\rho}^{(1)}_{UP}\right)}{8\pi^3}\int d^3R\,\Gamma(\mathbf{R})\,\exp\left(-i\mathbf{k}\cdot\mathbf{R}\right)\end{aligned}\right\}, \tag{5.50}$$

[1]The first–order SPFT estimate is identical to the zeroth–order SPFT estimate which is represented by the comparison material, as shown in §4.6.

with

$$\begin{aligned}\Gamma(\mathbf{R}) = \Gamma(\mathbf{r}-\mathbf{r}') &= \langle\, \Phi^{(1)}(\mathbf{r})\, \Phi^{(1)}(\mathbf{r}')\,\rangle - \langle\, \Phi^{(1)}(\mathbf{r})\,\rangle\, \langle\, \Phi^{(1)}(\mathbf{r}')\,\rangle \\ &\equiv \langle\, \Phi^{(2)}(\mathbf{r})\, \Phi^{(2)}(\mathbf{r}')\,\rangle - \langle\, \Phi^{(2)}(\mathbf{r})\,\rangle\, \langle\, \Phi^{(2)}(\mathbf{r}')\,\rangle. \end{aligned} \tag{5.51}$$

In order to make the integrals in the expressions for $\breve{C}^{(spft)}_{lMPq}$ and $\breve{\rho}^{(spft)}_{MP}$ presented in equations (5.48) and (5.49) numerically tractable, we simplify them as follows. Let us begin with the integral on the right sides of equations (5.50). Upon implementing the step function–shaped covariance function (3.12) and utilizing (3.11), we find

$$\int d^3R\ \Gamma(\mathbf{R})\, \exp\left(-i\mathbf{k}\cdot\mathbf{R}\right) = f^{(1)} f^{(2)} \int_{|\mathbf{R}|\leq L} d^3R\ \exp\left[-i\left(\underline{\underline{\mathbf{U}}}\cdot\mathbf{k}\right)\cdot\mathbf{R}\right]. \tag{5.52}$$

Thereby, the expressions for $\breve{B}^{lMRs}_{tUPq}(\mathbf{k})$ and $\breve{B}_{MSUP}(\mathbf{k})$ reduce to [38]

$$\left.\begin{aligned}\breve{B}^{lMRs}_{tUPq}(\mathbf{k}) &= \frac{f^{(1)} f^{(2)} \left(\breve{\xi}^{(2)}_{lMRs} - \breve{\xi}^{(1)}_{lMRs}\right)\left(\breve{\xi}^{(2)}_{tUPq} - \breve{\xi}^{(1)}_{tUPq}\right)}{2\left(\pi k\sigma\right)^2} \times \\ &\qquad \left[\frac{\sin\left(k\sigma L\right)}{k\sigma} - L\cos\left(k\sigma L\right)\right] \\ \breve{B}_{MSUP}(\mathbf{k}) &= \frac{f^{(1)} f^{(2)} \left(\breve{\rho}^{(2)}_{MS} - \breve{\rho}^{(1)}_{MS}\right)\left(\breve{\rho}^{(2)}_{UP} - \breve{\rho}^{(1)}_{UP}\right)}{2\left(\pi k\sigma\right)^2} \times \\ &\qquad \left[\frac{\sin\left(k\sigma L\right)}{k\sigma} - L\cos\left(k\sigma L\right)\right] \end{aligned}\right\}, \tag{5.53}$$

wherein the scalar function

$$\sigma \equiv \sigma(\theta,\phi) = \sqrt{a^2\sin^2\theta\cos^2\phi + b^2\sin^2\theta\sin^2\phi + c^2\cos^2\theta} \tag{5.54}$$

is introduced.

Now we turn to the integrals in (5.48) and (5.49). In analogy with the corresponding expression for the elastodynamic SPFT, the spectral Green function $\underline{\underline{\breve{\mathbf{G}}}}^{(ocm)}(\mathbf{k})$ may be conveniently expressed as, §4.3,

$$\underline{\underline{\breve{\mathbf{G}}}}^{(ocm)}(\mathbf{k}) = \frac{\underline{\underline{\breve{\mathbf{N}}}}(\mathbf{k})}{\breve{\Delta}(\mathbf{k})}, \tag{5.55}$$

where the 4×4 matrix function

$$\underline{\underline{\breve{\mathbf{N}}}}(\mathbf{k}) = \text{adj}\,\left[\, k^2\,\underline{\underline{\breve{\mathbf{a}}}}(\hat{\mathbf{k}}) - \omega^2\underline{\underline{\breve{\boldsymbol{\rho}}}}^{(ocm)}\right] \tag{5.56}$$

and the scalar function

$$\begin{aligned}\breve{\Delta}(\mathbf{k}) \;=\;& k^8 \det\left[\underline{\underline{\breve{\mathbf{a}}}}(\hat{\mathbf{k}})\right] - \text{tr}\left\{\text{adj}\left[k^2\underline{\underline{\breve{\mathbf{a}}}}(\hat{\mathbf{k}})\right]\cdot\omega^2\underline{\underline{\breve{\boldsymbol{\rho}}}}^{(ocm)}\right\} - \\ & k^2\,\text{tr}\left[\text{adj}(\omega^2\underline{\underline{\breve{\boldsymbol{\rho}}}}^{(ocm)})\cdot\underline{\underline{\breve{\mathbf{a}}}}(\hat{\mathbf{k}})\right] + k^4\Big(\text{tr}\Big\{\left[\underline{\underline{\breve{\mathbf{a}}}}(\hat{\mathbf{k}})\right]_{44}\left[\underline{\underline{\breve{\mathbf{a}}}}^{\sharp}(\hat{\mathbf{k}})\cdot\text{adj}(\omega^2\underline{\underline{\breve{\boldsymbol{\rho}}}}^{\sharp})\right]\Big\} - \\ & \left[\underline{\underline{\breve{\mathbf{a}}}}(\hat{\mathbf{k}})\right]_{41}\left[\underline{\underline{\breve{\mathbf{a}}}}(\hat{\mathbf{k}})\right]_{14}\left[\text{adj}(\omega^2\underline{\underline{\breve{\boldsymbol{\rho}}}}^{\sharp})\right]_{11} - \left[\underline{\underline{\breve{\mathbf{a}}}}(\hat{\mathbf{k}})\right]_{42}\left[\underline{\underline{\breve{\mathbf{a}}}}(\hat{\mathbf{k}})\right]_{24}\left[\text{adj}(\omega^2\underline{\underline{\breve{\boldsymbol{\rho}}}}^{\sharp})\right]_{22} - \\ & \left[\underline{\underline{\breve{\mathbf{a}}}}(\hat{\mathbf{k}})\right]_{31}\left[\underline{\underline{\breve{\mathbf{a}}}}(\hat{\mathbf{k}})\right]_{13}\left[\text{adj}(\omega^2\underline{\underline{\breve{\boldsymbol{\rho}}}}^{\sharp})\right]_{33}\Big),\end{aligned} \tag{5.57}$$

with the 3×3 matrices $\underline{\underline{\breve{\mathbf{a}}}}^{\sharp}$ and $\underline{\underline{\breve{\boldsymbol{\rho}}}}^{\sharp}$ having entries

$$\begin{aligned}\underline{\underline{\breve{\mathbf{a}}}}^{\sharp}(\mathbf{k}) \;&=\; \begin{pmatrix} \left[\underline{\underline{\breve{\mathbf{a}}}}(\hat{\mathbf{k}})\right]_{11} & \left[\underline{\underline{\breve{\mathbf{a}}}}(\hat{\mathbf{k}})\right]_{12} & \left[\underline{\underline{\breve{\mathbf{a}}}}(\hat{\mathbf{k}})\right]_{13} \\ \left[\underline{\underline{\breve{\mathbf{a}}}}(\hat{\mathbf{k}})\right]_{21} & \left[\underline{\underline{\breve{\mathbf{a}}}}(\hat{\mathbf{k}})\right]_{22} & \left[\underline{\underline{\breve{\mathbf{a}}}}(\hat{\mathbf{k}})\right]_{23} \\ \left[\underline{\underline{\breve{\mathbf{a}}}}(\hat{\mathbf{k}})\right]_{31} & \left[\underline{\underline{\breve{\mathbf{a}}}}(\hat{\mathbf{k}})\right]_{32} & \left[\underline{\underline{\breve{\mathbf{a}}}}(\hat{\mathbf{k}})\right]_{33} \end{pmatrix}, \\ \underline{\underline{\breve{\boldsymbol{\rho}}}}^{\sharp} \;&=\; \begin{pmatrix} \left[\underline{\underline{\breve{\boldsymbol{\rho}}}}^{(ocm)}\right]_{11} & \left[\underline{\underline{\breve{\boldsymbol{\rho}}}}^{(ocm)}\right]_{12} & \left[\underline{\underline{\breve{\boldsymbol{\rho}}}}^{(ocm)}\right]_{13} \\ \left[\underline{\underline{\breve{\boldsymbol{\rho}}}}^{(ocm)}\right]_{21} & \left[\underline{\underline{\breve{\boldsymbol{\rho}}}}^{(ocm)}\right]_{22} & \left[\underline{\underline{\breve{\boldsymbol{\rho}}}}^{(ocm)}\right]_{23} \\ \left[\underline{\underline{\breve{\boldsymbol{\rho}}}}^{(ocm)}\right]_{31} & \left[\underline{\underline{\breve{\boldsymbol{\rho}}}}^{(ocm)}\right]_{32} & \left[\underline{\underline{\breve{\boldsymbol{\rho}}}}^{(ocm)}\right]_{33} \end{pmatrix}. \end{aligned} \tag{5.58}$$

Through exploiting equations (5.53) and (5.55), the integrals in equations (5.48) and (5.49) with respect to k can be evaluated by means of calculus of residues: The roots of $\breve{\Delta}(\mathbf{k}) = 0$ give rise to seven poles in the complex–k plane, located at $k = 0, \pm\breve{p}_1, \pm\breve{p}_2, \pm\breve{p}_3$, which are chosen such that $\breve{p}_n$ $(n = 1, 2, 3)$ lie in the upper half of the complex plane. From equation (5.57), we find that the

nonzero poles satisfy

$$\breve{p}_1^2 = \mathcal{P}_A - \frac{1}{3}\left(\frac{2^{1/3}\mathcal{P}_B}{\mathcal{P}_C} - \frac{\mathcal{P}_C}{2^{1/3}}\right), \tag{5.59}$$

$$\breve{p}_2^2 = \mathcal{P}_A + \frac{1}{3}\left(\frac{(1+i\sqrt{3})\mathcal{P}_B}{2^{2/3}\mathcal{P}_C} - \frac{(1-i\sqrt{3})\mathcal{P}_C}{2^{4/3}}\right), \tag{5.60}$$

$$\breve{p}_3^2 = \mathcal{P}_A + \frac{1}{3}\left(\frac{(1-i\sqrt{3})\mathcal{P}_B}{2^{2/3}\mathcal{P}_C} - \frac{(1+i\sqrt{3})\mathcal{P}_C}{2^{4/3}}\right), \tag{5.61}$$

wherein

$$\mathcal{P}_A = \frac{\omega^2 \mathrm{tr}\left\{\mathrm{adj}\left[\underline{\underline{\breve{\mathbf{a}}}}(\hat{\mathbf{k}})\right] \cdot \underline{\underline{\breve{\boldsymbol{\rho}}}}^{(ocm)}\right\}}{3\det\left[\underline{\underline{\breve{\mathbf{a}}}}(\hat{\mathbf{k}})\right]}, \tag{5.62}$$

$$\mathcal{P}_B = -\mathcal{C}_A^2 + 3\,\mathcal{C}_B, \tag{5.63}$$

$$\mathcal{P}_C = \left[\mathcal{P}_D + \left(4\mathcal{P}_B^3 + \mathcal{P}_D^2\right)^{1/2}\right]^{1/3}, \tag{5.64}$$

$$\mathcal{P}_D = -2\,\mathcal{C}_A^3 + 9\,\mathcal{C}_A\,\mathcal{C}_B - 27\,\mathcal{C}_C, \tag{5.65}$$

with

$$\mathcal{C}_A = \frac{-\omega^2\,\mathrm{tr}\left\{\mathrm{adj}\left[\underline{\underline{\breve{\mathbf{a}}}}(\hat{\mathbf{k}})\right] \cdot \underline{\underline{\breve{\boldsymbol{\rho}}}}^{(ocm)}\right\}}{\det\left[\underline{\underline{\breve{\mathbf{a}}}}(\hat{\mathbf{k}})\right]}, \tag{5.66}$$

$$\begin{aligned}\mathcal{C}_B = \frac{\omega^4}{\det\left[\underline{\underline{\breve{\mathbf{a}}}}(\hat{\mathbf{k}})\right]}\Bigg\{ & \left[\underline{\underline{\breve{\mathbf{a}}}}(\hat{\mathbf{k}})\right]_{44} \mathrm{tr}\left[\underline{\underline{\breve{\mathbf{a}}}}^{\sharp}(\hat{\mathbf{k}}) \cdot \mathrm{adj}\left(\underline{\underline{\breve{\boldsymbol{\rho}}}}^{\sharp}\right)\right] + \\ & \left[\underline{\underline{\breve{\mathbf{a}}}}(\hat{\mathbf{k}})\right]_{41}\left[\underline{\underline{\breve{\mathbf{a}}}}(\hat{\mathbf{k}})\right]_{14}\left[\mathrm{adj}\left(\underline{\underline{\breve{\boldsymbol{\rho}}}}^{(ocm)}\right)\right]_{11} + \\ & \left[\underline{\underline{\breve{\mathbf{a}}}}(\hat{\mathbf{k}})\right]_{42}\left[\underline{\underline{\breve{\mathbf{a}}}}(\hat{\mathbf{k}})\right]_{24}\left[\mathrm{adj}\left(\underline{\underline{\breve{\boldsymbol{\rho}}}}^{(ocm)}\right)\right]_{22} + \\ & \left[\underline{\underline{\breve{\mathbf{a}}}}(\hat{\mathbf{k}})\right]_{43}\left[\underline{\underline{\breve{\mathbf{a}}}}(\hat{\mathbf{k}})\right]_{34}\left[\mathrm{adj}\left(\underline{\underline{\breve{\boldsymbol{\rho}}}}^{(ocm)}\right)\right]_{33}\Bigg\},\end{aligned} \tag{5.67}$$

$$\mathcal{C}_C = \frac{-\omega^6\,\mathrm{tr}\left\{\mathrm{adj}\left[\underline{\underline{\breve{\boldsymbol{\rho}}}}^{(ocm)}\right] \cdot \underline{\underline{\breve{\mathbf{a}}}}(\hat{\mathbf{k}})\right\}}{\det\left[\underline{\underline{\breve{\mathbf{a}}}}(\hat{\mathbf{k}})\right]}. \tag{5.68}$$

We must calculate the residue of $\underline{\underline{\breve{\mathbf{G}}}}^{(ocm)}$ at each of the poles of $\breve{\Delta}(\mathbf{k}) = 0$. Furthermore, a simple pole is introduced by the covariance function (5.53). The

function we wish to find the residue of is

$$\frac{\breve{\underline{\underline{\mathbf{N}}}}(\mathbf{k})}{\acute{\breve{\mathcal{F}}}(k)}\left[\frac{e^{iL\sigma k}-e^{-iL\sigma k}}{2i\sigma k}-\frac{L(e^{iL\sigma k}+e^{-iL\sigma k})}{2}\right] \tag{5.69}$$

with

$$\acute{\breve{\mathcal{F}}}(k)=k^2(k-\breve{p}_1)(k-\breve{p}_2)(k-\breve{p}_3)(k+\breve{p}_1)(k+\breve{p}_2)(k+\breve{p}_3). \tag{5.70}$$

We calculate the residue using contour integration, exactly as in the elastodynamic SPFT, §3.2.4. Splitting (5.69) into 4 separate functions;

$$\breve{\mathcal{F}}_1(k) = \frac{\breve{\underline{\underline{\mathbf{N}}}}(\mathbf{k})}{\acute{\breve{\mathcal{F}}}(k)}\frac{e^{iL\sigma k}}{2i\sigma k} \tag{5.71}$$

$$\breve{\mathcal{F}}_2(k) = \frac{\breve{\underline{\underline{\mathbf{N}}}}(\mathbf{k})}{\acute{\breve{\mathcal{F}}}(k)}\frac{-Le^{iL\sigma k}}{2} \tag{5.72}$$

$$\breve{\mathcal{F}}_3(k) = \frac{\breve{\underline{\underline{\mathbf{N}}}}(\mathbf{k})}{\acute{\breve{\mathcal{F}}}(k)}\frac{-e^{-iL\sigma k}}{2i\sigma k} \tag{5.73}$$

$$\breve{\mathcal{F}}_4(k) = \frac{\breve{\underline{\underline{\mathbf{N}}}}(\mathbf{k})}{\acute{\breve{\mathcal{F}}}(k)}\frac{-Le^{-iL\sigma k}}{2}. \tag{5.74}$$

For the functions $\breve{\mathcal{F}}_1(k)$ and $\breve{\mathcal{F}}_2(k)$ we use a semi–circle in the upper half plane as the contour, calculating the residue at $\breve{p}_1$, $\breve{p}_2$, $\breve{p}_3$ and 0. The residues are given by

$$\mathrm{Res}(\breve{\mathcal{F}}_1(\breve{p}_1)) = \frac{-i\breve{\underline{\underline{\mathbf{N}}}}(\breve{p}_1\underline{\underline{\mathbf{U}}}\cdot\hat{\mathbf{k}})e^{iL\sigma\breve{p}_1}}{4\sigma\breve{p}_1^4(\breve{p}_1^2-\breve{p}_2^2)(\breve{p}_1^2-\breve{p}_3^2)} \tag{5.75}$$

$$\mathrm{Res}(\breve{\mathcal{F}}_1(\breve{p}_2)) = \frac{i\breve{\underline{\underline{\mathbf{N}}}}(\breve{p}_2\underline{\underline{\mathbf{U}}}\cdot\hat{\mathbf{k}})e^{iL\sigma\breve{p}_2}}{4\sigma\breve{p}_2^4(\breve{p}_1^2-\breve{p}_2^2)(\breve{p}_2^2-\breve{p}_3^2)} \tag{5.76}$$

$$\mathrm{Res}(\breve{\mathcal{F}}_1(\breve{p}_3)) = \frac{-i\breve{\underline{\underline{\mathbf{N}}}}(\breve{p}_3\underline{\underline{\mathbf{U}}}\cdot\hat{\mathbf{k}})e^{iL\sigma\breve{p}_3}}{4\sigma\breve{p}_3^4(\breve{p}_1^2-\breve{p}_3^2)(\breve{p}_2^2-\breve{p}_3^2)} \tag{5.77}$$

$$\begin{aligned}\mathrm{Res}(\breve{\mathcal{F}}_1(0)) = \frac{1}{4i\sigma\breve{p}_1^4\breve{p}_2^4\breve{p}_3^4}\times\Bigg\{\breve{p}_1^2\breve{p}_2^2\breve{p}_3^2\Bigg(&\breve{\underline{\underline{\mathbf{N}}}}(\mathbf{0})\sigma^2L^2-2i\frac{\partial}{\partial k}\breve{\underline{\underline{\mathbf{N}}}}(\mathbf{0})\sigma L-\\ &\frac{\partial^2}{\partial k^2}\breve{\underline{\underline{\mathbf{N}}}}(\mathbf{0})\Bigg)-2\breve{\underline{\underline{\mathbf{N}}}}(\mathbf{0})\left(\breve{p}_1^2\breve{p}_2^2+\breve{p}_1^2\breve{p}_3^2+\breve{p}_2^2\breve{p}_3^2\right)\Bigg\}\end{aligned} \tag{5.78}$$

$$\mathrm{Res}(\breve{\mathcal{F}}_2(\breve{p}_1)) = \frac{-L\underline{\underline{\breve{\mathbf{N}}}}(\breve{p}_1\underline{\underline{\mathbf{U}}}\cdot\hat{\mathbf{k}})e^{iL\sigma\breve{p}_1}}{4\sigma\breve{p}_1^3(\breve{p}_1^2-\breve{p}_2^2)(\breve{p}_1^2-\breve{p}_3^2)} \tag{5.79}$$

$$\mathrm{Res}(\breve{\mathcal{F}}_2(\breve{p}_2)) = \frac{L\underline{\underline{\breve{\mathbf{N}}}}(\breve{p}_2\underline{\underline{\mathbf{U}}}\cdot\hat{\mathbf{k}})e^{iL\sigma\breve{p}_2}}{4\sigma\breve{p}_2^3(\breve{p}_1^2-\breve{p}_2^2)(\breve{p}_2^2-\breve{p}_3^2)} \tag{5.80}$$

$$\mathrm{Res}(\breve{\mathcal{F}}_2(\breve{p}_3)) = \frac{-L\underline{\underline{\breve{\mathbf{N}}}}(\breve{p}_3\underline{\underline{\mathbf{U}}}\cdot\hat{\mathbf{k}})e^{iL\sigma\breve{p}_3}}{4\sigma\breve{p}_3^3(\breve{p}_1^2-\breve{p}_3^2)(\breve{p}_2^2-\breve{p}_3^2)} \tag{5.81}$$

$$\mathrm{Res}(\breve{\mathcal{F}}_2(0)) = \frac{iL\left(\underline{\underline{\breve{\mathbf{N}}}}(\mathbf{0})\sigma L - i\frac{\partial}{\partial k}\underline{\underline{\breve{\mathbf{N}}}}(\mathbf{0})\right)}{2\breve{p}_1^2\breve{p}_2^2\breve{p}_3^2}, \tag{5.82}$$

Similarly, for the functions $\breve{\mathcal{F}}_3(k)$ and $\breve{\mathcal{F}}_4(k)$ we use a semi–circle in the lower half plane as the contour, calculating the residue at $-\breve{p}_1$, $-\breve{p}_2$, $-\breve{p}_3$ and 0. These residues are given by

$$\mathrm{Res}(\breve{\mathcal{F}}_3(-\breve{p}_1)) = \frac{i\underline{\underline{\breve{\mathbf{N}}}}(\breve{p}_1\underline{\underline{\mathbf{U}}}\cdot\hat{\mathbf{k}})e^{iL\sigma\breve{p}_1}}{4\sigma\breve{p}_1^4(\breve{p}_1^2-\breve{p}_2^2)(\breve{p}_1^2-\breve{p}_3^2)} \tag{5.83}$$

$$\mathrm{Res}(\breve{\mathcal{F}}_3(-\breve{p}_2)) = \frac{-i\underline{\underline{\breve{\mathbf{N}}}}(\breve{p}_2\underline{\underline{\mathbf{U}}}\cdot\hat{\mathbf{k}})e^{iL\sigma\breve{p}_2}}{4\sigma\breve{p}_2^4(\breve{p}_1^2-\breve{p}_2^2)(\breve{p}_2^2-\breve{p}_3^2)} \tag{5.84}$$

$$\mathrm{Res}(\breve{\mathcal{F}}_3(-\breve{p}_3)) = \frac{i\underline{\underline{\breve{\mathbf{N}}}}(\breve{p}_3\underline{\underline{\mathbf{U}}}\cdot\hat{\mathbf{k}})e^{iL\sigma\breve{p}_3}}{4\sigma\breve{p}_3^4(\breve{p}_1^2-\breve{p}_3^2)(\breve{p}_2^2-\breve{p}_3^2)} \tag{5.85}$$

$$\begin{aligned}\mathrm{Res}(\breve{\mathcal{F}}_3(0)) \;=\; & \frac{-1}{4i\sigma\breve{p}_1^4\breve{p}_2^4\breve{p}_3^4}\times\left\{\breve{p}_1^2\breve{p}_2^2\breve{p}_3^2\left(\underline{\underline{\breve{\mathbf{N}}}}(\mathbf{0})\sigma^2L^2+2i\frac{\partial}{\partial k}\underline{\underline{\breve{\mathbf{N}}}}(\mathbf{0})\sigma L-\right.\right.\\ & \left.\left.\frac{\partial^2}{\partial k^2}\underline{\underline{\breve{\mathbf{N}}}}(\mathbf{0})\right)-2\underline{\underline{\breve{\mathbf{N}}}}(\mathbf{0})\left(\breve{p}_1^2\breve{p}_2^2+\breve{p}_1^2\breve{p}_3^2+\breve{p}_2^2\breve{p}_3^2\right)\right\}\end{aligned} \tag{5.86}$$

$$\mathrm{Res}(\breve{\mathcal{F}}_4(-\breve{p}_1)) = \frac{L\underline{\underline{\breve{\mathbf{N}}}}(\breve{p}_1\underline{\underline{\mathbf{U}}}\cdot\hat{\mathbf{k}})e^{iL\sigma\breve{p}_1}}{4\sigma\breve{p}_1^3(\breve{p}_1^2-\breve{p}_2^2)(\breve{p}_1^2-\breve{p}_3^2)} \tag{5.87}$$

$$\mathrm{Res}(\breve{\mathcal{F}}_4(-\breve{p}_2)) = \frac{-L\underline{\underline{\breve{\mathbf{N}}}}(\breve{p}_2\underline{\underline{\mathbf{U}}}\cdot\hat{\mathbf{k}})e^{iL\sigma\breve{p}_2}}{4\sigma\breve{p}_2^3(\breve{p}_1^2-\breve{p}_2^2)(\breve{p}_2^2-\breve{p}_3^2)} \tag{5.88}$$

$$\mathrm{Res}(F_4(-\breve{p}_3)) = \frac{L\underline{\underline{\breve{\mathbf{N}}}}(\breve{p}_3\underline{\underline{\mathbf{U}}}\cdot\hat{\mathbf{k}})e^{iL\sigma\breve{p}_3}}{4\sigma\breve{p}_3^3(\breve{p}_1^2-\breve{p}_3^2)(\breve{p}_2^2-\breve{p}_3^2)} \tag{5.89}$$

$$\mathrm{Res}(\breve{\mathcal{F}}_4(0)) = \frac{iL\left(\underline{\underline{\breve{\mathbf{N}}}}(\mathbf{0})\sigma L+i\frac{\partial}{\partial k}\underline{\underline{\breve{\mathbf{N}}}}(\mathbf{0})\right)}{2\breve{p}_1^2\breve{p}_2^2\breve{p}_3^2}. \tag{5.90}$$

The values of the residues provided by the pole at zero are halved as the pole lies on both contours. We sum the residues in the following way because each residue has to be evaluated by moving anti-clockwise around the contour.

$$\begin{aligned}\text{Residue} &= \text{Res}(\breve{\mathcal{F}}_1(\breve{p}_1)) + \text{Res}(\breve{\mathcal{F}}_1(\breve{p}_2)) + \text{Res}(\breve{\mathcal{F}}_1(\breve{p}_3)) + \frac{1}{2}\text{Res}(\breve{\mathcal{F}}_1(0)) + \\ &\quad \text{Res}(\breve{\mathcal{F}}_2(\breve{p}_1)) + \text{Res}(\breve{\mathcal{F}}_2(\breve{p}_2)) + \text{Res}(\breve{\mathcal{F}}_2(\breve{p}_3)) + \frac{1}{2}\text{Res}(\breve{\mathcal{F}}_2(0)) - \\ &\quad \text{Res}(\breve{\mathcal{F}}_3(-\breve{p}_1)) - \text{Res}(\breve{\mathcal{F}}_3(-\breve{p}_2)) - \text{Res}(\breve{\mathcal{F}}_3(-\breve{p}_3)) - \frac{1}{2}\text{Res}(\breve{\mathcal{F}}_3(0)) - \\ &\quad \text{Res}(\breve{\mathcal{F}}_4(-\breve{p}_1)) - \text{Res}(\breve{\mathcal{F}}_4(-\breve{p}_2)) - \text{Res}(\breve{\mathcal{F}}_4(-\breve{p}_3)) - \frac{1}{2}\text{Res}(\breve{\mathcal{F}}_4(0)).\end{aligned} \tag{5.91}$$

Thus, by this application of the Cauchy residue theorem [39], the SPFT estimates are delivered in terms of two–dimensional integrals as

$$\begin{aligned}\breve{C}^{(spft)}_{lMPq} &= \breve{C}^{(ocm)}_{lMPq} + \frac{\omega^2 f^{(1)} f^{(2)}}{4\pi i} \int_{\phi=0}^{2\pi} \int_{\theta=0}^{\pi} d\phi\, d\theta\, \frac{k_t \sin\theta}{(k\sigma)^2 \, \det\left[\underline{\underline{\breve{\mathbf{a}}}}(\hat{\mathbf{k}})\right]} \left[\underline{\underline{\breve{\boldsymbol{\rho}}}}^{(ocm)}\right]_{XY} \times \\ &\quad \left[\underline{\underline{\breve{\mathbf{b}}}}(\hat{\mathbf{k}})\right]_{YU} \Bigg(\left\{\breve{\xi}^{(2)}_{lMrs} - \breve{\xi}^{(1)}_{lMrs}\right\} \left\{k_s \left[\underline{\underline{\breve{\mathbf{a}}}}^{-1}(\hat{\mathbf{k}})\right]_{rX} + k_r \left[\underline{\underline{\breve{\mathbf{a}}}}^{-1}(\hat{\mathbf{k}})\right]_{sX}\right\} + \\ &\quad \left\{\breve{\xi}^{(2)}_{lm4s} - \breve{\xi}^{(1)}_{lm4s}\right\} \left\{k_s \left[\underline{\underline{\breve{\mathbf{a}}}}^{-1}(\hat{\mathbf{k}})\right]_{4X}\right\} \Bigg) \left(\breve{\xi}^{(2)}_{tUPq} - \breve{\xi}^{(1)}_{tUPq}\right)\end{aligned} \tag{5.92}$$

and

$$\begin{aligned}\breve{\rho}^{(spft)}_{MP} &= \breve{\rho}^{(ocm)}_{MP} - \frac{\omega^2 f^{(1)} f^{(2)} \left(\breve{\rho}^{(2)}_{MS} - \breve{\rho}^{(1)}_{MS}\right) \left(\breve{\rho}^{(2)}_{UP} - \breve{\rho}^{(1)}_{UP}\right)}{2\pi i} \times \\ &\quad \int_{\phi=0}^{2\pi} \int_{\theta=0}^{\pi} d\phi\, d\theta\, \frac{\sin\theta}{\det\left[\underline{\underline{\breve{\mathbf{a}}}}(\hat{\mathbf{k}})\right]} \left[\underline{\underline{\breve{\mathbf{b}}}}(\hat{\mathbf{k}})\right]_{SU},\end{aligned} \tag{5.93}$$

where the residue is given by the 4×4 matrix

$$\begin{aligned}\breve{\underline{\underline{\mathbf{b}}}}(\hat{\mathbf{k}}) \;=\; & \frac{1}{2i}\Bigg\{\frac{e^{iL\sigma\breve{p}_1}\breve{\underline{\underline{\mathbf{N}}}}(\breve{p}_1\underline{\underline{\mathbf{U}}}\cdot\hat{\mathbf{k}})}{\sigma\breve{p}_1^4(\breve{p}_1^2-\breve{p}_2^2)(\breve{p}_1^2-\breve{p}_3^2)}\Big(1-iL\sigma\breve{p}_1\Big)- \\ & \frac{e^{iL\sigma\breve{p}_2}\breve{\underline{\underline{\mathbf{N}}}}(\breve{p}_2\underline{\underline{\mathbf{U}}}\cdot\hat{\mathbf{k}})}{\sigma\breve{p}_2^4(\breve{p}_1^2-\breve{p}_2^2)(\breve{p}_2^2-\breve{p}_3^2)}\Big(1-iL\sigma\breve{p}_2\Big)+ \\ & \frac{e^{iL\sigma\breve{p}_3}\breve{\underline{\underline{\mathbf{N}}}}(\breve{p}_3\underline{\underline{\mathbf{U}}}\cdot\hat{\mathbf{k}})}{\sigma\breve{p}_3^4(\breve{p}_2^2-\breve{p}_3^2)(\breve{p}_1^2-\breve{p}_3^2)}\Big(1-iL\sigma\breve{p}_3\Big)- \\ & \frac{1}{\sigma\breve{p}_1^2\breve{p}_2^2\breve{p}_3^2}\Big[\breve{\underline{\underline{\mathbf{N}}}}(\mathbf{0})\Big(\frac{1}{\breve{p}_1^2}+\frac{1}{\breve{p}_2^2}+\frac{1}{\breve{p}_3^2}+\frac{\sigma^2L^2}{2}\Big)+\frac{1}{2}\frac{\partial^2}{\partial k^2}\breve{\underline{\underline{\mathbf{N}}}}(\mathbf{0})\Big]\Bigg\}.\end{aligned} \tag{5.94}$$

The expressions for the second–order SPFT estimates $\breve{C}_{lMPq}^{(spft)}$ and $\breve{\rho}_{MP}^{(spft)}$ in equations (5.92) and (5.93) may be evaluated by standard numerical methods [40].

It is particularly noteworthy that $\breve{C}_{lMPq}^{(spft)}$ and $\breve{\rho}_{MP}^{(spft)}$ are complex–valued for $L>0$, even when the corresponding quantities for the component materials, i.e., $\breve{C}_{lMPq}^{(\ell)}$ and $\breve{\rho}_{MP}^{(\ell)}$ $(\ell=1,2)$, are real–valued. This reflects the fact that the SPFT accommodates losses due to scattering [10].

5.1.7 Energy considerations

Due to energy considerations, the imaginary part of the extended compliance matrix, $\breve{\underline{\underline{\mathbf{M}}}}^{(spft)}$ [54], is required to be positive definite for passive materials [55].

We begin with the constitutive equation for the extended stiffness matrix

$$\breve{\boldsymbol{\sigma}} = \breve{\underline{\underline{\mathbf{C}}}}\cdot\breve{\mathbf{S}} \tag{5.95}$$

where

$$\breve{\underline{\underline{\mathbf{C}}}} = \begin{pmatrix} \underline{\underline{\mathbf{C}}} & -\underline{\underline{\mathbf{e}}}^T \\ \underline{\underline{\mathbf{e}}} & \underline{\underline{\boldsymbol{\epsilon}}} \end{pmatrix}, \quad \breve{\boldsymbol{\sigma}} = \begin{pmatrix} \boldsymbol{\sigma} \\ \mathbf{D} \end{pmatrix} \quad \text{and} \quad \breve{\mathbf{S}} = \begin{pmatrix} \mathbf{S} \\ \mathbf{E} \end{pmatrix}. \tag{5.96}$$

Herein, $\boldsymbol{\sigma}$, $\mathbf{D}$, $\mathbf{S}$ and $\mathbf{E}$ are the vector forms of the stress, electric displacement, strain and electric field respectively. Therefore, we can rewrite (5.95) as

$$\boldsymbol{\sigma} = \underline{\underline{\mathbf{C}}}\cdot\mathbf{S} - \underline{\underline{\mathbf{e}}}^T\cdot\mathbf{E} \tag{5.97}$$

and

$$\mathbf{D} = \underline{\underline{\mathbf{e}}} \cdot \mathbf{S} + \underline{\underline{\boldsymbol{\epsilon}}} \cdot \mathbf{E}. \tag{5.98}$$

Now, multiplying (5.97) by $\underline{\underline{\mathbf{C}}}^{\dagger}$ [54] gives us

$$\underline{\underline{\mathbf{C}}}^{\dagger} \cdot \boldsymbol{\sigma} = \underline{\underline{\mathbf{C}}}^{\dagger} \cdot \underline{\underline{\mathbf{C}}} \cdot \mathbf{S} - \underline{\underline{\mathbf{C}}}^{\dagger} \cdot \underline{\underline{\mathbf{e}}}^{T} \cdot \mathbf{E} = \mathbf{S} - \underline{\underline{\mathbf{C}}}^{\dagger} \cdot \underline{\underline{\mathbf{e}}}^{T} \cdot \mathbf{E} \tag{5.99}$$

or rather

$$\mathbf{S} = \underline{\underline{\mathbf{C}}}^{\dagger} \cdot \boldsymbol{\sigma} + \underline{\underline{\mathbf{C}}}^{\dagger} \cdot \underline{\underline{\mathbf{e}}}^{T} \cdot \mathbf{E}. \tag{5.100}$$

Substituting this into (5.98) produces

$$\begin{aligned} \mathbf{D} &= \underline{\underline{\mathbf{e}}} \cdot (\underline{\underline{\mathbf{C}}}^{\dagger} \cdot \boldsymbol{\sigma} + \underline{\underline{\mathbf{C}}}^{\dagger} \cdot \underline{\underline{\mathbf{e}}}^{T} \cdot \mathbf{E}) + \underline{\underline{\boldsymbol{\epsilon}}} \cdot \mathbf{E} && (5.101) \\ &= \underline{\underline{\mathbf{e}}} \cdot \underline{\underline{\mathbf{C}}}^{\dagger} \cdot \boldsymbol{\sigma} + (\underline{\underline{\mathbf{e}}} \cdot \underline{\underline{\mathbf{C}}}^{\dagger} \cdot \underline{\underline{\mathbf{e}}}^{T} + \underline{\underline{\boldsymbol{\epsilon}}}) \cdot \mathbf{E}, && (5.102) \end{aligned}$$

which gives the extended compliance matrix as

$$\underline{\underline{\breve{\mathbf{M}}}} = \begin{pmatrix} \underline{\underline{\mathbf{C}}}^{\dagger} & \underline{\underline{\mathbf{C}}}^{\dagger} \cdot \underline{\underline{\mathbf{e}}}^{T} \\ \underline{\underline{\mathbf{e}}} \cdot \underline{\underline{\mathbf{C}}}^{\dagger} & \underline{\underline{\mathbf{e}}} \cdot \underline{\underline{\mathbf{C}}}^{\dagger} \cdot \underline{\underline{\mathbf{e}}}^{T} + \underline{\underline{\boldsymbol{\epsilon}}} \end{pmatrix}. \tag{5.103}$$

Explicitly, for our SPFT results, we have

$$\underline{\underline{\breve{\mathbf{M}}}}^{(spft)} = \begin{pmatrix} \left(\underline{\underline{\mathbf{C}}}^{(spft)}\right)^{\dagger} & \left(\underline{\underline{\mathbf{C}}}^{(spft)}\right)^{\dagger} \cdot \left(\underline{\underline{\mathbf{e}}}^{(spft)}\right)^{T} \\ \underline{\underline{\mathbf{e}}}^{(spft)} \cdot \left(\underline{\underline{\mathbf{C}}}^{(spft)}\right)^{\dagger} & \underline{\underline{\boldsymbol{\epsilon}}}^{(spft)} + \underline{\underline{\mathbf{e}}}^{(spft)} \cdot \left(\underline{\underline{\mathbf{C}}}^{(spft)}\right)^{\dagger} \cdot \left(\underline{\underline{\mathbf{e}}}^{(spft)}\right)^{T} \end{pmatrix} \tag{5.104}$$

where † is the elastodynamic 9×9 dagger operation (3.6).

5.2 Numerical results

5.2.1 Mori–Tanaka estimate

In order to illustrate the theory presented in §5.1, let us now consider a representative numerical example. A comparison for the SPFT estimate of the HCM constitutive parameters is provided by the corresponding results computed using the Mori–Tanaka formalism [20, 32, 43, 56]. In the case of orthorhombic $mm2$

piezoelectric component materials, the Mori-Tanaka estimate of the extended stiffness matrix for the HCM is given by [57]

$$\breve{\underline{\underline{\mathbf{C}}}}^{(MT)} = \breve{\underline{\underline{\mathbf{C}}}}^{(1)} + f^{(2)} \left(\breve{\underline{\underline{\mathbf{C}}}}^{(2)} - \breve{\underline{\underline{\mathbf{C}}}}^{(1)} \right) \cdot \breve{\underline{\underline{\mathbf{B}}}}^{(MT)} \cdot \left[f^{(1)} \breve{\underline{\underline{\boldsymbol{\tau}}}} + f^{(2)} \breve{\underline{\underline{\mathbf{B}}}}^{(MT)} \right]^{\ddagger}, \tag{5.105}$$

where the 12×12 matrix

$$\breve{\underline{\underline{\mathbf{B}}}}^{(MT)} = \left[\breve{\underline{\underline{\boldsymbol{\tau}}}} + \breve{\underline{\underline{\mathbf{S}}}}^{(esh)} \cdot \left(\breve{\underline{\underline{\mathbf{C}}}}^{(1)} \right)^{\ddagger} \cdot \left(\breve{\underline{\underline{\mathbf{C}}}}^{(2)} - \breve{\underline{\underline{\mathbf{C}}}}^{(1)} \right) \right]^{\ddagger}, \tag{5.106}$$

with $\breve{\underline{\underline{\mathbf{S}}}}^{(esh)}$ being the 12×12 matrix representation of the piezoelectric extension of the Eshelby tensor [44, 45, 48].

The piezoelectric extension of the Eshelby tensor, for orthorhombic component materials distributed with either spherical or ellipsoidal inclusion particles, is given by [48]

$$\breve{S}^{(esh)}_{MnAb} = \begin{cases} \dfrac{1}{8\pi} \breve{C}^{(1)}_{iJAb} \displaystyle\int_{-1}^{+1} d\zeta_3 \int_0^{2\pi} d\omega \ \left[\breve{F}^{(esh)}_{mJin}(\overline{\vartheta}) + \breve{F}^{(esh)}_{nJim}(\overline{\vartheta}) \right] & M = 1,\, 2,\, 3 \\ \dfrac{1}{4\pi} \breve{C}^{(1)}_{iJAb} \displaystyle\int_{-1}^{+1} d\zeta_3 \int_0^{2\pi} d\omega \ \breve{F}^{(esh)}_{4Jin}(\overline{\vartheta}) & M = 4 \end{cases} \tag{5.107}$$

wherein

$$\left. \begin{array}{lll} \breve{F}^{(esh)}_{MJin}(\overline{\vartheta}) = \overline{\vartheta}_i \overline{\vartheta}_n \breve{\mathcal{K}}^{-1}_{MJ}, & \breve{\mathcal{K}}_{JR} = \overline{\vartheta}_i \breve{C}^{(1)}_{iJRn} \overline{\vartheta}_n, & \\ \overline{\vartheta}_1 = \dfrac{\zeta_1}{a}, \qquad \overline{\vartheta}_2 = \dfrac{\zeta_2}{b}, & \overline{\vartheta}_3 = \dfrac{\zeta_3}{c} & \\ \zeta_1 = (1 - \zeta_3^2)^{1/2} \cos(\omega), \qquad \zeta_2 = (1 - \zeta_3^2)^{1/2} \sin(\omega), & \zeta_3 = \zeta_3 & \end{array} \right\}, \tag{5.108}$$

The integrals in (5.107) can be evaluated using standard numerical methods [40]. The piezoelectric extension of the Eshelby tensor is converted to a 12×12 matrix as described in §5.1.3.

5.2.2 Preliminaries

In the following, we present the numerical evaluation of the 12×12 extended stiffness matrix of the HCM, namely $\breve{\underline{\underline{\mathbf{C}}}}^{(hcm)}$, as estimated by the lowest–order

SPFT (i.e., $hcm = ocm$), the second–order SPFT (i.e., $hcm = spft$) and the Mori–Tanaka formalism (i.e., $hcm = MT$). The matrix $\underline{\underline{\breve{\mathbf{C}}}}^{(hcm)}$ has the form represented in equation (5.2). The second–order SPFT estimate of the extended density tensor $\breve{\rho}_{MP}^{(spft)}$ is also evaluated; the numerical evaluation of the lowest–order SPFT density $\breve{\rho}_{MP}^{(ocm)}$ need not be presented here as this quantity is simply the volume average of the densities of the component materials. An angular frequency of $\omega = 2\pi \times 10^6$ s^{-1} was selected for all second–order SPFT computations. As before we consider the HCM to be constructed of particles of component material '2' distributed in a matrix of component material '1'.

The eccentricities of the ellipsoidal inclusion particles are specified by the shape parameters $\{a, b, c\}$, per equations (3.8) and (3.9). To allow direct comparison with results from previous studies [57], component material '1' was taken to be the piezoelectric material polyvinylidene fluoride (PVDF) while component material '2' was taken to be the thermoplastic polyimide LaRC-SI, which has no piezoelectric properties. The stiffness constitutive parameters of the component materials are tabulated in Table 5.2. The nonzero piezoelectric constitutive parameters of PVDF are: $e_{113} \equiv e_{31} = 0.024$, $e_{223} \equiv e_{32} = 0.001$ and $e_{333} \equiv e_{33} = -0.027$ in units of C m^{-2}. The dielectric constitutive parameters of PVDF are: $\epsilon_{11} = 7.4$, $\epsilon_{22} = 9.6$ and $\epsilon_{33} = 7.6$, whereas those of LaRC-SI are: $\epsilon_{11} = \epsilon_{22} = \epsilon_{33} = 2.8$, all in units of $\epsilon_0 = 8.854 \times 10^{-12}$ F m^{-1} (the permittivity of free space). Lastly, the densities of PVDF and LaRC-SI are 1750 and 1376, respectively, in units of kg m^{-3}.

Stiffness parameter	PVDF (GPa)	LaRC-SI (GPa)
$C_{1111} \equiv C_{11}$	3.8	8.1
$C_{1122} \equiv C_{12}$	1.9	5.4
$C_{1133} \equiv C_{13}$	1.0	5.4
$C_{2222} \equiv C_{22}$	3.2	8.1
$C_{2233} \equiv C_{23}$	0.9	5.4
$C_{3333} \equiv C_{33}$	1.2	8.1
$C_{2323} \equiv C_{44}$	0.7	1.4
$C_{1313} \equiv C_{55}$	0.9	1.4
$C_{1212} \equiv C_{66}$	0.9	1.4

Table 5.2: The stiffness constitutive parameters of the component materials in units of GPa (after [57]).

5.2.3 Lowest–order SPFT

We begin by considering the lowest–order SPFT estimates of the HCM constitutive parameters. In Figs. 5.1–5.3, components of the HCM extended stiffness matrix $\underline{\underline{\breve{\mathbf{C}}}}^{(hcm)}$, as computed using the lowest–order SPFT and the Mori–Tanaka formalism, are plotted as functions of volume fraction $f^{(2)}$ for the case where the inclusion particles are spherical (i.e., $a = b = c$). Only relatively minor differences between the lowest–order SPFT estimates and the Mori–Tanaka estimates are observed, with the differences between the two being greatest for mid–range values of $f^{(2)}$. Plots for both the SPFT and Mori–Tanaka estimates are necessarily constrained by the limits

$$\lim_{f^{(2)}\to 0} \underline{\underline{\breve{\mathbf{C}}}}^{(hcm)} = \underline{\underline{\breve{\mathbf{C}}}}^{(1)}, \qquad \lim_{f^{(2)}\to 1} \underline{\underline{\breve{\mathbf{C}}}}^{(hcm)} = \underline{\underline{\breve{\mathbf{C}}}}^{(2)}. \tag{5.109}$$

The corresponding graphs for the cases where the inclusion particles are described by the shape parameters $\{a/c = 5,\, b/c = 1.5\}$ and $\{a/c = 10,\, b/c = 2\}$ are provided in Figs. 5.4–5.6 and 5.7–5.9, respectively. A comparison of Figs. 5.1–5.9 reveals that the differences between the lowest–order SPFT and Mori–Tanaka estimates are accentuated as the inclusion particles become more eccentric in shape, especially at mid–range values of $f^{(2)}$ for the piezoelectric parameters and the dielectric parameters.

5.2.4 Second–order SPFT estimate

Now let us turn to the second–order SPFT estimates of the HCM constitutive parameters. We considered these quantities as functions of $\breve{\bar{k}}L$, where $\breve{\bar{k}}$ is an approximate upper bound on the wavenumbers supported by the HCM, similar to that used in the elastodynamic SPFT §3.4, as estimated by

$$\breve{\bar{k}} = \frac{\omega}{2}\left(\sqrt{\frac{\bar{\rho}}{\bar{\lambda}+2\bar{\mu}}} + \sqrt{\frac{\bar{\rho}}{\bar{\mu}}}\right), \tag{5.110}$$

wherein

$$\left.\begin{aligned}
\bar{\lambda} &= \frac{1}{6}\sum_{\ell=1}^{2}\Big(\Big|\Big[\underline{\underline{\mathbf{C}}}^{(\ell)}\Big]_{12}\Big| + \Big|\Big[\underline{\underline{\mathbf{C}}}^{(\ell)}\Big]_{13}\Big| + \Big|\Big[\underline{\underline{\mathbf{C}}}^{(\ell)}\Big]_{23}\Big|\Big) \\
\bar{\mu} &= \frac{1}{6}\sum_{\ell=1}^{2}\Big(\Big|\Big[\underline{\underline{\mathbf{C}}}^{(\ell)}\Big]_{44}\Big| + \Big|\Big[\underline{\underline{\mathbf{C}}}^{(\ell)}\Big]_{55}\Big| + \Big|\Big[\underline{\underline{\mathbf{C}}}^{(\ell)}\Big]_{66}\Big|\Big) \\
\bar{\rho} &= \frac{1}{2}\sum_{\ell=1}^{2}\rho^{(\ell)}
\end{aligned}\right\}; \tag{5.111}$$

and L is the correlation length associated with the two–point covariance function (3.12). The real and imaginary parts of the components of $\underline{\underline{\tilde{\breve{\mathbf{C}}}}}^{(spft)} = \underline{\underline{\breve{\mathbf{C}}}}^{(spft)} - \underline{\underline{\breve{\mathbf{C}}}}^{(ocm)}$ are plotted against $\bar{\bar{k}}L$ for $f^{(2)} = 0.5$ in Figs. 5.10–5.12 and Figs. 5.13–5.15 respectively. The values of the shape parameters $\{a, b, c\}$ correspond to those used in the calculations for Figs. 5.1–5.9.

The second–order corrections to the lowest–order SPFT estimates are observed in Fig. 5.10–5.15 to grow exponentially in magnitude as the correlation length increases. Furthermore, the magnitudes of both the real and imaginary parts of $\underline{\underline{\breve{\mathbf{C}}}}^{(spft)}$ generally grow faster with increasing correlation length when the inclusion particles are more eccentric in shape. At $L = 0$, the second–order and lowest–order SPFT estimates coincide. While the second–order corrections are relatively small compared to the lowest–order SPFT estimates, a highly significant feature of the second–order corrections is that these are complex–valued with nonzero imaginary parts, even though $\underline{\underline{\breve{\mathbf{C}}}}^{(1,2)}$ and $\underline{\underline{\breve{\mathbf{C}}}}^{(ocm)}$ are purely real–valued. We note that for all computations the imaginary part of the extended compliance matrix $\underline{\underline{\breve{\mathbf{M}}}}^{(spft)}$ was found to be positive definite, which corresponds to positive loss [55]. Thus, the emergence of nonzero imaginary parts of $\underline{\underline{\breve{\mathbf{C}}}}^{(spft)}$ indicates that the HCM has acquired a dissipative nature, despite the component materials being nondissipative. The dissipation is attributed to scattering losses, since the second–order SPFT takes into account interactions between spatially–distinct scattering particles via the two–point covariance function (5.53). As the correlation length increases, the number of scattering particles that can mutually interact also increases, thereby increasing the scattering loss per unit volume.

Finally, we turn to the second–order SPFT estimate of the HCM density. The

real and imaginary parts of the matrix entry $\left[\underline{\underline{\breve{\tilde{\boldsymbol{\rho}}}}}^{(spft)}\right]_{jj}$, $j = 1, 2$ and 3 wherein $\underline{\underline{\breve{\tilde{\boldsymbol{\rho}}}}}^{(spft)} = \underline{\underline{\breve{\boldsymbol{\rho}}}}^{(spft)} - \underline{\underline{\breve{\boldsymbol{\rho}}}}^{(ocm)}$, are plotted as functions of $\bar{\bar{k}}L$ in Fig. 5.16. The second–order SPFT estimates of the HCM density exhibit characteristics similar to those of the corresponding HCM stiffness, piezoelectric and dielectric constitutive parameters. That is, $\lim_{L\to 0} \breve{\rho}_{jj}^{(spft)} = \breve{\rho}_{jj}^{(ocm)}$ and $\left|\breve{\tilde{\rho}}_{jj}^{(spft)}\right| \ll \left|\breve{\rho}_{jj}^{(ocm)}\right|$ for $j = 1, 2$ and 3. Also, the differences between $\underline{\underline{\breve{\boldsymbol{\rho}}}}^{(spft)}$ and $\underline{\underline{\breve{\boldsymbol{\rho}}}}^{(ocm)}$ increase exponentially as the correlation length increases, and this effect is most accentuated when the component particles are most eccentric in shape.

We remark that the second–order elastodynamic SPFT for orthotropic HCMs also produced a complex–valued, anisotropic density, §3.4, as well as in other homogenization scenarios [41, 42].

5.3 Closing remarks

We have now fully developed the piezoelectric SPFT for the case of orthorhombic mm2 piezoelectric HCMs. In doing this we have produced simplified versions of (4.103) and (4.104) that can be evaluated numerically evaluated. From the theoretical results and the numerical examples we can draw the following conclusions:

- The lowest–order SPFT estimate of the stiffness, piezoelectric and dielectric properties of the HCM are qualitatively similar to those estimates provided by the Mori–Tanaka formalism.

- Differences between the estimates of the lowest–order SPFT and the Mori–Tanaka formalism are greatest at mid–range values of the volume fraction, and accentuated when the inclusion particles are eccentric in shape.

- The second–order SPFT provides a correction to the lowest–order estimate of the HCM constitutive properties. The magnitude of this correction is generally larger when the inclusion particles are more eccentric in shape.

- While the correction provided by the second–order SPFT is relatively small in magnitude, it is highly significant as it indicates dissipation due to scattering loss.

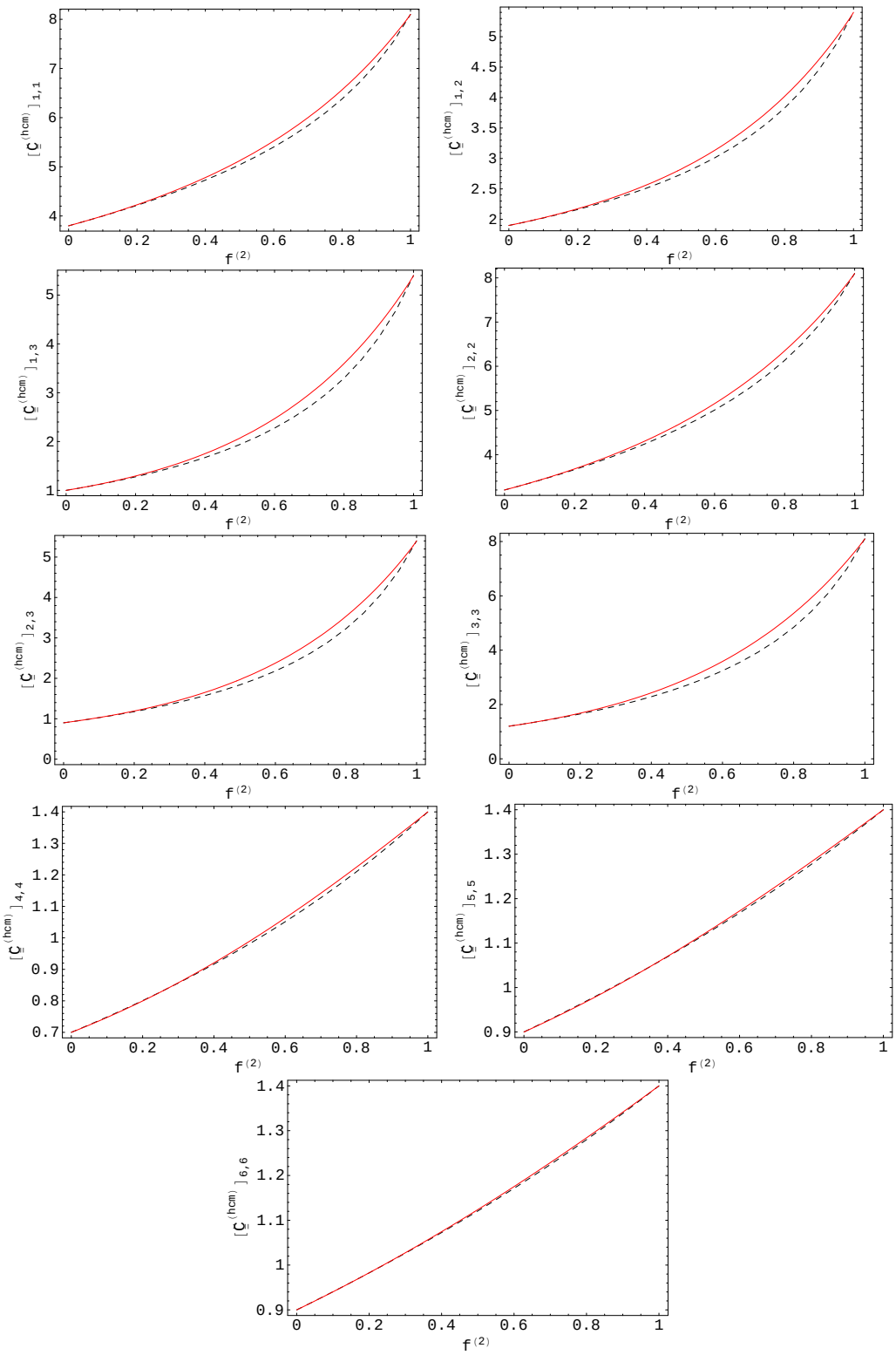

Figure 5.1: Plots of $\left[\underline{\underline{\breve{\mathbf{C}}}}^{(hcm)}\right]_{r,s}$, with $r,s \in \{1,1;\ 1,2;\ 1,3;\ 2,2;\ 2,3;\ 3,3;\ 4,4;\ 5,5;\ 6,6\}$ (in GPa) as estimated using the lowest–order SPFT (i.e., $hcm = ocm$) (red, solid curves) and the Mori–Tanaka mean–field formalism (i.e., $hcm = MT$) (black, dashed curves), against the volume fraction of component material '2'. Component material '1' is PVDF and component material '2' is LaRC-SI. The component materials are distributed as spheres (i.e., $a = b = c$).

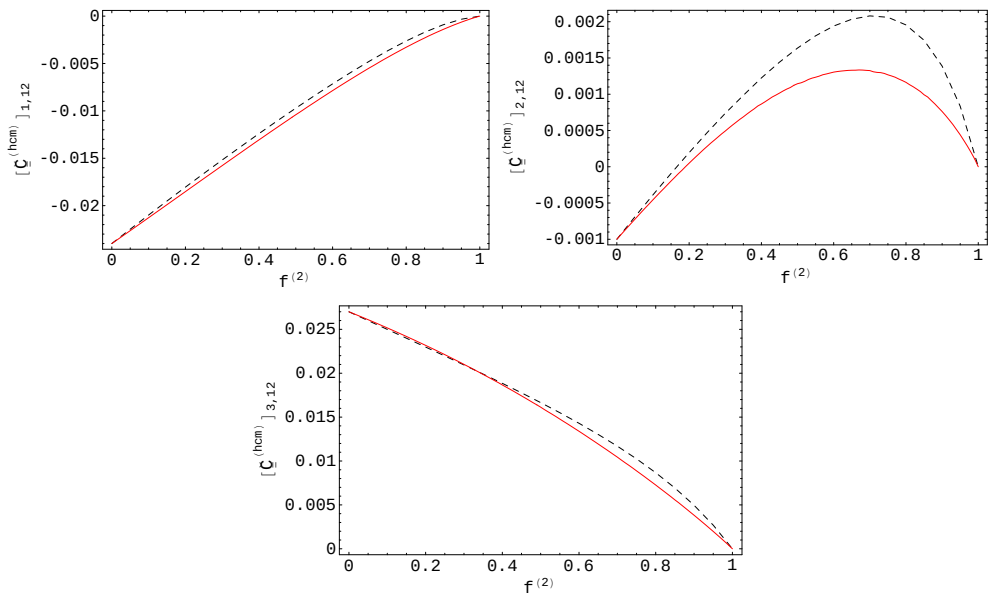

Figure 5.2: Plots of $\left[\underline{\underline{\breve{C}}}^{(hcm)}\right]_{r,s}$, with $r, s \in \{1, 12;\ 2, 12;\ 3, 12\}$ (in C/m^2), as estimated using the lowest–order SPFT (i.e., $hcm = ocm$) (red, solid curves) and the Mori–Tanaka mean–field formalism (i.e., $hcm = MT$) (black, dashed curves), against the volume fraction of component material '2'. Component material '1' is PVDF and component material '2' is LaRC-SI. The component materials are distributed as spheres (i.e., $a = b = c$).

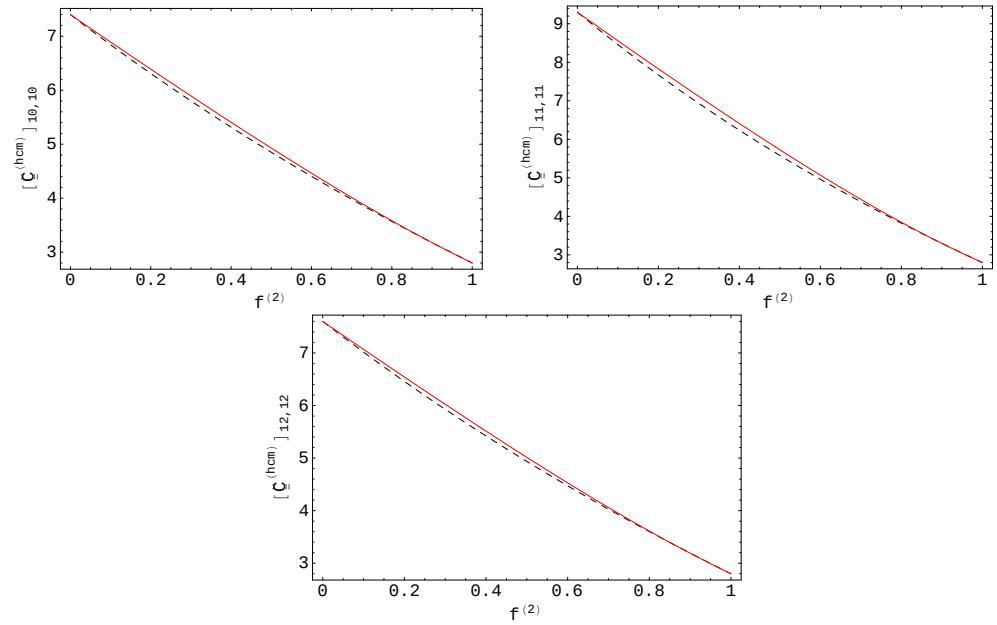

Figure 5.3: Plots of $\left[\underline{\underline{\breve{C}}}^{(hcm)}/\epsilon_0\right]_{r,s}$, with $r, s \in \{10, 10;\ 11, 11;\ 12, 12\}$ as estimated using the lowest–order SPFT (i.e., $hcm = ocm$) (red, solid curves) and the Mori–Tanaka mean–field formalism (i.e., $hcm = MT$) (black, dashed curves), against the volume fraction of component material '2'. Component material '1' is PVDF and component material '2' is LaRC-SI. The component materials are distributed as spheres (i.e., $a = b = c$).

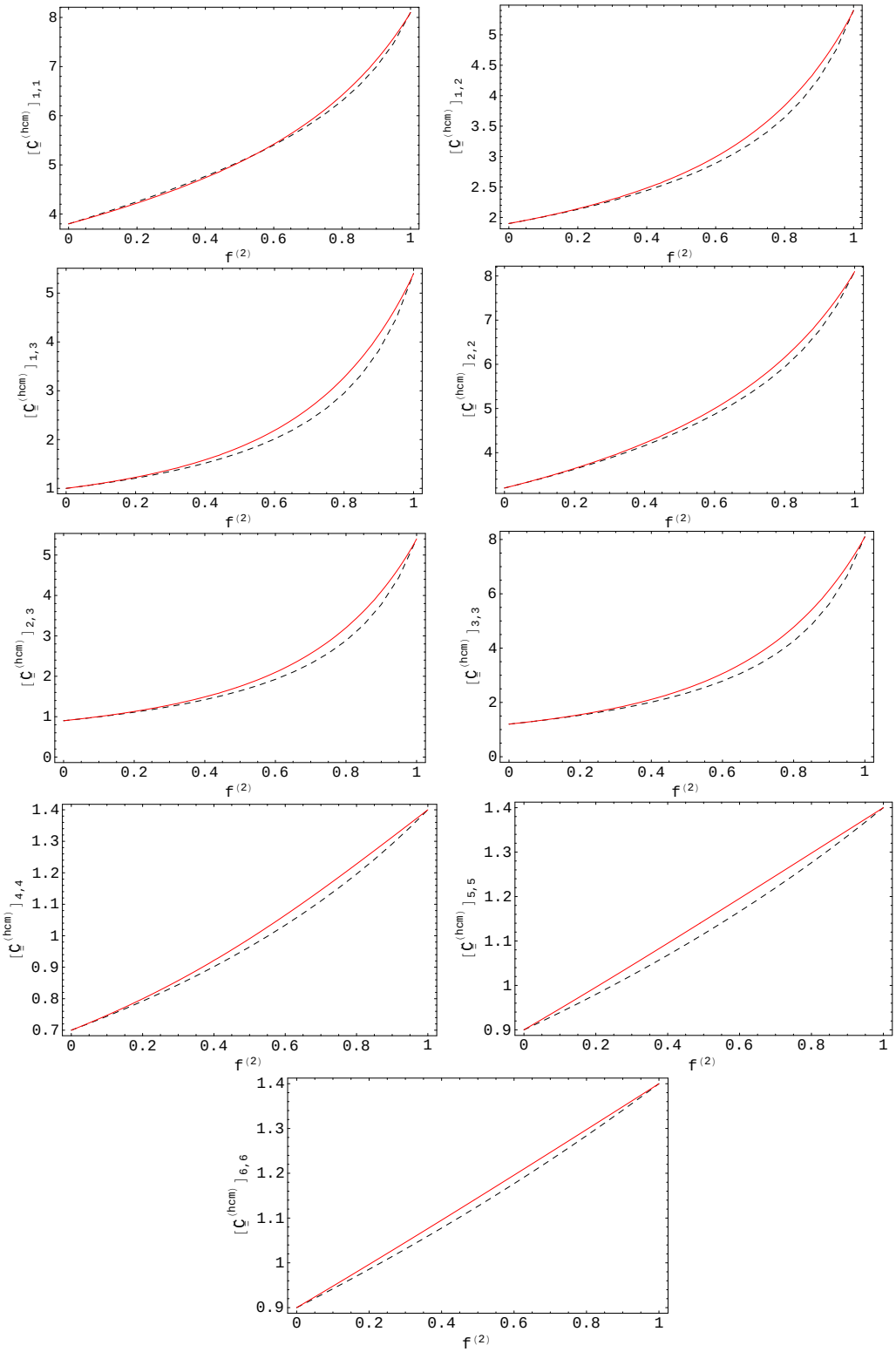

Figure 5.4: As Fig 5.1 but with the component materials distributed as ellipsoids with ($a/c = 5$ and $b/c = 1.5$).

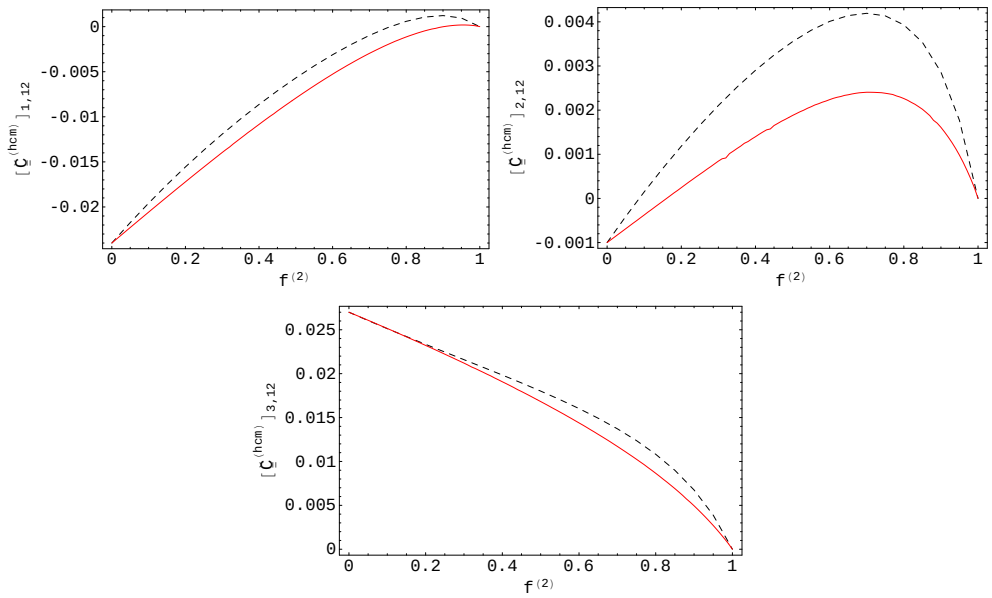

Figure 5.5: As Fig 5.2 but with the component materials distributed as ellipsoids with ($a/c = 5$ and $b/c = 1.5$).

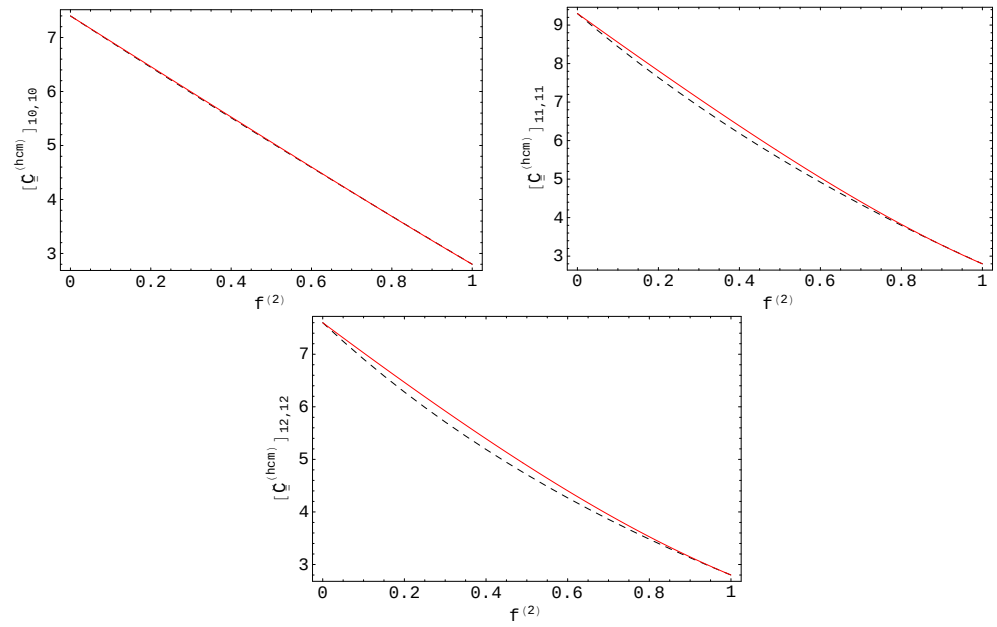

Figure 5.6: As Fig 5.3 but with the component materials distributed as ellipsoids with ($a/c = 5$ and $b/c = 1.5$).

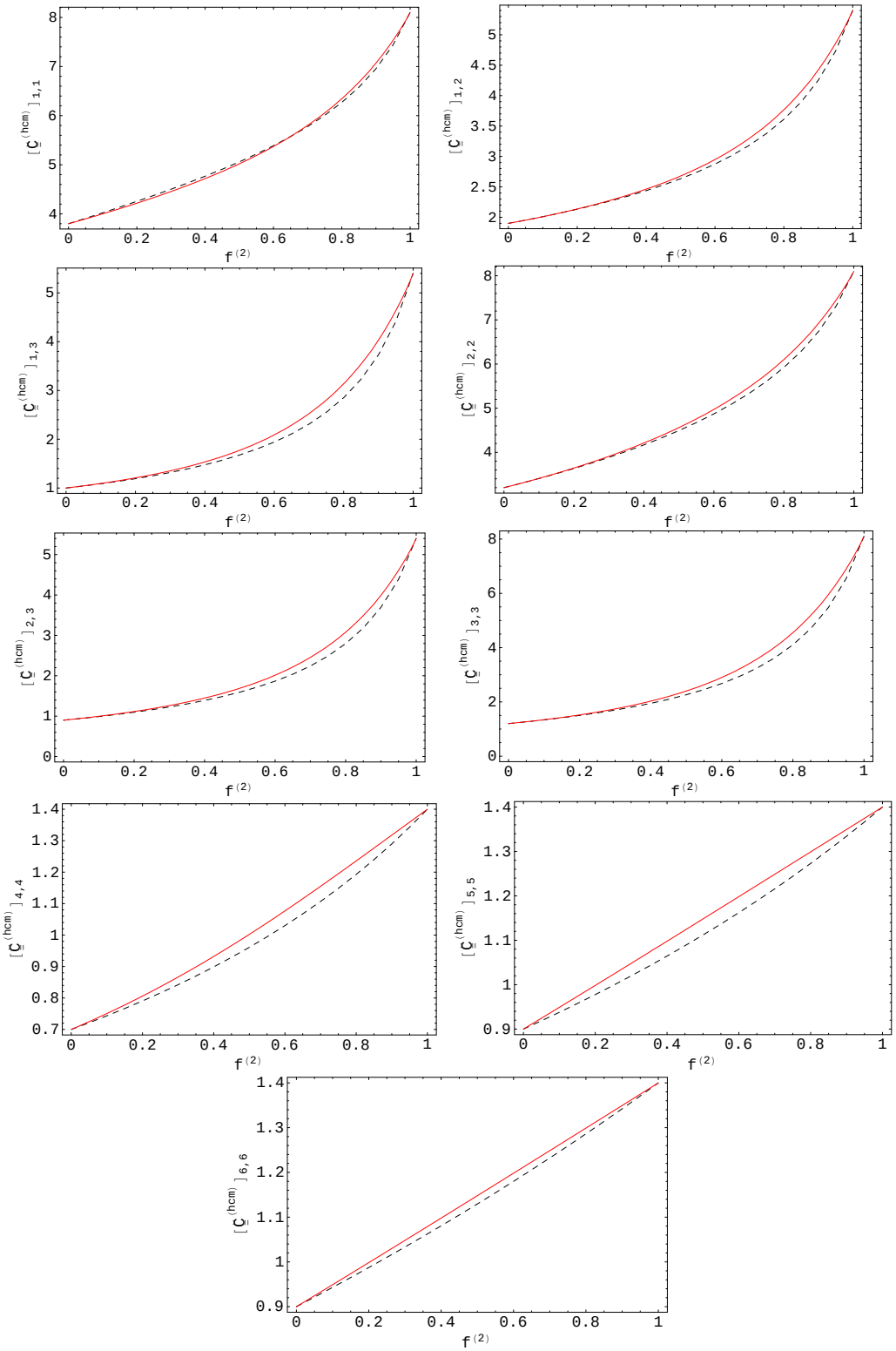

Figure 5.7: As Fig 5.1 but with the component materials distributed as ellipsoids with ($a/c =$ 10 and $b/c = 2$).

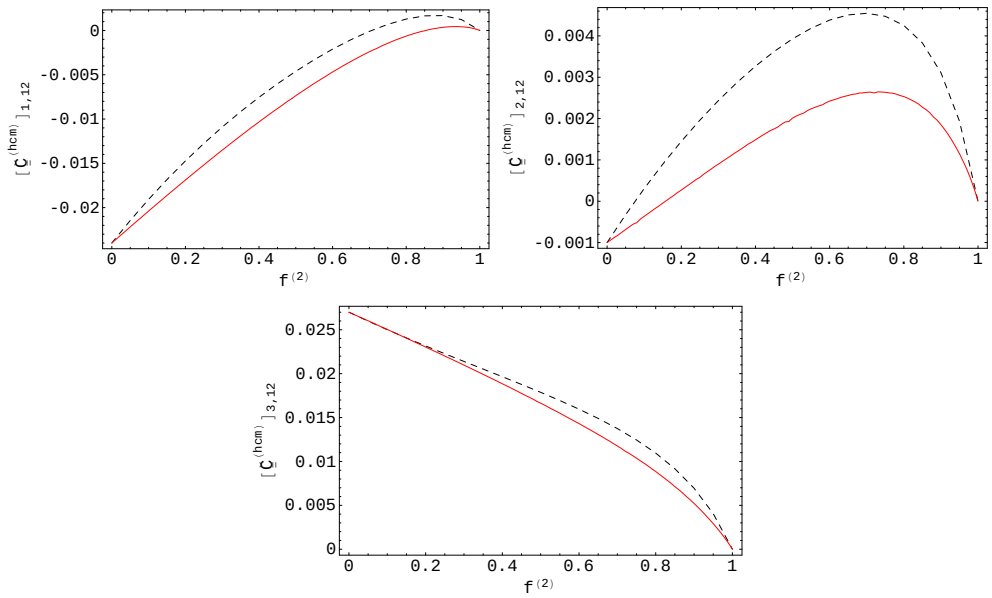

Figure 5.8: As Fig 5.2 but with the component materials distributed as ellipsoids with ($a/c =$ 10 and $b/c = 2$).

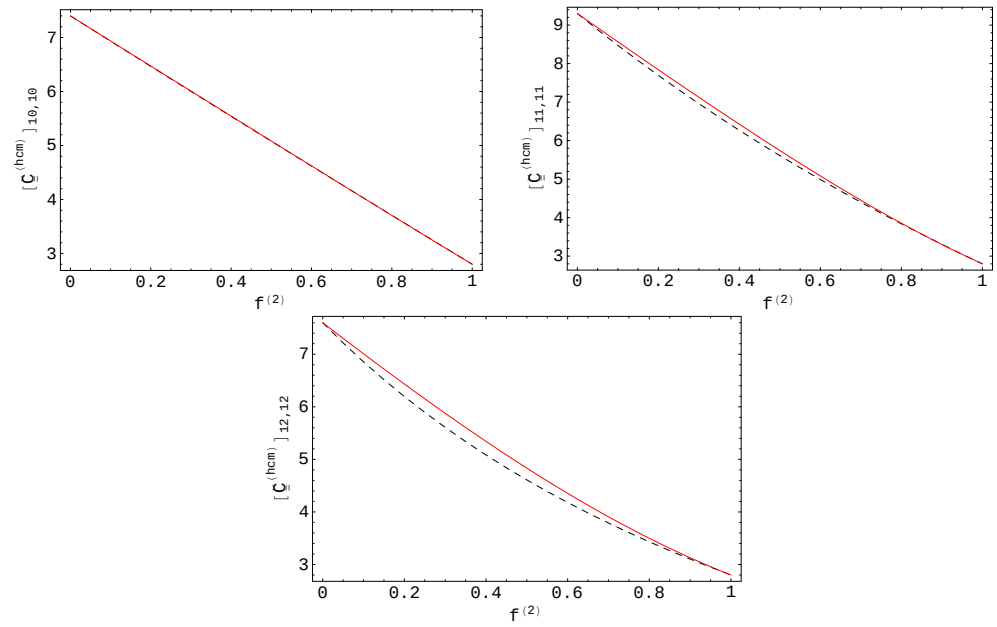

Figure 5.9: As Fig 5.3 but with the component materials distributed as ellipsoids with ($a/c =$ 10 and $b/c = 2$).

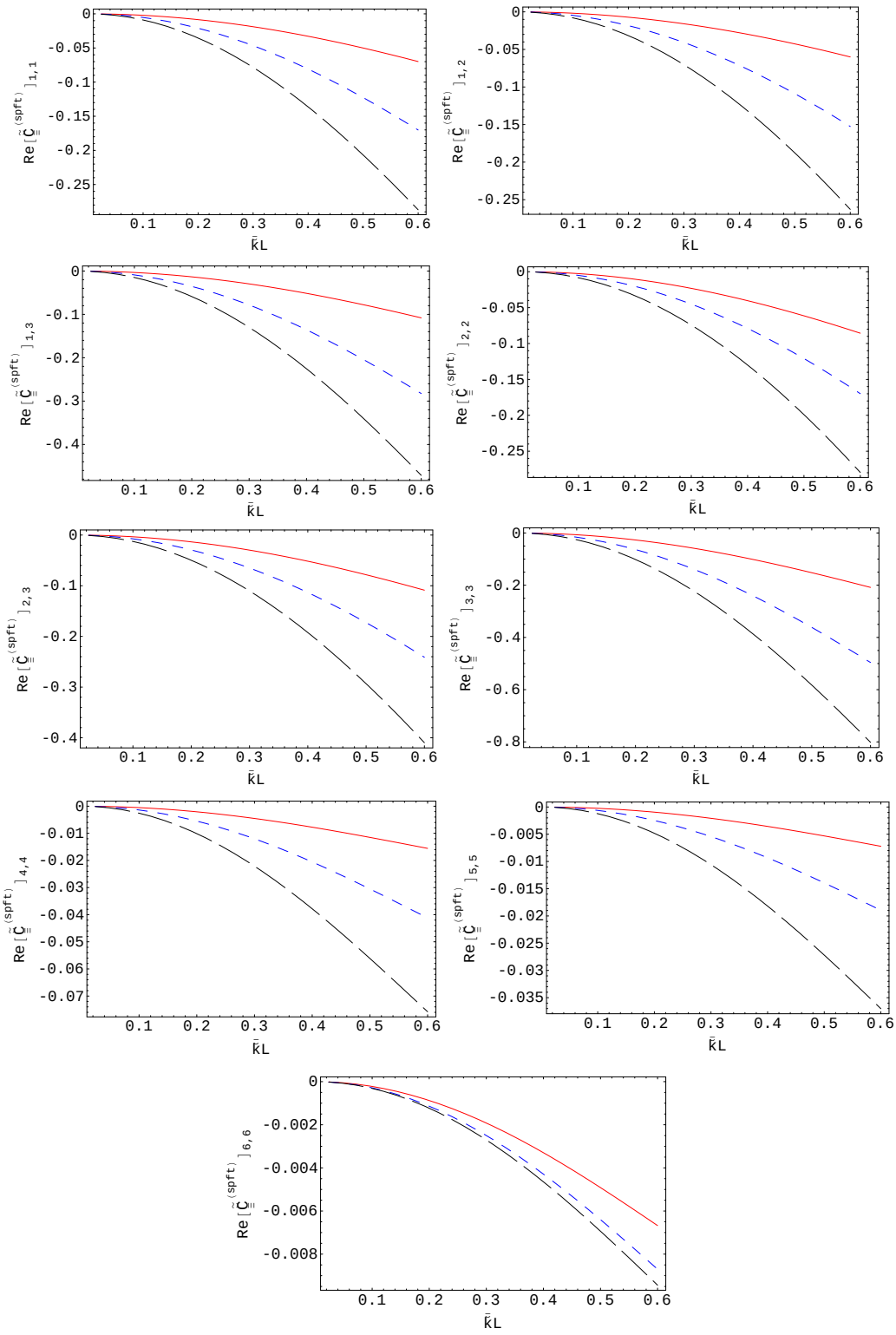

Figure 5.10: Plots of the real parts of $\left[\underline{\underline{\tilde{\mathbf{C}}}}^{(spft)}\right]_{r,s}$, with $r,s \in \{1,1;\ 1,2;\ 1,3;\ 2,2;\ 2,3;\ 3,3;\ 4,4;\ 5,5;\ 6,6\}$ (in GPa) plotted as functions of $\bar{k}L$, with $f^{(2)} = 0.5$. The results from the spherical inclusion case (red, solid line) are plotted alongside the cases with elliptical inclusions $a = 5$, $b = 1.5$, $c = 1$ (blue, short-dashed line) and $a = 10$, $b = 2$, $c = 1$ (black, long-dashed line). Component material '1' is PVDF and component material '2' is LaRC-SI.

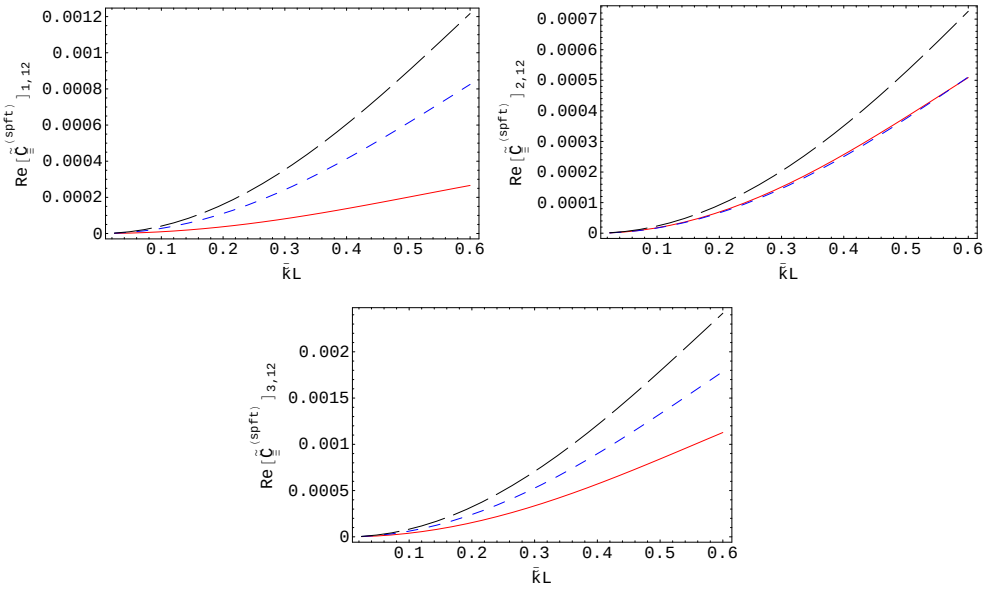

Figure 5.11: Plots of the real parts of $\left[\underline{\underline{\tilde{\mathbf{C}}}}^{(spft)}\right]_{r,s}$, with $r,s \in \{1,12;\ 2,12;\ 3,12\}$, the piezoelectric parts. The results from the spherical inclusion case (red, solid line) are plotted alongside the cases with elliptical inclusions $a = 5$, $b = 1.5$, $c = 1$ (blue, short-dashed line) and $a = 10$, $b = 2$, $c = 1$ (black, long-dashed line). Component material '1' is PVDF and component material '2' is LaRC-SI.

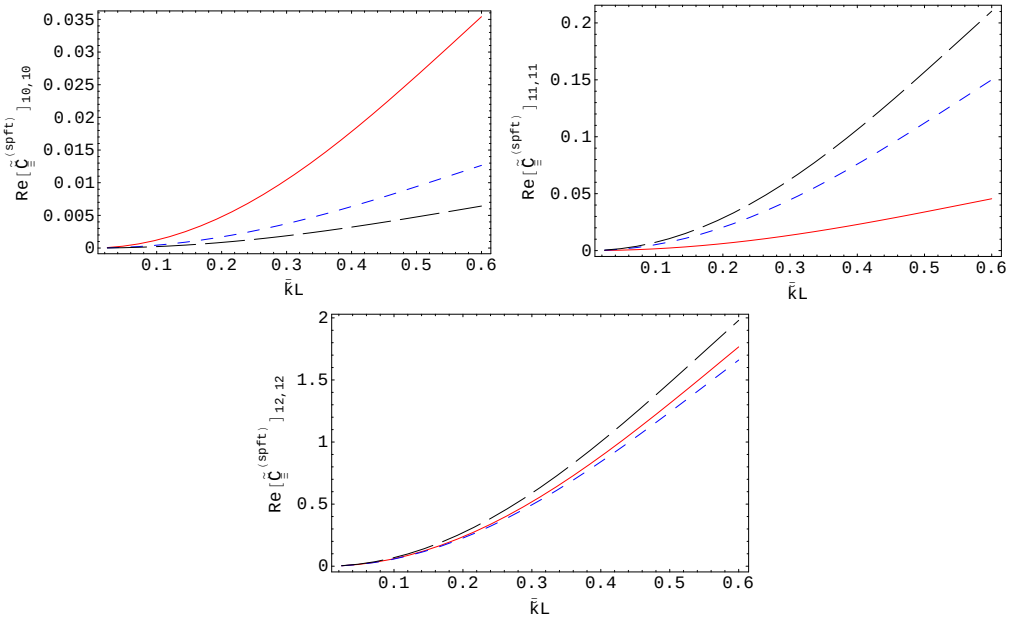

Figure 5.12: Plots of the real parts of $\left[\underline{\underline{\tilde{\mathbf{C}}}}^{(spft)}\right]_{r,s}$, with $r,s \in \{10,10;\ 11,11;\ 12,12\}$, the dielectric parts. The results from the spherical inclusion case (red, solid line) are plotted alongside the cases with elliptical inclusions $a = 5$, $b = 1.5$, $c = 1$ (blue, short-dashed line) and $a = 10$, $b = 2$, $c = 1$ (black, long-dashed line). Component material '1' is PVDF and component material '2' is LaRC-SI.

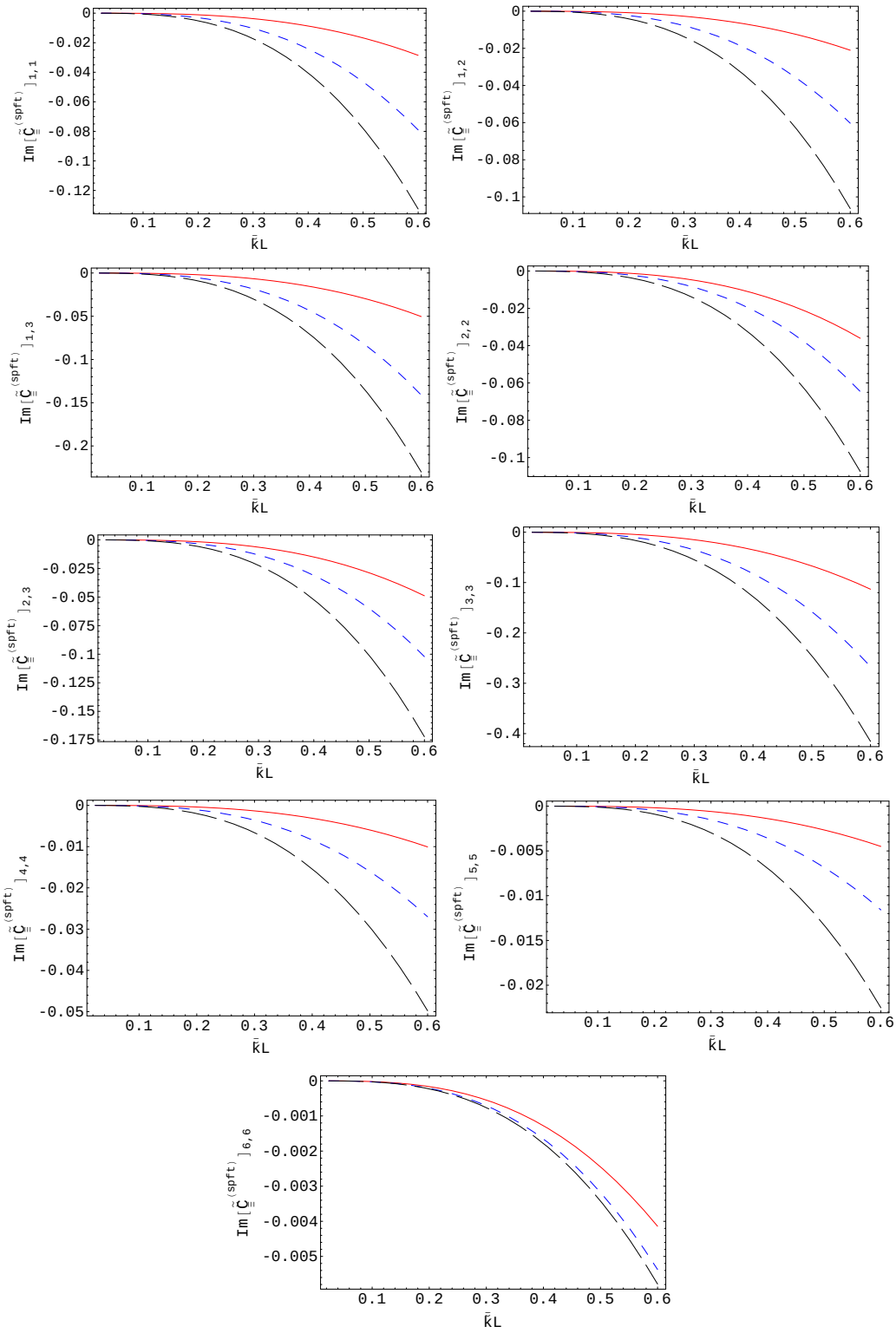

Figure 5.13: As figure 5.10 but for the imaginary parts.

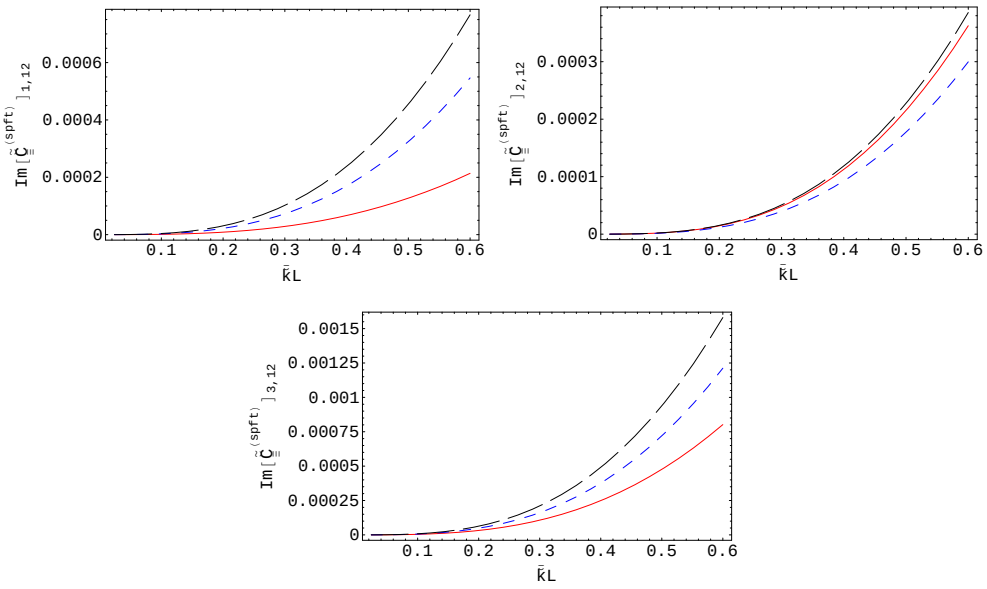

Figure 5.14: As figure 5.11 but for the imaginary parts.

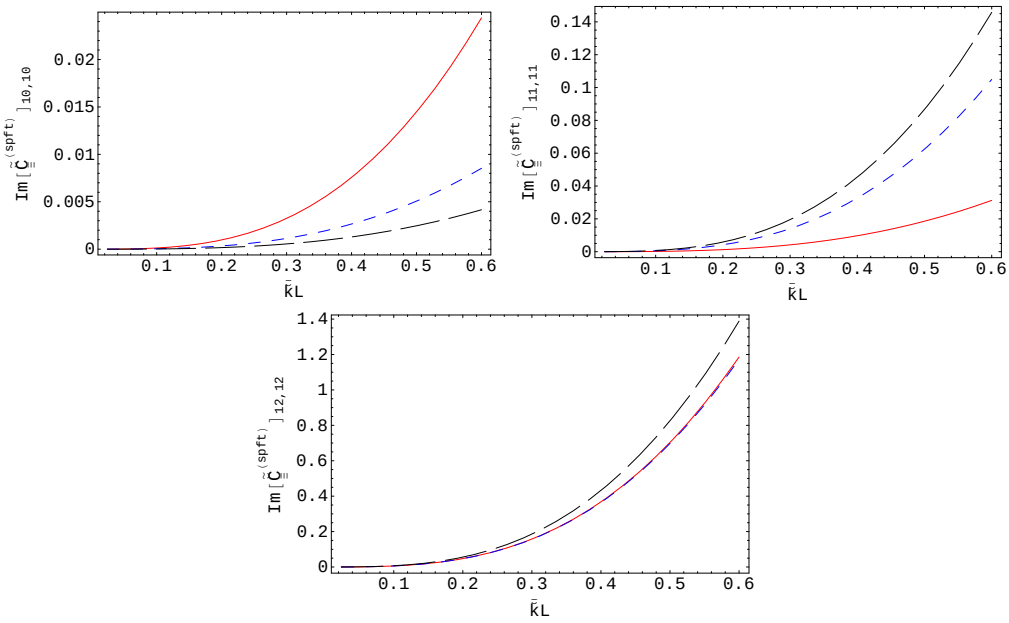

Figure 5.15: As figure 5.12 but for the imaginary parts.

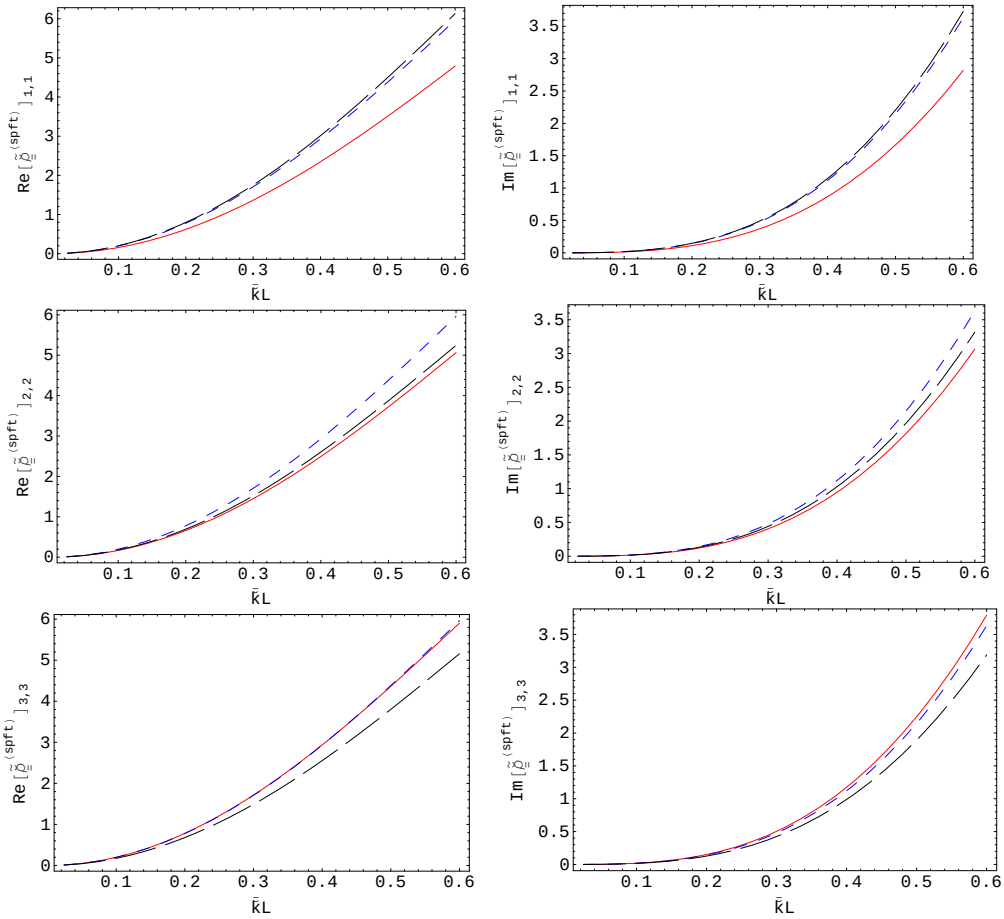

Figure 5.16: Plots of the real and imaginary parts of $\underline{\underline{\tilde{\rho}}}^{(spft)}_{11}$, $\underline{\underline{\tilde{\rho}}}^{(spft)}_{22}$ and $\underline{\underline{\tilde{\rho}}}^{(spft)}_{33}$ plotted as functions of $\breve{\bar{k}}L$, with $f^{(2)} = 0.5$. The results from the spherical inclusion case (red, solid line) are plotted alongside the cases with elliptical inclusions $a = 5$, $b = 1.5$, $c = 1$ (blue, short-dashed line) and $a = 10$, $b = 2$, $c = 1$ (black, long-dashed line).

Chapter 6

Conclusions and further work

Within this thesis we have explored the estimation of the electromagnetic, elastodynamic and piezoelectric properties of homogenized composite materials.

For electromagnetic HCMs we re–examined the Bergman–Milton bounds and Maxwell Garnett estimates on ϵ, in light of recent advances in material manufacture. It was shown that the Bergman–Milton bounds do not provide tight limits on the relative permittivity of the HCM if the real parts of the composite materials' relative permittivities are of opposite sign and the magnitude of the real parts are much larger than the magnitude of the imaginary parts.

In elastodynamics the SPFT was further developed for orthotropic HCMs and numerical studies undertaken. The piezoelectric SPFT was developed for orthorhombic HCMs as an extension of the elastodynamic SPFT and numerical examples were produced. For both SPFT estimates, elastodynamic and piezoelectric, it has been shown that the lowest–order estimates are qualitatively similar to those produced by the respective estimates from the Mori–Tanaka formalism. Furthermore, the second–order SPFT estimate provides a relatively small, but highly significant, correction to the lowest–order estimate which indicates dissipation due to scattering loss.

The work described in this thesis leads to several possibilities for further work. Firstly, the path has how been cleared towards the development of the SPFT for piezoelectric/piezomagnetic HCMs [58], with bianisotropic electromagnetic properties [10]. Secondly, as with the electromagnetic SPFT [59] it may be of interest

to investigate the 3rd–order approximation of both the elastodynamic and the piezoelectric SPFT. Thirdly, a wavenumber study would allow comparison with a greater number of multi-scattering homogenization theories [60]. Finally, it would be interesting to use the piezoelectric SPFT to investigate the possibility of negative phase velocity through the application of certain stress or strain [9].

Acknowledgements

The work described herein was partially undertaken during a research visit to Prof. Akhlesh Lakhtakia at Pennsylvania State University. The author thanks Prof. Lakhtakia for his hospitality, and the Engineering and Physical Sciences Research Council, the Royal Academy of Engineering and the School of Mathematics at the University of Edinburgh for funding.

Bibliography

[1] Lakhtakia, A., (Ed.), 1996, *Selected Papers on Linear Optical Composite Materials*, SPIE, Bellingham, WA, USA.

[2] Milton, G.W., 2002, *The Theory of Composites*, Cambridge, UK: Cambridge University Press.

[3] Aspnes, D.E., 1982 Local-field effects and effective–medium theory: A microscopic perspective, *Am. J. Phys.*, **50**, 704-709. (Reproduced in [1]).

[4] Bergman, D.J., 1981, Bounds for the complex dielectric constant of a two-component material, *Phys. Rev. B.*, **23**, 3058-3065.

[5] Bergman, D.J., 1978, The dielectric constant of a composite material - a problem in classical physics, *Phys. Rep.*, **43**, 377-407.

[6] Bergman, D.J., 1982, Rigorous bounds for the complex dielectric constant of a two-component composite, *Annals. Phys.*, **138**, 78-114.

[7] Bergman, D.J., 1993, Hierarchies of stieltjes functions and their application to the calculation of bounds for the dielectric constant of a two–component medium, *SIAM J. Appl. Math.*, **53**, 915-930.

[8] Milton, G.W., 1981, Bounds on the complex permittivity of a two-component composite material, *J. Appl. Phys.*, **52**, 5286-5293.

[9] Mackay, T.G., 2005, Linear and nonlinear homogenized composite mediums as metamaterials, *Electromag.*, **25**, 461–481.

[10] Mackay, T.G., Lakhtakia, A. & Weiglhofer, W. S., 2000, Strong-property-fluctuation theory for homgenization of bianisotropic composites: Formulation, *Phys. Rev. E*, **62**, 6052-6064.

[11] Mackay, T.G., Lakhtakia, A. & Weiglhofer, W. S., 2001, Ellipsoidal Topology, Orientation Diversity and Correlation Length in Bianiostropic Composite Mediums, *Int. J. Electron. Commun.*, **55**, 243-251.

[12] Mackay, T.G., Lakhtakia, A. & Weiglhofer, W. S., 2001, Homogenization of similarly oriented, metallic, ellipsiodal inclusions using the bilocally approximated strong-property-fluctuation theory, *Opt. Commun.*, **197**, 89-95.

[13] Zhuck, N.P., 1996, Strong fluctuation theory for a mean acoustic field in a random fluid medium with statistically anisotropic perturbations. *J. Acoust. Soc. Am.*, **99**, 46–54.

[14] Zhuck, N.P. & Lakhtakia, A., 1999, Effective constitutive properties of a disordered elastic solid medium via the strong-fluctuation approach. *Proc R. Soc. Lond. A*, **455**, 543–566.

[15] Hashin, Z. & Shtrikman, S., 1962, On some variational principles in anisotropic and nonhomogeneous elasticity. *J. Mech. Phys. Solids* **10**, 335–342.

[16] Kröner, E., 1977, Bounds for the effective elastic moduli of disordered materials. *J. Mech. Phys. Solids*, **25**, 137–155.

[17] Willis, J.R., 1981, Variational and related methods for the overall properties of composites. *Advances in Applied Mechanics*, **21**, 1–79.

[18] Talbot, D.R.S. & Willis, J.R., 1982, Variational estimates for the dispersion and attenuation of waves in random composites I: General theory, *Int. J. Solids Structures*, **18**, 673–683.

[19] Hashin, Z., 1983, Analysis of composite materials — a survey. *J. Appl. Mech.*, **50**, 481–505.

[20] Mori, T. & Tanaka, K., 1993, Average stress in matrix and average elastic energy of materials misfitting inclusions, *Acta Metallurgica*, **21**, 571–574.

[21] Lorrain, P., Corson, D.R.& Lorrain, F., 1988, *Electromagnetic Fields and Waves*, 3rd. ed. New York, NY, USA: W.H. Freeman and Company.

[22] Weiglhofer, W.S., 2003, A Flavour of Constitutive Relations: The Linear Regime, in *Advances in Electromagnetics of Complex Media and Metamaterials*, Zouhdi, S., Sihvola, A. & Arsalane, M., (Eds.), Kluwer, Dordrecht.

[23] Weiglhofer, W.S., & Lakhtakia, A., (Eds.), 2003, *Introduction to Complex Mediums for Optics and Electromagnetics*, SPIE, Bellingham, WA, USA.

[24] Singh, O.N., & Lakhtakia, A., (Eds.), , 2000, *Electromagnetic Fields in Unconventional Materials and Structures*, Wiley, New York, NY, USA.

[25] Walser, R.M., 2003, Metamaterials: an introduction, in *Introduction to Complex Mediums for Optics and Electromagnetics*, Weiglhofer, W.S. & Lakhtakia, A., (Eds.), SPIE, Bellingham, WA, USA.

[26] Milton, G.W., 1980, Bounds on the complex dielectric constant of a composite material, *Appl. Phys. Lett.*, **37**, 300-301.

[27] Hashin, Z. & Shtrikman, S., 1962, A variational approach to the theory of the effective magnetic permeability of multimedium materials, *J. Appl. Phys.*, **33**, 3125-3130.

[28] Mackay, T.G &, Lakhtakia, A., 2004, A limitation of the bruggeman formalism for homogenization, *Opt. Commun.* **234**, 35-42.

[29] Hill R., 1963, A self–consistent mechanics of composite materials. *J. Mech. Phys. Solids*, **13**, 213–222.

[30] Hill R., 1965, Elastic properties of reinforced solids: some theoretical principles. *J. Mech. Phys. Solids*, **11**, 357–372.

[31] Budiansky B., 1965, On the elastic moduli of some heterogeneous materials. *J. Mech. Phys. Solids*, **13**, 223–227.

[32] Lakhtakia, A., 2002, Microscopic model for elastostatic and elastodynamic excitation of chiral sculptured thin films, *J. Compos. Mater.*, **36**, 1277–1298.

[33] Červený, V. & Pšenčik, I., 2006, Energy flux in viscolelastic anisotropic media, *Geophys. J. Int.*, **166**, 1299–1317.

[34] Tsang, L., Kong, J.A. & Newton, R.W., 1982, Application of strong fluctuation random medium theory to scattering of electromagnetic waves from a half–space of dielectric mixture, *IEEE Trans. Antennas Propagat.*, **30**, 292–302.

[35] Ting, T.C.T., 1996, *Anisotropic Elasticity*. New York, NY, USA: Oxford University Press.

[36] Narasimhan, M.N.L., 1993, *Principles of Continuum Mechanics*. New York, NY, USA: Wiley.

[37] Bagnara, R., 1995, A unified proof for the convergence of Jacobi and Gauss–Seidel methods, *SIAM Review*, **37**, 93–97.

[38] Michel, B., 1997, A Fourier space approach to the pointwise singularity of an anisotropic dielectric medium, *Int. J. Appl. Electromagn. Mech.*, **8**, 219–227.

[39] Kwok, Y.K., 2002, *Applied Complex Variables for Scientists and Engineers*. Cambridge, UK: Cambridge University Press.

[40] Press, W.H., Flannery, B.P., Teukolsky, S.A. & Vetterling, W.T., 1992, *Numerical Recipes in Fortran*, 2nd. edition. Cambridge, UK: Cambridge University Press.

[41] Willis, J.R., 1985, The nonlocal influence of density variations in a composite. *Int. J. Solids Structures* **21**, 805–817.

[42] Milton, G.W., 2007, New metamaterials with macroscopic behavior outside that of continuum elastodynamics. *New J. Physics* **9**, 359.

[43] Mura, T., 1987, *Micromechanics of Defects in Solids*. Dordrecht, The Netherlands: Martinus Nijhoff Publishers.

[44] Eshelby, J.D., 1957, The determination of the elastic field of an ellipsoidal inclusion, and related problems. *Proc. R. Soc. Lond. A*, **241**, 376–396.

[45] Gavazzi, A.C. & Lagoudas, D.C., 1990, On the numerical evaluation of Eshelby's tensor and its application to elastoplastic fibrous composites. *Comp. Mech.*, **7**, 13–19.

[46] James, A.M. & Lord, M.P., 1992, *MacMillan's Chemical and Physical Data*. London, UK: MacMillan Press.

[47] Shackelford, J.F., 2005, *Introduction to Materials Science for Engineers*, 6th. edition. Upper Saddle River, NJ, USA: Pearson Prentice Hall.

[48] Dunn, M.L. & Taya, M., 1993, An analysis of piezoelectric composite materials containing ellipsoidal inhomogeneities, *Proc. R. Soc.: Math. Phys. Sci.*, **443**, 265–287.

[49] Ma, H. & Wang, B., 2005, The scattering of electrostatic waves by an ellipsoidal inclusion in piezoelectric medium, *Int. J. Solids Structures*, **42**, 4541–4554.

[50] Lifshitz, I.M. & Rosenzveig, L.N., 1946, On the theory of elastic polycrystals, *Zh. Eksp. Teor. Fiz.*, **20**, 175–184. (In Russian)

[51] Tsang, L. & Kong, J.A., 1981, Scattering of electromagnetic waves from random media with strong permittivity fluctuations, *Radio Sci.*, **16**, 303–320.

[52] Huang, J.H. & Kuo, W–S., 1996, The analysis of piezoelectric/piezomagnetic composite materials containing ellipsoidal inclusions, *J. Appl. Phys.*, **81**, 1378—1386.

[53] Nye, J.F., 1985, *Physical Properties of Crystals*, Oxford, UK: Clarendon.

[54] Auld, B.A., 1990, *Acoustic Fields and Waves in Solids*, 2nd edn Malabar, FL, USA: Krieger Publishing Company.

[55] Holland, R., 1967, Representation of dielectric, elastic, and piezoelectric losses by complex coefficients, *IEEE Trans. Son. Ultrason.*, **14**, 18–20.

[56] Dunn, M.L. & Taya, M., 1993, Micromechanics predictions of the effective electroelastic moduli of piezoelectric composites, *Int. J. Solids Structures*, **30**, 161–175.

[57] Odegard, G.M., 2004, Constitutive modeling of piezoelectric polymer composites, *Acta Mater.*, **52**, 5315–5330.

[58] Nan, C–W., 1994, Magnetoelectric effect in composites of piezoelectric and piezomagnetic phases, *Phys. Rev. B*, **50**, 6082–6088.

[59] Mackay, T.G., Lakhtakia, A. & Weiglhofer, W. S., 2002, Homogenisation of isotropic, cubically nonlinear, composite mediums by the strong-permittivity-fluctuation theory: third–order considerations, *Opt. Commun.*, **204**, 219–228.

[60] Twersky, V., 1962, On scattering of waves by random distributions. I. Free space scatterer formalism, *J. Math. Phys.*, **4**, 700–715.